Physics Reports 975 (2022) 1–61

Contents lists available at ScienceDirect

Physics Reports

journal homepage: www.elsevier.com/locate/physrep

Precision spectroscopy of positronium: Testing bound-state QED theory and the search for physics beyond the Standard Model

G.S. Adkins [a], D.B. Cassidy [b], J. Pérez-Ríos [c,*]

[a] Department of Physics and Astronomy, Franklin & Marshall College, Lancaster, PA 17604, United States
[b] Department of Physics and Astronomy, University College London, Gower Street, London, WC1E 6BT, United Kingdom
[c] Department of Physics and Astronomy, Stony Brook University, Stony Brook, NY 11794, United States

ARTICLE INFO

Article history:
Received 1 April 2021
Received in revised form 8 January 2022
Accepted 5 May 2022
Available online xxxx
Editor: Andreas Buchleitner

Keywords:
Positronium spectroscopy
Bound states QED
Physics beyond the standard model

ABSTRACT

Positronium (Ps) is an exotic hydrogenic atom composed of an electron bound to a positron via the Coulomb force. Being composed of two low-mass leptons, positronium is, for all practical purposes, fully described by quantum electrodynamics (QED). The absence of hadronic components suggests that positronium energy levels and decay rates can be calculated to very high precision, limited only by the order of the corresponding perturbative expansion and the tiny effects of heavy or weakly interacting virtual particles and exotic decay modes. Moreover, as it is a low-mass particle–antiparticle system, the QED description of positronium is strongly affected by annihilation and recoil effects that are either weaker or not present in other atoms. As a result, sufficiently precise measurements of Ps energy levels and decay properties can serve as stringent tests of bound-state QED theory, and may be sensitive to processes not present in the theory, such as axion-like particles (beyond the QCD axion), or a fifth fundamental force. In addition, since positronium is an eigenstate of the fundamental symmetries C and P, various symmetry violating mechanisms can be probed through searches for anomalous decay modes. In the last three decades, there have been significant experimental advances in positron and positronium physics which open up the possibility to test QED bound-state theory with unprecedented precision. Here we present the current state-of-the-art in experimental positronium spectroscopy, and discuss explicitly how such measurements can be used to test bound-state QED theory, and how such tests may contribute to the search for physics beyond the Standard Model.

Contents

* Corresponding author.
E-mail address: jesus.perezrios@stonybrook.edu (J. Pérez-Ríos).

https://doi.org/10.1016/j.physrep.2022.05.002
0370-1573/

1. Introduction

The simplicity of single electron (hydrogenic) atoms offers clear advantages from a theoretical perspective, as evidenced by early studies of hydrogen and the concomitant development of quantum theory (e.g., [1]). Such atoms are therefore also attractive systems for precision measurements (e.g., [2]). Experimentally, the advantages of dealing with hydrogenic systems are less obvious, and indeed vary considerably among the various possible systems that are available for study. In addition to hydrogen, simple atoms of current interest include the exotic systems of positronium, muonium and muonic hydrogen and antihydrogen. Systems containing muons or antiprotons can only be studied at large facilities, and such experimentation is therefore rare [3–5]. More accessible is the electron–positron bound state, positronium (Ps) [6] which can be generated using positron beams based on radioactive isotopes [7]. While Ps atoms can be readily produced, they are intrinsically metastable and in the triplet ground state will decay by self-annihilation in 142 ns [8]. Compared to hydrogen, the wavelengths needed to drive transitions from the ground states are more convenient, being scaled by the ratio of the Ps and hydrogen reduced masses, which is almost a factor of two (actually 1.9989). A schematic representation of H and Ps energy levels for $n = 1$ and $n = 2$ is shown in Fig. 1.

The experimentally accessible properties of Ps that can be measured with sufficient precision to test QED theory, including searches for violations of discrete symmetries, are (i) energy intervals (ii) decay rates, and (iii) decay modes. These are measured using a variety of techniques, as described in Section 3: Ps energy levels are measured using laser or microwave spectroscopy, whereas lifetimes are measured using positronium annihilation lifetime spectroscopy (PALS) [9]. Decay mode measurements are specific to the type of symmetry being studied but generally consist of using gamma radiation detectors to look for forbidden correlations between annihilation quanta properties (polarization and momentum) or simply for missing decay quanta.

At the lowest (Bohr) order, all two-body Coulombic bound states are described by the nonrelativistic Schrödinger equation with reduced mass. Relativistic and other corrections related to spin can be introduced by use of the Dirac equation with a Coulomb potential [10]. The Dirac equation works well for hydrogen, where the mass ratio and hence recoil corrections are small, but not for positronium where the mass ratio obtains its maximum value of one and recoil effects are large. Furthermore, virtual annihilation comes into play at the next level of approximation. More advanced techniques such as the use of effective potentials [11], the Bethe–Salpeter equation [12], or effective quantum field theories [13,14] are required even at the level of the fine structure at $O(\alpha^4)$.

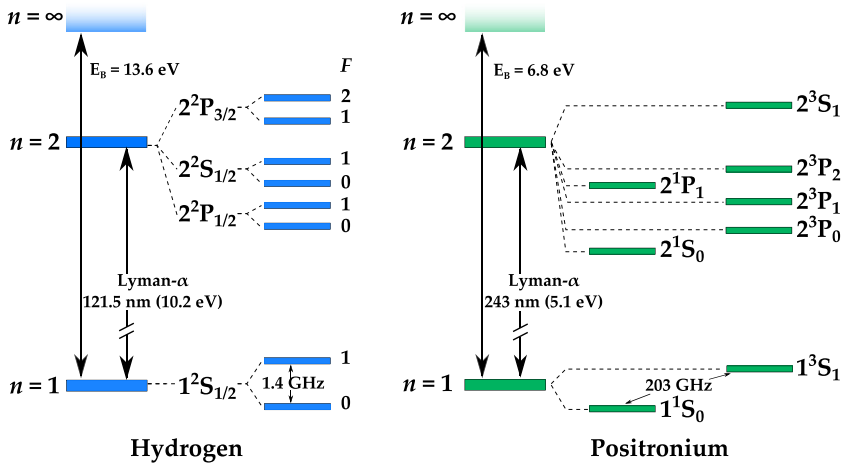

Fig. 1. Comparison of hydrogen and positronium energy level structures. The $n = 1$ and $n = 2$ levels indicated refer to the Bohr levels.

Nevertheless, despite these complications the nature of Ps makes it the only true two-body atomic system available for study [2]. The lack of hadronic components, and attendant substructure means that Ps is (almost [15]) fully described by QED theory [16]. Thus, calculations can in principle be performed to any arbitrary precision. In reality of course this precision is not arbitrary, as it depends on generating complex high-order expansions with a multitude of terms, and requires correspondingly precise knowledge of fundamental constants [17].

QED is the most precisely tested theory in physics, and agrees with all observations performed so far, having been tested at the part per trillion level (i.e. parts in 10^{12}) [18]. Because the theory is so well established it is possible to use precision measurements of Ps to search for effects that may be caused by elements not included in the theory. Ps is also free of complications arising from nuclear effects; hydrogen is of course also an excellent QED probe, but it has the limitation of nuclear structure corrections. Incomplete knowledge of the proton structure is currently a limiting factor in the interpretation of some high-precision measurements [2]. As they are governed by quark interactions (i.e., by the strong nuclear force), details of the proton structure cannot be directly calculated with sufficiently high precision [19] and have to be measured; attempts to do so using muonic hydrogen [20] have revealed a discrepancy with previous measurements that has not yet been resolved (this is known as the proton radius puzzle [21,22]).

The search for new physics (NP) (that is, particles or fields not currently included in the Standard Model (SM)) is driven by various unexplained phenomena, which may be cosmological in scale, as in the matter–antimatter asymmetry of the Universe or the nature of Dark Matter and Energy, or may arise from inconsistencies within the SM itself. The latter are well known, and include neutrino oscillations, the mass hierarchy problem and the so-called strong CP problem. All of these phenomena (and more) indicate that SM physics is more of an effective model rather than a complete theory of nature. The Large Hadron Collider (LHC) was built with the hope that it would generate data able to point the way towards NP; the observation of the Higgs Boson [23] was a triumph of modern physics, but nevertheless all LHC observations so far can be accommodated within the SM. As a result there is a growing interest in exploring other routes to NP. One of them is via precision spectroscopy [24], including measurements of Ps energy levels and decay modes/rates.

An interpretation of the spectroscopy of Ps as a sensitive probe of new physics requires equally precise theoretical calculations of the energy levels within the framework of the SM. Given that Ps is purely leptonic, this amounts to a precise test of perturbative QED at high loop orders. The current theoretical precision is 0.58 MHz in calculating the $1\,^3S_1$ - $2\,^3S_1$ transition frequency, with loop corrections in the fine structure constant α up to $\mathcal{O}(m_e\alpha^7\ln^2(1/\alpha))$ included [25]. This is a factor of five better than the current experimental precision ($\pm$3.2 MHz, or 2.6 ppb), but will likely need to improve to $\mathcal{O}(m_e\alpha^7)$ in the near future as new experiments are completed [26]. We note that, as discussed below, some $\mathcal{O}(m_e\alpha^7)$ terms have already been calculated, and continued progress can be expected [27]. Other transitions are also being re-measured, including the Ps $n = 2$ fine structure [28] and ground state hyperfine interval [29]. Experimental progress will thus drive theoretical efforts, and while QED is the best tested theory in physics, a precise understanding of its simplest bound state is crucial for verification and a requirement for any new physics searches. In fact, it is necessary to improve the theoretical understanding of Ps in order to fully capitalize on experimental improvements.

High precision spectroscopy in simple atomic systems can also act as a probe with which to search for exotic forces [30,31]. One can distinguish between spin dependent and spin independent forces [32]: spin-dependent interactions may result from a pseudo-scalar or pseudo-vector mediator, while spin-independent interactions may come from a scalar or vector mediator. For example, a light exotic scalar or vector boson, ϕ, that couples to SM leptons will give rise to a spin-independent Yukawa potential

$$V_{ij}(r) = -\frac{g_i g_j}{4\pi}\frac{e^{-m_\phi r}}{r}, \tag{1}$$

between two leptonic species i and j [33]. Here, g_i and g_j are the associated coupling constants, m_ϕ is the mass of the exotic boson and r is the distance between the leptons. In bound states of leptonic systems, the potential from Eq. (1) induces shifts in energy levels compared to QED predictions. Specifically, for Ps as a bound state of an electron and a positron, such a force may be probed through measuring the frequency of the $1\,^3S_1 \rightarrow 2\,^3S_1$ transition or the spectroscopy of Rydberg states with high, $n \lesssim 30$ principal quantum numbers [34]. Using the precision of current $1\,^3S_1 \rightarrow 2\,^3S_1$ measurements, couplings of order $g_e \approx 10^{-5}$ can be probed for exotic mediator masses $m_\phi \lesssim 1$ keV [32]. This is only slightly worse than the sensitivity from measurements of the anomalous magnetic moment of the electron $(g-2)_e$ [35], and improving the sensitivity by a factor of 3 can provide the most stringent laboratory constraint in this regime. It should also be noted that $(g-2)_e$ will be induced at the quantum loop level and several contributions can cancel each other in the case of a more complex dark sector. On the other hand, these laboratory constraints are much less sensitive than those coming from cooling considerations in astroparticle physics, $g_e \lesssim 10^{-14}$ applicable for $m_\phi \lesssim 300$ keV [36]. It is nevertheless important to push the envelope of laboratory measurements, especially given that it is possible to avoid the constraints from astrophysics if the force potential depends on the surrounding matter density and can be screened, e.g. as it is in chameleon models [37].

There are already hints from neutrino oscillations that the combined symmetry of charge-conjugation and spatial parity (CP) is violated in the lepton sector of the SM [38]. Future oscillation experiments will aim to confirm this. Despite the potential impact on the origin of the matter–antimatter asymmetry of the Universe, the connection between neutrino CP violation and Baryogenesis will remain ambiguous and further searches will be important. The photonic decays of Ps, specifically that of $^3S_1$ Ps into three photons, is a sensitive probe not only to CP violation, but also that of time-reversal (T) symmetry and the combination CPT [39]. The latter symmetry will hold in any consistent relativistic quantum field theory (QFT) and searches for CPT violation thus probe a fundamental tenet of particle physics. We note that performing a CPT test by spectroscopy of antihydrogen has been a long term goal and primary motivation of the low-energy antimatter program at CERN [40]. For Ps, anomalous angular correlations between the momenta of the photons produced in the decay of polarized $^3S_1$ atoms to 3γ are odd in CP, T and CPT and their observation would point to the violation of the respective symmetry. Underlying models of CP and T violation would induce mixing terms in the Ps mass matrix, generated by effective operators beyond the SM coupling four electron fields or electrons with one or more photon fields [39]. While bounds on the strength of such operators are expected to be severe generically, especially coming from the stringent constraints on the electric dipole moment (EDM) of the electron [41], the correlation between the EDM and CP and T-odd observables is model-dependent.

In this review we discuss the current situation and future prospects of experimental Ps studies with respect to the intertwined areas of QED tests and new physics. We start with a review of the theoretical situation, including the methods that have been found useful for performing QED bound state calculations for situations where recoil plays a major role. We present the state-of-the-art for calculations of positronium energy levels and decay rates and discuss the uncertainty estimates associated with these results as well as the implications for fundamental constants that can be expected from the comparison between theory and experiment for positronium properties. We then evaluate all existing experimental data regarding Ps energy levels, decay rates, and decay modes, and their implications regarding various aspects of physics beyond the standard model in the context of QED theory. Finally, we critically evaluate the next generation of experimental and theoretical advances, and suggest how these might best contribute to the ongoing search for new physics.

A number of review articles and books have been written covering various areas of positronium physics and QED theory. DeBenedetti and Corben [42] cover theory and experiment up to 1954, and an in-depth exposition of the discovery of Ps has been given by Maglich [43]. A review calculation of positronium decay rates and energy levels, as well as Stark and Zeeman effects in Ps up to 1975 has been given by Stroscio [44]. The theory of the Ps hyperfine structure is described by Murota [45]. Comprehensive review articles by Berko and Pendleton [46] and Rich [47] were published in 1980, and have been indispensable for generations of Ps physicists. However, they both predate optical Ps experiments, which were not conducted until 1982 [48] (as discussed also by Mills and Chu [49]). Rich and co-workers have also discussed the use of Ps in studies of fundamental symmetries [50], with a more recent contribution by Bass [51]. Rubbia [52] and Gninenko [53] have written concerning Ps studies as probes for physics beyond the standard model, including connections to mirror matter and Dark matter. Karshenboim has described how precision studies of simple atoms (specifically (anti)hydrogen, positronium, and muonium) can be used to probe QED, nuclear structure and fundamental constants [2,16]. The 2001 book by Charlton and Humberston [54] is focused mainly on low energy positron and positronium scattering (covering both experiment and theory in some detail). More recently (2016) Mills has discussed high-density Ps physics [55,56], and Cassidy has published a review concerning Ps-laser physics up to 2018 [57].

Theoretical developments related to Ps physics have continued steadily up to the present day (see Section 2), and various technological advances (e.g., [58]) have led to a resurgence in experimental Ps work. Moreover, there is no comprehensive summary of both experimental and theoretical developments of the last few decades and their relation to New Physics. As a result, there is a need for an updated review article.

2. Theoretical description of positronium

Shortly after the prediction of the antielectron (or positron) by Dirac in 1931 [59], and its discovery by Anderson in 1933 [60], the existence of an electron–positron bound state "electrum" was suggested by Mohorovičić [61]. Mohorovičić

calculated the electrum spectrum at the Bohr level of precision and searched for its spectral lines in stellar spectra, but made no mention of the possibility that this bound system might be subject to annihilation. (The impact of Mohorovičić's work has been discussed in [62,63].) Positronium was named by Ruark in 1945 [64], who also obtained its spectrum at the Bohr level and made comments about its structure and annihilation. A more general discussion of electron–positron bound systems was given by Wheeler in 1946 [6]. Wheeler also obtained the positronium spectrum, and was the first to calculate the lowest-order spin-0 (singlet) lifetime, obtaining 1.24×10^{-10} s. He noted that the lifetime of the spin-1 states would be "several orders of magnitude greater". The lowest-order spin-0 lifetime was also obtained by Pirenne in the course of a major investigation [65–68]. The lowest-order spin-1 triplet lifetime was calculated by Ore and Powell in 1949 [8]. By the time positronium was first produced in the laboratory by Martin Deutsch [69] in 1951, the calculation of corrections to the energy levels and decay rates of positronium had already begun. In this section we will outline the theoretical work that has been done on positronium energy levels and decay rates and describe the current state of the art. We will discuss the theoretical methods that have been and are being used to perform these calculations, and consider the sensitivity of the results to the values of fundamental constants.

The internal structure of positronium is described by a number of quantum numbers. These are the principal quantum number n, the orbital angular momentum ℓ, the combined spin of the electron and positron s (which can be 0 or 1, the total angular momentum j (associated with the total angular momentum operator $\vec{J} = \vec{L} + \vec{S}$), and the z component of j. Energies and decay rates will depend on all of these quantum numbers except (in the absence of external fields) j_z. In pure QED, with the neglect of small corrections due to the weak interaction, parity (P) and charge parity (C) are conserved, and their conservation lets us define "good" quantum numbers for positronium states. The parity of a positronium state is determined by the spatial wave function and the opposite intrinsic parities of the constituents to be $P = (-1)^{\ell+1}$. The charge parity of a positronium state can be determined by the requirement that complete interchange of the two fermions yields a factor of -1. Complete interchange entails spatial interchange (with factor $(-1)^{\ell}$), spin state interchange (with factor $(-1)^{s+1}$), and charge state interchange (with factor C). For the charge parity C we find $C = (-1)^{\ell+s}$, and for the combined parity CP we have $CP = (-1)^{s+1}$. States with $CP = -1$ have anti-parallel spins and are called "parapositronium" (p-Ps), while states with $CP = +1$ have parallel spins and are called "orthopositronium" (o-Ps). Since charge parity is conserved in QED and n-photon states have $C = (-1)^n$, ground state parapositronium decays to an even number of photons ($\ell = 0$ for the ground state), and ground state orthopositronium decays to an odd number of photons. In general, the conservation law

$$(-1)^{\ell+s} = (-1)^n \tag{2}$$

governs positronium decays.

We can draw the following conclusions about the eigenstates of positronium in pure QED. The states can be classified as either singlet ($s = 0$) or triplet ($s = 1$) since these are the only options for total spin and CP is conserved. Total angular momentum j will certainly be conserved. Parity conservation in pure QED implies that the value of ℓ for eigenstates is either odd or even. However, states with a given value of j and s must have $\ell = j$ for singlets and $\ell = j \pm 1$ for triplets. In principle, the eigenstates of positronium will be mixtures having $\ell = j - 1$ and $\ell = j + 1$. However, this mixing is small. Degeneracy in positronium is broken at the level of the fine structure ($O(m_e\alpha^4)$), but the matrix elements of operators that mix states with $\ell = j \pm 1$ have magnitude $O(m_e\alpha^6)$ [70] and energy shifts due to this mixing sets in at $O(m_e\alpha^8)$, so for practical purposes we can label the states by n, ℓ, j, and j_z. The small corrections due to weak interactions are discussed in [71,72].

2.1. History and present status of positronium theory

2.1.1. Energy levels

Positronium energy levels as calculated from QED are all proportional to $m_e c^2$ times a function of the fine structure constant α (including possibly logs of α). They have the form

$$E = m_e c^2 \Big\{ A_{20}\alpha^2 + A_{40}\alpha^4 + (A_{51}L + A_{50})\,\alpha^5 + (A_{61}L + A_{60})\,\alpha^6 + \left(A_{72}L^2 + A_{71}L + A_{70}\right)\alpha^7 + \cdots \Big\} \tag{3}$$

where $L = \ln(1/\alpha) \approx 4.92$ and m_e is the electron mass.[1] In this section we will describe what is known about the various coefficients A_{ij}. The Bohr energy factor $A_{20} = -1/(4n^2)$ was obtained by Mohorovičić, Ruark, and Wheeler as described above. The first corrections requiring a relativistic treatment, those at $O(m_e\alpha^4)$, were obtained by the time of positronium's discovery. Pirenne, in a series of papers [65–68], developed a formalism for the electron–positron interaction and used it

[1] In this section from now on we will employ natural units where $\hbar = c = 1$ (with $\hbar = h/(2\pi)$). In these units m_e represents a mass (the electron mass), an energy, and a frequency. Appropriate factors of $\hbar$ and c should be inserted as needed to obtain quantities with the required units. It is convenient to note that $\hbar \approx 6.582\,120 \times 10^{-16}$ eV s, $\hbar c \approx 197.327$ eV nm, $h \approx 4.135\,668 \times 10^{-15}$ eV/Hz, and $m_e c^2 \approx 510\,999$ eV. Since $m_e c^2/\hbar$ is a frequency in units of rad/s we see that $m_e c^2/(2\pi\hbar) = mc^2/h$ is a frequency in Hz. In fact, $m_e c^2\alpha^2/(2h) \approx 3.289\,842 \times 10^{15}$ Hz is the Rydberg constant in frequency units. The inverse fine structure constant has the value $\alpha^{-1} \approx 137.036$. Precise values of the fundamental constants were obtained from the 2018 CODATA adjustment [73]. The relation of natural units to atomic units is discussed in Section 4.3.

to obtain the energies at order $m_e\alpha^4$. This work involved consideration of the relativistic kinetic energy, the spin–orbit and Darwin interactions, magnetic interactions (involving transverse photon exchange), and a new interaction involving electron–positron annihilation into a virtual photon followed by the re-constitution of the electron–positron state. Building on the electron–positron Hamiltonian of Berestetskii and Landau [74], Berestetskii also obtained the $O(m_e\alpha^4)$ energies [75]. Both of these works contained errors that were corrected by Ferrell in the course of his PhD research [76,77]. His result is

$$\Delta E^{(4)} = \frac{m_e\alpha^4}{n^3}\left\{\frac{11}{64n} - \frac{1}{2(2\ell+1)} + \frac{7}{12}\delta_{\ell=0}\delta_{s=1} + \frac{\delta_{\ell\neq 0}\delta_{s=1}}{4\ell(\ell+1)(2\ell+1)}c_{j\ell}^{(0)}\right\} \tag{4}$$

where the Kronecker delta factors are one if the condition in the subscript is true and zero if not,

$$c_{j\ell}^{(0)} = \begin{cases} -\frac{(\ell+1)(3\ell-1)}{2j+1} & \ell = j+1 \\ -1 & \ell = j \\ \frac{\ell(3\ell+4)}{2j+1} & \ell = j-1, \end{cases} \tag{5}$$

and j, ℓ, and s are the quantum numbers of total angular momentum, orbital angular momentum, and total spin.

Ferrell worked on the $O(m_e\alpha^5)$ corrections and pointed out a number of factors that make the calculation of intervals between states having different values of ℓ challenging compared to intervals for states with the same ℓ but different total spin. The S-state triplet–singlet splitting has come to be called the "hyperfine splitting" and the intervals between other states (having the same principal quantum number) the "fine structure". The name "hyperfine", which arose no doubt by analogy with the triplet–singlet splitting in hydrogen, is actually a misnomer since there is no particular factor that makes hyperfine intervals smaller than fine structure intervals in positronium. (In hydrogen, the small electron to proton mass ratio $m_e/m_p \approx 1/1836$, which arises from the inverse mass dependence of the magnetic moments, cuts down the hyperfine splitting relative to other intervals.) Both fine and hyperfine intervals are typically in the microwave range in positronium (for small values of n). Intervals between states of different values of n (when both values of n are not too large) are sometimes called "optical" transitions since their associated wavelengths are in or near the range of visible light. For many years the hyperfine transition was given the greatest amount of attention both in terms of experiment and theory. Ferrell's thesis result for the $O(m_e\alpha^5)$ hyperfine splitting was not complete [76]. The correct result appeared in the 1952 calculation of Karplus and Klein [78]:

$$\Delta E_{n=1;\,\mathrm{hfs}} = m_e\alpha^4\left\{\frac{7}{12} - \left(\frac{1}{2}\ln 2 + \frac{8}{9}\right)\frac{\alpha}{\pi}\right\}. \tag{6}$$

Shortly thereafter some theory improvements were made related to a more physical treatment of the infrared [79], and Fulton and Martin were able to obtain results for the full energies at $O(m_e\alpha^5)$ for the $n = 2$ states [80,81]. The expression for the energies at $O(m_e\alpha^5)$ for all ℓ were given by Pineda and Soto [14] as an example of the use of potential NRQED. They gave their result in a convenient form:

$$\begin{aligned}\Delta E^{(5)} = \frac{m_e\alpha^5}{8\pi n^3}\Bigg\{ & 6\ln\left(\frac{1}{\alpha}\right)\delta_{\ell=0} - \frac{16}{3}\ln k_0(n,\ell) \\ & + \left(\frac{14}{3}\left[H_n - \ln n - \frac{1}{2n}\right] + \frac{28}{3}\ln 2 + \frac{203}{45}\right)\delta_{\ell=0} \\ & + \left(-4\ln 2 - \frac{64}{9}\right)\delta_{\ell=0}\delta_{s=1} - \frac{7\delta_{\ell\neq 0}}{3\ell(\ell+1)(2\ell+1)} \\ & + \frac{\delta_{\ell\neq 0}\delta_{s=1}}{\ell(\ell+1)(2\ell+1)}c_{j\ell}^{(1)}\Bigg\},\end{aligned} \tag{7}$$

where

$$c_{j\ell}^{(1)} = \begin{cases} -\frac{(\ell+1)(4\ell-1)}{(2j+1)} & \ell = j+1 \\ -1 & \ell = j \\ \frac{\ell(4\ell+5)}{(2j+1)} & \ell = j-1. \end{cases} \tag{8}$$

Here $\ln k_0(n,\ell)$ represents the Bethe log, which has been tabulated for example in [82, Ch. 3], and $H_n = \sum_{i=1}^{n}\frac{1}{i}$ is the nth harmonic number. At about the same time, the non-recoil energies for hydrogen-like atoms were computed using traditional NRQED [83]. Non-relativistic QED (NRQED) was proposed in 1986 [13] as an alternative to standard QED as the basis for calculations of bound-state properties. NRQED is an effective quantum field theory in which the relativistic effects are subsumed into a set of additional interactions and only non-relativistic degrees of freedom are explicitly present. Calculations involving non-relativistic bound systems such as positronium are significantly simpler in NRQED than in QED. Potential QED (pNRQED) is a derived effective field theory in which the effects of "soft" energy scales (those with energies $\sim m_e\alpha$) are also encoded into new interactions, leaving only "ultrasoft" ($\sim m_e\alpha^2$) dynamical degrees of freedom [14,84]. See Section 2.2.3.)

The next big push was to calculate corrections at $O(m_e\alpha^6 \ln(1/\alpha))$ for the ground state hyperfine splitting (hfs). This work commenced in 1970 and involved many workers [85–92]. It was not clear at first exactly where all the logs would come from, and inefficient perturbative schemes made the calculations delicate. The calculation of A_{61} for the hfs was completed by the end of the decade [93–95], with the result for the ground state hfs

$$A_{61} = \frac{5}{24}. \tag{9}$$

Results for the A_{61} coefficients for individual S states were obtained somewhat later [96–99].

The pure $O(m_e\alpha^6)$ correction was an even greater challenge, partly because there were so many disparate terms to calculate, partly because some of them required methods that were not available when work on them commenced in 1973. (These methods are discussed in Sections 2.2.2 and 2.2.3.) At $O(m_e\alpha^6)$ the effort required to find the energies of the $s = 0$ and $s = 1$ spin states separately, at least for S states, is not appreciably more than for the hfs only, so by the time the complete hfs result was complete the correction for individual S states was done as well. It took a quarter of a century for final results to be obtained with contributions from many workers [13,25,88,91,100–129]. In the mean time results were also obtained for P states. These states with $\ell = 1$ have some extra complexity due to their non-vanishing angular momentum, but there are also crucial simplifications coming from the softer behavior of the wave function at short distances (the lowest order wave function vanishes at $r = 0$). The P state results were obtained in [117,126,130–132]. Convenient expressions for the positronium S and P state energies were given by Czarnecki, Melnikov, and Yelkhovsky [126]. Energies for states with $\ell > 1$ at order $m_e\alpha^6$ are also known [70,133].

Results for the $O(m_e\alpha^6)$ energy level contributions (including the logs) for S and P states are as follows [126]. The S state hyperfine splitting at $O(m_e\alpha^6)$ is

$$\Delta E^{(6)}_{\ell=0;\,\mathrm{hfs}} = \frac{m_e\alpha^6}{8n^3}\left[\frac{5}{3}\ln\left(\frac{n}{\alpha}\right) - \frac{5}{3}H_n + \frac{20}{3n} - \frac{85}{12n^2} + \frac{1}{\pi^2}\left(-\frac{53}{4}\zeta(3) + \frac{221}{3}\zeta(2)\ln 2 - \frac{4297}{72}\zeta(2) + 4\ln 2 + \frac{1367}{81}\right)\right]. \tag{10}$$

The triplet S state correction is

$$\Delta E^{(6)}_{\ell=0;\,s=1} = \frac{m_e\alpha^6}{32n^3}\left[\frac{8}{3}\ln\left(\frac{n}{\alpha}\right) - \frac{8}{3}H_n + \frac{2}{3n} - \frac{17}{3n^2} - \frac{69}{16n^3} + \frac{1}{\pi^2}\left(22\zeta(3) + \frac{632}{3}\zeta(2)\ln 2 - \frac{187}{2}\zeta(2) - 64\ln 2 + \frac{5630}{81}\right)\right], \tag{11}$$

while the singlet S state correction is

$$\Delta E^{(6)}_{\ell=0;\,s=0} = \frac{m_e\alpha^6}{32n^3}\left[-4\ln\left(\frac{n}{\alpha}\right) + 4H_n - \frac{26}{n} + \frac{68}{3n^2} - \frac{69}{16n^3} + \frac{1}{\pi^2}\left(75\zeta(3) - 84\zeta(2)\ln 2 + \frac{1307}{9}\zeta(2) - 80\ln 2 + 2\right)\right]. \tag{12}$$

The P state energy corrections are

$$\Delta E^{(6)}_{^3P_2} = \frac{m_e\alpha^6}{8n^3}\left[-\frac{169}{600n} + \frac{559}{600n^2} - \frac{69}{64n^3} + \frac{1}{\pi^2}\left(\frac{9}{20}\zeta(3) - \frac{9}{5}\zeta(2)\ln 2 + \frac{20677}{9000}\zeta(2) + \frac{13}{16}\right)\right], \tag{13}$$

$$\Delta E^{(6)}_{^3P_1} = \frac{m_e\alpha^6}{8n^3}\left[-\frac{25}{24n} + \frac{77}{40n^2} - \frac{69}{64n^3} + \frac{1}{\pi^2}\left(-\frac{1}{4}\zeta(3) + \zeta(2)\ln 2 + \frac{493}{360}\zeta(2) - \frac{179}{432}\right)\right], \tag{14}$$

$$\Delta E^{(6)}_{^3P_0} = \frac{m_e\alpha^6}{8n^3}\left[-\frac{8}{3n} + \frac{119}{30n^2} - \frac{69}{64n^3} + \frac{1}{\pi^2}\left(-\frac{3}{2}\zeta(3) + 6\zeta(2)\ln 2 - \frac{923}{90}\zeta(2) - \frac{203}{72}\right)\right], \tag{15}$$

and

$$\Delta E^{(6)}_{^1P_0} = \frac{m_e\alpha^6}{8n^3}\left[-\frac{2}{3n} + \frac{23}{15n^2} - \frac{69}{64n^3} + \frac{163}{540}\right]. \tag{16}$$

Corrections at $O(m_e\alpha^6)$ for $\ell > 1$ can be found in Refs. [70,133].

Table 1
Theoretical results for contributions at various orders to the energies of selected transitions of positronium (in MHz). The transitions shown are the $1^3S_1 - 2^3S_1$ optical transition, the ground state hyperfine, and the most precisely measured of the $n = 2$ fine structures splittings. The Bohr energies at $O(m_e\alpha^2)$ only contribute to transitions having differing principal quantum numbers. Fine structure corrections set in at $O(m_e\alpha^4)$. Corrections at $O(\alpha^7 L)$ where $L = \ln(1/\alpha) \approx 4.92$ are known only for the hyperfine transitions. The theoretical uncertainties were estimated to be half of the magnitude of the $O(m_e\alpha^7 L^2)$ contribution.

Term	$1^3S_1 \to 2^3S_1$	$1^3S_1 \to 1^1S_0$	$2^3S_1 \to 2^3P_0$
$A_{20}\alpha^2$	1 233 690 735.09	0	0
$A_{40}\alpha^4$	−82 005.57	204 386.63	18 248.81
$A_{51}\alpha^5 L$	−2 627.89	0	375.41
$A_{50}\alpha^5$	1 126.45	−1 005.50	−128.08
$A_{61}\alpha^6 L$	−6.69	19.13	0.96
$A_{60}\alpha^6$	−0.42	−7.33	1.32
$A_{72}\alpha^7 L^2$	1.16	−0.92	−0.17
$A_{71}\alpha^7 L$	–	−0.32	–
Total	1 233 607 222.12(58)	203 391.69(46)	18 498.25(8)

Some of the α^7 terms with logs are also known. As early as 1993, Karshenboim obtained the $O(m_e\alpha^7 \ln^2(1/\alpha))$ contribution to the hfs [134]. In 1999 this result was generalized by two groups to give the $O(m_e\alpha^7 \ln^2(1/\alpha))$ contribution to a general state [135,136], with the result

$$\Delta E_{\rm hfs} = -\left(\frac{499}{480} + \frac{7}{32}\vec{\sigma}_1 \cdot \vec{\sigma}_2\right) \frac{m_e\alpha^7 L^2}{\pi n^3}\delta_{\ell,0}, \tag{17}$$

where $\vec{\sigma}_1 \cdot \vec{\sigma}_2 = \delta_{s,1} - 3\delta_{s,0}$ and $L = \ln(1/\alpha)$. The $O(m_e\alpha^7 \ln(1/\alpha))$ correction to the ground state hfs was computed by three groups shortly thereafter using various implementations of NRQED, with the result [137–139]

$$\Delta E_{\rm hfs} = \left(\frac{217}{90} - \frac{17}{3}\ln 2\right)\frac{m_e\alpha^7 L}{\pi}. \tag{18}$$

A number of the pure $O(m_e\alpha^7)$ contributions have been obtained, but many more remain to be computed [140–154]. Of particular interest are the "ultrasoft" corrections, which involve virtual photons having energy and momentum of the same order as the positronium binding energy. A calculation of the one-photon-annihilation contribution (including ultrasoft effects) at $O(m_e\alpha^7)$ gives $\delta_{1\gamma A}A_{70} = 1.595(10)$, leading to an energy shift $\delta_{1\gamma A}E = 0.22$ MHz [143], of which the ultrasoft contribution (∼95% of the total) forms the dominant part. A calculation of the complete $O(m_e\alpha^7)$ ultrasoft contribution to the hfs results in $\delta_{\rm US}A_{70} = 3.50279(32)$, leading to an energy shift of $\delta_{\rm US}E = 0.48$ MHz [142]. We note the partial cancellation of the ultrasoft contribution against that of the sub-leading log (which contributes −0.32 MHz to the hfs). Other known contributions at $O(m_e\alpha^7)$ that do not involve ultrasoft photons [144–154] are significantly smaller. It seems likely that the ultrasoft contributions give the numerically leading contribution at $O(\alpha^7)$, and that an uncertainty estimate of half of the leading $O(\alpha^7 L^2)$ log squared contribution is appropriate.

Despite the presence of non-analytic logarithms, the perturbation series in the fine structure constant for transition energies seem to be behaving well. We illustrate this by giving numerical values for the contributions at the various orders of α and $L \equiv \ln(1/\alpha)$ to three representative transitions in Table 1. The logarithmic contributions generally dominate non-logarithmic ones at the same order in α, as might be expected given that $L \approx 4.92$. Terms with higher powers of α are significantly smaller than terms with lower powers, but by a factor that seems to be decreasing as the order gets higher.

Other corrections to the transition energies are small. The hadronic vacuum polarization contribution to the ground state Ps hfs has been estimated to be or order 0.12 kHz [112]. The weak interaction contribution is 1.15×10^{-2} kHz [72]. Manohar and Stewart used renormalization group methods in an effective field theory to compute the leading $O(m_e\alpha^8 L^3)$ energy shift [155]. They found a spin independent shift (so there is no contribution to the hfs at this order) that gives only $\Delta E = -4.4$ kHz when $n = 1$.

In Table 2 we have given the current best estimates for the energies of transitions involving $n = 1$ and $n = 2$ states of positronium, as these are the transitions that have been measured with high precision. We have included the $1^3S_1 - 2^3S_1$ optical transition, the hyperfine transitions, the $n = 2$ fine structure intervals, and the "ultrafine" transition. The ultrafine transition (for P states) is defined as the interval between the 2^1P_1 state and an average of 2^3P_J states: [156,157]

$$\Delta E^{\rm ultrafine}_{n,P} = E(n^1P_1) - \frac{1}{9}\left[E(n^3P_0) + 3E(n^3P_1) + 5E(n^3P_2)\right]. \tag{19}$$

Of the four spin-dependent operators that enter into positronium energies (the identity 1, the hyperfine operator $S_1 \cdot S_2$, the spin–orbit operator $S \cdot L$, and the tensor operator $S_1 \cdot \hat{r} S_2 \cdot \hat{r} - \frac{1}{3}S_1 \cdot S_2$) only the hyperfine operator contributes to the ultrafine transition. The expectation value of the radial operator multiplying $S_1 \cdot S_2$ vanishes at orders α^4 and α^5 for P states, leaving the pure α^6 prediction

$$\Delta E^{\rm ultrafine}_{2,P} = \frac{683}{172800}m\alpha^6 \approx 74(3)\ \text{kHz}. \tag{20}$$

Table 2
Theoretical results for the $n = 1$ and $n = 2$ transition energies of positronium (in MHz). The calculations include all terms through $m_e\alpha^7 L^2$ where $L = \ln(1/\alpha)$ except for the $n = 1$ and $n = 2$ ($n^3S_1 \to n^1S_0$) hyperfine transitions, which also include the $m_e\alpha^7 L$ contribution. The theoretical uncertainties (expressed in MHz) are discussed in the text.

Transition		Theory (MHz)	Uncertainty
$1^3S_1 \to 2^3S_1$	Optical	1233607222.12	0.58
$1^3S_1 \to 1^1S_0$	$n = 1$ hfs	203391.69	0.46
$2^3S_1 \to 2^1S_0$	$n = 2$ hfs	25424.67	0.06
$2^3S_1 \to 2^1P_1$	$n = 2$ fine structure	11185.37	0.08
$2^3S_1 \to 2^3P_0$	$n = 2$ fine structure	18498.25	0.08
$2^3S_1 \to 2^3P_1$	$n = 2$ fine structure	13012.41	0.08
$2^3S_1 \to 2^3P_2$	$n = 2$ fine structure	8626.71	0.08
$2^1P_1 \to 2^3P_{\bar{J}}$	$n = 2$ ultrafine	0.074	0.003

The uncertainty of 3 kHz was discussed by Lamm [156]. It has been suggested that a precise measurement of the ultrafine transition could be used to constrain the effects of the exchange of hypothetical axion-like particles as it is discussed in Section 4.

2.1.2. Decay rates

Positronium is an unstable system that almost always decays into two or more photons. There is an extremely small branching ratio for decays involving neutrinos. (For example, the branching ratio for o-Ps decay to $\nu_e\bar{\nu}_e$ relative to the dominant 3γ mode is $\sim 6.2 \times 10^{-18}$ [158]. The p-Ps to $\nu\bar{\nu}$ rate is suppressed by an additional factor of $(m_\nu/m_e)^2$ [15].) Possible decays into hypothetical light particles have, of course, also been considered, as reviewed in [52,159]. The decays that have been measured with high precision are those from the $n = 1$ singlet (220 ppm [160]) and triplet (150 ppm [161]) states. These decays will be the focus of this section.

Spin-singlet ground-state parapositronium decays into an even number of photons as required by the charge conjugation invariance of QED (see Eq. (2)). The dominant mode is $1^1S_0 \to 2\gamma$ because each additional photon in the final state brings with it an additional power of α. Orders of alpha for a decay mode may be estimated as follows: one power of α for each photon in the final state (the lowest-order $e^+e^- \to n\gamma$ amplitude is proportional to e^n, so the corresponding cross-section has a factor of α^n), and a factor of α^3 from the density of positronium atoms available to decay (the square of the wave function at the origin). The $n\gamma$ decay rate has the form of a constant times α^{n+3}, where the constant is determined primarily by the phase space volume available for the n photon final state. The two photon phase space is trivial since the two photons are constrained by energy–momentum conservation to go off back-to-back with the same energy (half the energy of the original state). The only free variable is the direction of the decay line, which is unconstrained. The lowest order rate for ground state p-Ps decay to two photons is

$$\Gamma_{\text{p-Ps},0} = \frac{1}{2} m_e \alpha^5 = 8.0325\,\text{ns}^{-1}, \tag{21}$$

as calculated by Wheeler [6] and Pirenne [68]. The corresponding lifetime is $\tau_{\text{p-Ps}} = 0.124\,49\,\text{ns}$. The $O(\alpha)$ correction was obtained in 1957 by Harris and Brown [162]

$$\Gamma_{\text{p-Ps}} = \Gamma_{\text{p-Ps},0}\left\{1 - \frac{\alpha}{\pi}\left(5 - \frac{\pi^2}{4}\right)\right\} \tag{22}$$

based on the Brown and Feynman result for the one-loop correction to the Compton scattering cross-section [163]. The $O(\alpha^2 \ln \alpha)$ correction was obtained in 1990 [164], and the full $O(\alpha^2)$ correction ten years later [165–169]. The $O(\alpha^3 \ln^2 \alpha)$ correction was already known in 1993 [134], and the $O(\alpha^3 \ln \alpha)$ term was obtained in 2000 [170].

The lowest-order rate for p-Ps to decay to four photons has been calculated by several groups [171–175]. The most precise result was obtained in the course of a calculation of the $O(\alpha)$ radiative corrections to this rate [176]. The result for p-Ps $\to 4\gamma$ is

$$\Gamma_{\text{p-Ps}\to 4\gamma} = 0.274290(8)\left(\frac{\alpha}{\pi}\right)^2 \Gamma_{\text{p-Ps},0}\left\{1 - 14.5(6)\frac{\alpha}{\pi}\right\}. \tag{23}$$

More exotic decays – ones allowed by the weak interaction but forbidden in QED – have also been discussed, including the rate for p-Ps to decay to three photons [71,177] and for p-Ps decay to two neutrinos and a photon [178,179]. The branching ratios are too small by many orders of magnitude to be observed in the foreseeable future.

In all, the theoretical result for the p-Ps decay rate is

$$\Gamma_{\text{p-Ps}} = \Gamma_{\text{p-Ps},0}\left\{1 + A_{\text{p}}\frac{\alpha}{\pi} + 2\alpha^2 L + B_{\text{p}}\left(\frac{\alpha}{\pi}\right)^2 - \frac{3\alpha^3}{2\pi}L^2 + C_{\text{p}}\frac{\alpha^3}{\pi}L + D_{\text{p}}\left(\frac{\alpha}{\pi}\right)^3\right\} \tag{24}$$

where $A_{\text{p}} = \frac{\pi^2}{4} - 5$, $B_{\text{p}} = 5.3986(33)$ (including the effect of four-photon decay), $C_{\text{p}} = 2A_p - 10\ln 2 + \frac{367}{90}$, and D_{p} is, as yet, unknown. The numerical contributions of the various parts are detailed in Table 3. The total result for the p-Ps decay

Table 3
Theoretical results for the contributions to the p-Ps $\to 2\gamma$ decay rate. The first column gives the order in α of the contribution, including powers of π that typically accompany that order, relative to the lowest order rate $\Gamma_{\text{p-Ps},0}$. The second column gives the coefficient of the corresponding power of α relative to $\Gamma_{\text{p-Ps},0}$, and the third column (the product of the first two columns times $\Gamma_{\text{p-Ps},0}$) gives the numerical value of the corresponding contribution in $(\text{ns})^{-1}$.

Order	Coefficient	Contribution $(\text{ns})^{-1}$
1	1	8.032 502 928
$\frac{\alpha}{\pi}$	$A_\text{p} = -2.532\,598\,900$	−0.047 253 367
$\alpha^2 \ln(1/\alpha)$	2	0.004 209 186
$\left(\frac{\alpha}{\pi}\right)^2$	$B_\text{p} = 5.3986(33)$	0.000 233 97(14)
$\frac{\alpha^3}{\pi} \ln^2(1/\alpha)$	−1.5	−0.000 036 080
$\frac{\alpha^3}{\pi} \ln(1/\alpha)$	$C_\text{p} = -7.918\,892$	−0.000 038 712
$\left(\frac{\alpha}{\pi}\right)^3$	D_p	0.000 000 10 D_p

rate is

$$\Gamma_{\text{p-Ps}} = 7.989\,618(18)\,(\text{ns})^{-1}. \tag{25}$$

Uncertainties include $0.000\,0014\,(\text{ns})^{-1}$ from the 0.0033 uncertainty in B_p and $1.0 \times 10^{-7} D_\text{p}\,(\text{ns})^{-1}$ from the unknown value of D_p. We choose to estimate an uncertainty in Γ_p equal to half the contribution of the leading α^3 logarithmic term as we did for the transition energies. This corresponds to a sizeable value $D_p \sim 180$ of the α^3 correction, but one not out of line with the known large ultrasoft $O(\alpha^3)$ correction to the hfs.

The decay rate for orthopostronium is more complicated to evaluate than that for parapositronium for two reasons. First, the three-photon final state has a non-trivial phase-space in that the photon energies and relative directions are not determined but must be integrated over. Second, there are simply more diagrams to deal with for o-Ps due to the extra photon in the final state. The lowest order rate was obtained in 1949 by Ore and Powell [8]:

$$\Gamma_{\text{o-Ps},0} = \frac{2}{9\pi}(\pi^2 - 9) m_e \alpha^6 = 7.2112\ (\mu\text{s})^{-1}. \tag{26}$$

Measurement of the rate through the early 1970s gave a result somewhat higher. By 1974 the agreement had improved with the completion of the one-loop corrections by Stroscio and Holt [180,181]. New experiments, done in powder or in vacuum instead of in gas, gave results well below the previous experiments and theory. A new calculation [182] uncovered a mistake in a part of the "ladder" graph that led to a significant change in the final result: $\Gamma = \left\{1 - 10.348(70)\alpha/\pi\right\}\Gamma_{\text{o-Ps},0}$ instead of $\Gamma = \left\{1 + 1.8(6)\right\}\Gamma_{\text{o-Ps},0}$. Shortly thereafter, in 1979, the $O(\alpha^2 \ln \alpha)$ correction was obtained as well [95]. A re-calculation of the one-loop correction confirmed the new result [183], and some of the one-loop diagrams succumbed to analytic evaluation [184–186]. However, most of the one-loop graphs were too complicated to be done by traditional integration methods. New rounds of experiments, done in gas as well as powder or vacuum, were consistent with the revised theoretical results.

The $O(\alpha^2 \ln \alpha)$ correction was obtained in 1979 by Caswell and Lepage [95] and confirmed by Khriplovich and Yelkhovsky [164]. They found the value $\delta\Gamma_{\text{o-Ps}} = \frac{1}{3}\alpha^2 \ln \alpha$.

As experimental precision continued to improve, it became clear by the late 1990s that there was an "orthopositronium lifetime puzzle"—the highest-precision experimental results were clustered about 6–9 experimental standard deviations above the theoretical prediction [187–189]. A value of about 250 ± 40 for the coefficient B_o of the expansion for the o-Ps decay rate

$$\Gamma_{\text{o-Ps}} = \Gamma_{\text{o-Ps},0}\left\{1 + A_\text{o}\frac{\alpha}{\pi} - \frac{\alpha^2}{3}L + B_\text{o}\left(\frac{\alpha}{\pi}\right)^2 - \frac{3\alpha^3}{2\pi}L^2 + C_\text{o}\frac{\alpha^3}{\pi}L + D_\text{o}\left(\frac{\alpha}{\pi}\right)^3\right\} \tag{27}$$

would be required to bring theory and experiment into accord, which was thought by most to be unlikely. Work on the calculation of B_o commenced in 1983 with the evaluation of the rate for five-photon decay, which has the same order as two-loop corrections to three-photon decay. The o-Ps $\to 5\gamma$ contribution to B_o is small, $B_\text{o}(5\gamma) = 0.187(11)$ [173,174]. A number of gauge-invariant sets of contributions to $B_\text{o}(3\gamma)$ were obtained in the 1990s. The contribution from squaring the one-loop decay amplitudes was found to be $\delta B_\text{o} = 28.860(2)$ [190,191]. Corrections involving vacuum polarization were small: $\delta B_\text{o} = 0.964960(4)$ [192,193]. Radiative corrections to the electron loop in the o-Ps $\to 1\gamma \to e^+e^- \to 3\gamma$ diagrams gave a contribution $\delta B_\text{o} = 9.0074(9)$ [194,195]; this somewhat large coefficient is reduced when the ladder photon exchange is enhanced to include the exchange of any number of ladder photons [196]. The contribution from the light-by-light scattering of two final-state photons gives $\delta B_\text{o} = 0.350(4)$ [197]. The full result for B_o was obtained by Adkins, Fell, and Sapirstein in 2000: $B_\text{o} = 45.06(26)$ [198,199].

By this time the $O(\alpha^3 \ln^2 \alpha)$ contribution was already known, having been calculated by Karshenboim in 1993 [134]. Furthermore, the $O(\alpha^3 \ln \alpha)$ contribution was obtained in 2000 by three groups: Hill [200], Kniehl and Penin [170],

Table 4
Theoretical results for the contributions to the o-Ps $\to 3\gamma$ decay rate. The first column gives the order in α of the contribution, including powers of π that typically accompany that order, relative to the lowest order rate $\Gamma_{\text{o-Ps},0}$. The second column gives the coefficient of the corresponding power of α relative to $\Gamma_{\text{o-Ps},0}$, and the third column (the product of the first two columns times $\Gamma_{\text{o-Ps},0}$) gives the numerical value of the corresponding contribution in $(\mu s)^{-1}$.

Order	Coefficient	Contribution $(\mu s)^{-1}$
1	1	7.211 167 117
$\frac{\alpha}{\pi}$	$A_o = -10.286\,614\,809$	−0.172 303 260
$\alpha^2 \ln(1/\alpha)$	$-\frac{1}{3}$	−0.000 629 798
$\left(\frac{\alpha}{\pi}\right)^2$	$B_o = 45.06(26)$	0.001 753(10)
$\frac{\alpha^3}{\pi} \ln^2(1/\alpha)$	−1.5	−0.000 032 390
$\frac{\alpha^3}{\pi} \ln(1/\alpha)$	$C_o = -5.517\,027$	0.000 024 213
$\left(\frac{\alpha}{\pi}\right)^3$	D_o	0.000 000 090

and Melnikov and Yelkhovsky [201]: $C_o = -\frac{A_o}{3} - 8\ln 2 + \frac{229}{30}$. Neither the result for B_0 nor the $O(\alpha^3)$ logarithmic contributions provided an explanation for the orthopositronium lifetime puzzle, which was only resolved with the advent of new measurements and an improved understanding of systematic errors related to interaction with surrounding matter [202–204], as discussed in Section 3.4.2.

A new approach led to the analytic evaluation of the $O(\alpha)$ and $O(\alpha^2 \ln \alpha)$ lifetime corrections. It was found that the decay amplitude could be expressed in terms of three invariant functions that could be obtained analytically [191,205]. This development led to a much improved numerical result for the $O(\alpha)$ correction A_o. Evaluation of the remaining phase space integration then enabled Kniehl and Veretin to find analytic results for A_o and also C_o [206]. Their result for A_o is somewhat lengthy, consisting of 35 terms containing products of logarithms, zeta functions, polylogarithms, and generalized polylogarithms, but their analytic results can be evaluated to any desired precision. The values of A_o and C_o were found to be

$$A_o = -10.286\,614\,808\,628\ldots, \tag{28}$$

$$C_o = -5.517\,027\,491\,729\ldots. \tag{29}$$

Exotic decays of o-Ps allowed by the standard model but not by QED are also possible. These include non-photonic decays o-Ps $\to \nu\bar{\nu}$ [15,158], decays involving a single photon o-Ps $\to \nu\bar{\nu}\gamma$ [71], and four-photon decays o-Ps $\to 4\gamma$ [71]. All of the branching ratios for these processes involve the weak coupling constant and are much too small to be observed.

The complete result for the o-Ps decay rate is given in Eq. (27) and Table 4, with the pure $O(\alpha^3)$ correction D_o still uncalculated. The numerical result for the o-Ps decay rate is

$$\Gamma_{\text{o-Ps}} = 7.039\,979(19)\ (\mu s)^{-1}. \tag{30}$$

The uncertainty is a combination of $0.000\,010\ (\mu s)^{-1}$ from the 0.026 uncertainty in B_o and $0.000\,016\,(\mu s)^{-1}$ (half the contribution of the leading $O(\alpha^3)$ logarithmic term) to account for the unknown value of D_o.

2.2. Bound-state QED

2.2.1. General formalism: comparison with hydrogen

The theoretical description of weakly-bound Coulombic bound systems starts with the non-relativistic Schrödinger equation

$$\left\{\frac{p^2}{2m_r} + V(r)\right\}\psi = E\psi, \tag{31}$$

where $V(r) = -\frac{Z\alpha}{r}$ is the Coulomb potential, Z is the charge (in units of the electron charge magnitude e) of the positive constituent, and the reduced mass $m_r = (1/m_1 + 1/m_2)^{-1}$ is defined in terms of the masses m_1 and m_2 of the bound state constituents. Explicit solutions for the wavefunctions in terms of associated Laguerre functions and spherical harmonics can be found in most textbooks on quantum mechanics. The associated Bohr energy levels depend on the principal quantum number n only:

$$E_B = -\frac{m_r(Z\alpha)^2}{2n^2}. \tag{32}$$

Systems described in this way include hydrogen, hydrogen-like (*i.e.* one-electron) ions with $Z\alpha \ll 1$, muonium, positronium, etc. Nuclear recoil at this order is taken care of exactly by the introduction of the reduced mass. There are three important scales associated with these systems: the "hard" scale set by the electron mass $m_e c^2$, the "soft" scale

given by the typical size of the relative momentum $\langle p\rangle = m_r Z\alpha/n$, and the "ultra-soft" scale determined by the binding energy $|E_B|$. The binding is "weak" in the sense that the binding energy is much smaller than the electron rest energy and the typical momentum is much smaller than m_r. At this order of description, the spectra of hydrogen and positronium are identical except that the reduced mass $m_e/2$ for positronium, and hence the energies, are approximately half as large as those of hydrogen. The transition wavelengths are approximately twice the size of the corresponding ones for hydrogen.

The next level of description, appropriate for hydrogen and other systems where recoil can be neglected, is provided by the Dirac equation [207]

$$\left\{\vec{\alpha}\cdot\vec{p}+\beta m_e + V(r)\right\}\psi = E\psi, \tag{33}$$

where again $V(r)$ is the Coulomb potential and $\vec{\alpha}$ and β are related to the usual Dirac gamma matrices according to $\beta = \gamma^0$ and $\vec{\alpha} = \beta\vec{\gamma}$, with $\{\gamma^\mu, \gamma^\nu\} = 2g^{\mu\nu}$. The Dirac equation builds relativity and spin into the description of the electron. Recoil cannot be incorporated into the Dirac equation as is possible in the nonrelativistic case—the potential is that of a fixed external field and m_e is the electron, not the reduced, mass. Consequently, the Dirac equation is only appropriate for situations where the mass ratio of the electron to the nuclear mass is small. On the other hand, relativity is included, so the Dirac descriptions works even when $Z\alpha$ is not small. The Dirac equation for the Coulomb problem was solved for energies and wave functions shortly after its invention [10,208]. The energies are given by

$$E = m_e\left[1+\left(\frac{Z\alpha}{n-(j+1/2)+\sqrt{(j+1/2)^2-(Z\alpha)^2}}\right)^2\right]^{-1/2}, \tag{34}$$

The energy levels of the Dirac–Coulomb system depend on both the principal quantum number n and the total (orbital plus electron spin) angular momentum j. When $Z\alpha$ is small, the Dirac energy levels can be expanded as

$$E = m_e\left\{1-\frac{(Z\alpha)^2}{2n^2}-\frac{(Z\alpha)^4}{2n^3}\left(\frac{1}{j+1/2}-\frac{3}{4n}\right)+O((Z\alpha)^6)\right\}. \tag{35}$$

These energies through terms of $O((Z\alpha)^4)$ provide a good approximation for systems having weak coupling and a small mass ratio (*e.g.* $m_e/m_p \sim 1/1836 \ll 1$ for hydrogen). The Dirac energies do not differentiate between states having differing values of ℓ but the same j, so they predict the degeneracy of states such as $2^2S_{1/2}$ and $2^2P_{1/2}$ for hydrogen-like systems, a degeneracy broken at order $\alpha(Z\alpha)^4\ln(Z\alpha)$ as the "Lamb shift". Also, the Dirac equation does not account for nuclear spin, so, for example, the ground state $1^2S_{1/2}$ splits when nuclear spin is taken into account by an amount $\propto (Z\alpha)^4(m_e/m_p)$ for hydrogen, giving the ground state hyperfine splitting.

While the Dirac–Coulomb problem is completely solved with exact solutions for energy levels and wave function, it is useful for the development of physical understanding to transform the intrinsically relativistic Dirac Hamiltonian $\beta m_e + \vec{\alpha}\cdot\vec{p} + V(r)$ to a form more amenable to physical interpretation. This can be achieved either by an analysis of the "large" and "small" components of the Dirac wave function, with the elimination of the latter (preserving normalization), or systematically through the Foldy–Wouthuysen transformation [209]. The result of either approach is a bound state equation for two-component Pauli wave functions with Hamiltonian

$$H = \frac{p^2}{2m_e} + V - \frac{p^4}{8m_e^3} + \frac{Z\alpha}{2m_e^2}\frac{\vec{L}\cdot\vec{S}}{r^3} + \frac{\pi Z\alpha}{2m_e^2}\delta^3(\vec{x}) + \cdots. \tag{36}$$

The three new terms represent the relativistic correction to kinetic energy $\sqrt{p^2+m_e^2}-m_e-\frac{p^2}{2m_e} = -\frac{p^4}{8m_e^3}+\cdots$, the "spin–orbit" interaction between the electron's spin and the magnetic field induced by its orbital motion, and the "Darwin term", which can be interpreted as electron "zitterbewegung"—electron coordinate fluctuation of order of the Compton radius that lets it see a smeared out potential. Together, these three perturbations taken at first order reproduce the $O(m_e(Z\alpha)^4)$ term of (35).

The fixed-source approximation used in the Dirac equation must be relaxed in order to understand the hydrogen spectrum in greater detail. For systems like positronium, the dynamical nature of both constituents is central to their description. A dynamic nucleus produces a current that allows it to emit and absorb transverse photons. Taking recoil corrections into account along with the exchange of a single transverse photon, several new terms come into the Hamiltonian. Also, at least for particle–antiparticle bound systems such as positronium, the effect of virtual annihilation must be included as well.

A two-body relativistic equation that includes the effect of transverse photon exchange was proposed by Breit [210]. The Breit equation is

$$\left(P^0 - H_1 - H_2\right)\psi_{nk}(\vec{r}) = \left(-\frac{Z\alpha}{r}+H_B\right)\psi_{nk}(\vec{r}) \tag{37}$$

where P^0 is the total CM energy (including rest masses), $H_1 = \beta_1 m_1 + \vec{\alpha}_1\cdot\vec{p}$, $H_2 = \beta_2 m_2 - \vec{\alpha}_2\cdot\vec{p}$, the subscripts "1" and "2" refer to the two particles, $\vec{r} = \vec{r}_1 - \vec{r}_2$, $\vec{p} = -i\vec{\nabla}$, β_i and $\vec{\alpha}_i$ are the usual Dirac matrices acting on the indices of particle

i, and H_B is the Breit interaction

$$H_B = \frac{Z\alpha}{2}\left(\frac{\vec{\alpha}_1\cdot\vec{\alpha}_2}{r} + \frac{\vec{\alpha}_1\cdot\vec{r}\,\vec{\alpha}_2\cdot\vec{r}}{r^3}\right) \tag{38}$$

The Breit Hamiltonian is a 16×16 dimensional matrix operator acting on 16 component states (four for each of the two particles). The "Breit interaction" H_B was obtained from the expansion of the classical electromagnetic interaction between two particles to order $1/c^2$ [211]:

$$\delta H_{\rm int} = -\frac{q_1 q_2}{2m_1 m_2 c^2}\left(\frac{\vec{p}_1\cdot\vec{p}_2}{r} + \frac{\vec{p}_1\cdot\vec{r}\,\vec{p}_2\cdot\vec{r}}{r^3}\right) \tag{39}$$

with the substitution $\vec{p}_i \to m_i\dot{\vec{r}} \to m_i\vec{\alpha}_i$. The Breit equation cannot be interpreted as an exact (if incomplete) equation for the 16-component two-particle wave function Ψ with energy eigenvalue P^0 as a two-body extension of the Dirac–Coulomb equation (33). Analysis by elimination of the large–small, small–large, and small–small components of Ψ in favor of the large–large component [210], or by a generalized Foldy–Wouthuysen procedure [212,213], leads to a spurious term (coming from the small–small component) that is not in accord with experimental results for helium fine structure [214]. Problems with the Breit equation have been discussed in [213,215–217] and elsewhere. One issue is the fact that if the Breit operator is used in second order perturbation theory, contributions from negative energy intermediate states are obtained of an anomalously large order. It was shown that use of the Breit interaction should be restricted to first order perturbation theory.

The Breit interaction can be interpreted as an effective potential due to exchange of a transverse photon [217, Sec. 38]. The scattering of nonrelativistic spin-1/2 particles due to exchange of a single Coulomb or transverse photon is described by the following Hamiltonian [67,74,77,217]

$$\begin{aligned} H = {}& \frac{p^2}{2m_r} - \frac{Z\alpha}{r} - \frac{p^4}{8}\left(\frac{1}{m_1^3}+\frac{1}{m_2^3}\right) \\ & + \frac{Z\alpha}{2r^3}\left(\frac{\vec{L}\cdot\vec{S}_1}{m_1^2}+\frac{\vec{L}\cdot\vec{S}_2}{m_2^2}\right) + \frac{\pi Z\alpha}{2}\left(\frac{1}{m_1^2}+\frac{1}{m_2^2}\right)\delta^3(\vec{r}) \\ & - \frac{Z\alpha}{2m_1m_2r}\left(\delta_{ab}+\hat{r}_a\hat{r}_b\right)p_a p_b + \frac{Z\alpha}{m_1m_2}\frac{\vec{L}\cdot\vec{S}}{r^3} \\ & + \frac{8\pi Z\alpha}{3m_1m_2}\vec{S}_1\cdot\vec{S}_2\delta^3(\vec{r}) + \frac{Z\alpha}{m_1m_2r^3}\left(3\hat{r}_a\hat{r}_b-\delta_{ab}\right)S_{1a}S_{2b}, \end{aligned} \tag{40}$$

which includes the usual non-relativistic kinetic energy (with reduced mass) and potential terms plus the kinetic energy correction, some spin–orbit terms, the Darwin terms, the magnetic interaction, another spin–orbit contribution, and the spin–spin interactions. The last four terms come from the Breit interaction and can be interpreted as due to the exchange of a single transverse photon. These terms are sufficient to give all corrections through $O(m_e\alpha^4)$ for two-fermion atoms (but not including the effects of virtual annihilation that contribute in particle–antiparticle bound systems such as positronium, or sizeable values of $g-2$ as for a proton).

For positronium, there is one additional contribution at $O(m_e\alpha^4)$ coming from virtual annihilation of the electron and positron into a photon, followed by the reformation of positronium. The effective potential for this process is found from the QED scattering amplitude by an identification of the three-dimensional potential that would bring about this effect. The annihilation potential is

$$H_A = \frac{2\pi\alpha}{m_e^2}\delta_{s=1}\delta^3(\vec{r}), \tag{41}$$

where the Kronecker delta $\delta_{s=1}$, which vanishes unless the total spin is one, is present due to the charge conjugation selection rule.

With the Hamiltonian in hand, it is now just a matter of some angular momentum algebra and finding some expectation values from non-relativistic quantum mechanics to obtain the energy levels of a two-body system with the complete mass dependence, at least through order $(Z\alpha)^4$ [213,218,219]. For example, the $\vec{S}_1\cdot\vec{S}_2$ term gives the ground state hyperfine splitting of hydrogen:

$$\Delta H_{\rm hfs} = \frac{8m_r^3\gamma_p\alpha^4}{3m_em_p} \approx 1420\,{\rm MHz} \tag{42}$$

(where m_p is the proton mass), which is the 21 cm line so useful in astrophysics. Since the proton is not an elementary fermion, we had to supplement the proton spin factor to account for the proton magnetic moment by including the factor $\gamma_p = 2.7928$. The degeneracy over ℓ for states having the same value of j is broken by a contribution

$$\Delta E = \frac{m_r(Z\alpha)^4m_e^2}{2n^3(m_e+m_p)^2}\left[\frac{1}{j+1/2}-\frac{1}{\ell+1/2}\right], \tag{43}$$

This term contributes to the Lamb shift, but because of the small size of m_e/m_p, its contribution is small compared to the Lamb shift effect coming from the bound electron self-energy even though the Lamb shift has an extra power of α. The situation in positronium is more straightforward since both constituents are elementary. The corrections to the energy levels of positronium through $O(\alpha^4)$ can be found from (40) and (41) by first order perturbation theory and are given in Eq. (4). These corrections were first worked out in [68,75], then by Ferrell who made some corrections [76,77]. They are now textbook material [220,221]. (In Ferrell's journal article he is missing a factor of 7/12 in one term. Itzykson and Zuber write $1-2\delta_{\ell 0}$ instead of the correct $\delta_{\ell\neq 0}=1-\delta_{\ell 0}$.)

We can already see the consequences of the three major differences between positronium and hydrogen, which are (1) the different mass ratio, (2) the fact that the proton has structure, and (3) the fact that positronium is built from a particle and its antiparticle, so virtual and real annihilation are allowed. The mass ratio $m_e/m_p\approx 1/1836$ for hydrogen is quite small, so to first order all $1/m_p$ and $1/m_p^2$ terms in the effective Hamiltonian can be neglected. This approximation leads to a simpler Hamiltonian with less structure—and more degeneracy. In positronium the mass ratio is one and the full Hamiltonian comes into play. There is no degeneracy at $O(\alpha^4)$ for positronium. Since the proton magnetic moment is proportional to $1/m_p$, the proton spin is irrelevant at $O(\alpha^4)$ for hydrogen. One consequence is that the usual angular momentum coupling scheme for positronium and hydrogen are different: for positronium the spins are coupled first to give the total spin $\vec{S}_1+\vec{S}_2=\vec{S}$, which is then coupled to orbital angular momentum to give the total angular momentum $\vec{S}+\vec{L}=\vec{J}$. In hydrogen, the electron orbital angular momentum and spin are first coupled as $\vec{L}+\vec{S}_e=\vec{J}$, which is then coupled to the proton spin as $\vec{J}+\vec{S}_p=\vec{I}$. For hydrogen or other systems where one or both constituents are not fundamental, phenomenological parameters reflecting the size and composition of the constituents must be inserted into the theoretical description. For hydrogen, these parameters include the proton magnetic moment and other size-related parameters. Because positronium is formed from a particle and its antiparticle, its states can be taken to be eigenstates of charge conjugation (C) as well as parity (P). The conservation of P and C in QED leads to a number of selection rules for transitions in positronium. Crucially, real and virtual decays to photons are constrained to satisfy Eq. (2): $(-1)^{\ell+s}=(-1)^{n_\gamma}$, where ℓ represents orbital angular momentum, s the total positronium spin, and n_γ the number of photons in the final (or intermediate) state.

2.2.2. Bethe–Salpeter approach and generalizations

The Bethe–Salpeter equation allows for the systematic evaluation of bound state energies that includes corrections due to multi-photon processes. The Bethe–Salpeter equation was proposed in 1951 [12,222]. Essentially equivalent equations were developed at about the same time by several authors [223–225]. A quantum field theory (QFT) derivation of the Bethe–Salpeter equation was provided by Gell-Mann and Low [226]. In principle, the Bethe–Salpeter equation provides an exact description for Coulombic bound states such as positronium and muonium that are built from fundamental spin-1/2 particles. For systems involving composite constituents such as hydrogen, muonic hydrogen, deuterium, etc., various phenomenological aspects of that structure must be included in the analysis. For high precision work, it may be necessary to include weak interaction and additional strong interaction effects, depending on the system and the required precision.

At the heart of the Bethe–Salpeter approach is the two-to-two Green function

$$G(x_1,x_2;y_1,y_2)=\langle 0|T\psi_1(x_1)\psi_2(x_2)\bar{\psi}_1(y_1)\bar{\psi}_2(y_2)|0\rangle, \tag{44}$$

where ψ_1 and ψ_2 are the Heisenberg representation quantum fields for the two constituents, the electron and proton for example, $|0\rangle$ is the vacuum state, and T is the time ordering operation. The graphical expansion of G is shown in Fig. 2a. There are two crucial facts about the Green function G that allow us to extract the spectrum of two-body bound states. The first is that G contains poles at the energies of the two-body bound systems. The positions of these poles can be extracted from G, giving the bound state energies. The second crucial fact is that we can organize the infinite set of graphs contained in G in a way that allows us to extract the poles. The organization displayed in Fig. 2 is appropriate for scattering calculations, where only the simplest of these graphs make large contributions due to the smallness of the fine structure constant α and the fact that each photon in a graph contributes a factor of α to the value of that graph. Bound state poles are only produced when an infinite subset of graphs is summed, so a reorganization is required.

The Bethe–Salpeter equation can be written as

$$G=S+SKG, \tag{45}$$

where G is the two-to-two Green function discussed above, S is the product of two one-to-one Green functions for the two constituent particles, and K is the two-particle-irreducible "kernel" consisting of all diagrams of G that cannot be cut into two disjoint pieces by severing two of the fermion lines—one for each of the constituents. The kernel K does not include external fermion lines. The notation of (45) is quite condensed. Dirac indices for the fermions, including summations over indices in the products, are implicit. The space–time dependence is also implicit. It is useful to work in momentum space, and represent the center of mass momentum of the two fermions as P and the relative momentum as p, so the momentum of line 1 is $p_1=\xi_1 P+p$ and that of line 2 is $p_2=\xi_2 P-p$, where $\xi_i=m_i/(m_1+m_2)$. Translational invariance of the theory implies conservation of the center-of-mass momentum, which means that the Green functions and kernel contain

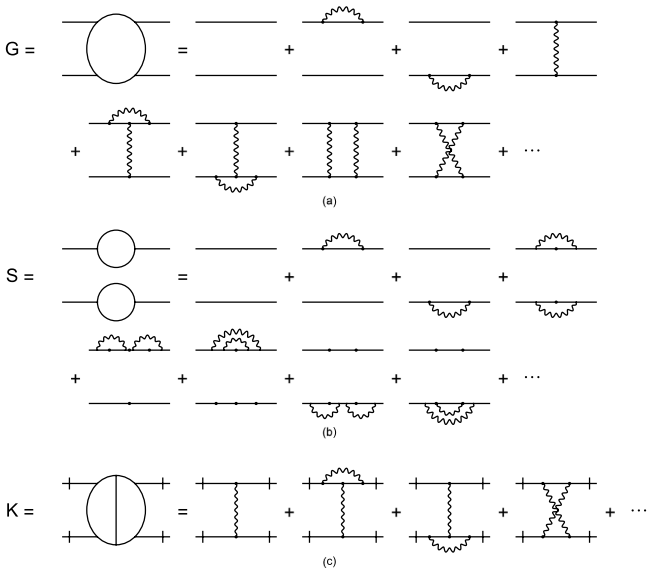

Fig. 2. Graphical representation of the elements of the Bethe–Salpeter equation. The two-to-two Green function G is shown in (a). Particle one (two) is shown at the top (bottom). Virtual photons are shown as wiggly lines. Part (b) shows the product S of two fully-corrected one-particle Green functions. The two-particle-irreducible kernel K is shown in (c). External fermion lines are not included in the kernel even though they are drawn in for clarity. Their absence is indicated by hash marks.

factors of $\delta^4(P-Q)$, which we factor out, and write $G(p_1,p_2;q_1,q_2)=(2\pi)^4\delta^4(P-Q)G(P;p,q)$, where the p momentum is for the final state and q for the initial state. A more explicit rendering of the Bethe–Salpeter equation is

$$G(P;p,q)=S(P;p,q) + S(P;p)\int\frac{d^4\ell}{(2\pi)^4}K(P;p,\ell)\,G(P;\ell,q), \tag{46}$$

where the non-interacting Green function can be written as $S(P;p,q)=(2\pi)^4\delta^4(p-q)S(P;p)$. (The delta function of relative momentum is present in S because there is no exchange of momentum between the two fermions.) The easiest "derivation" of the Bethe–Salpeter is to write out all graphs entering into the various terms of (46) and see that the graphs on the two sides of the equal sign are identical order by order in the fine structure constant.

The Bethe–Salpeter Eq. (46) is, to begin with, a function of the bare coupling and masses and contains the usual quantum field theory divergences. Renormalized quantities can be defined by

$$G=Z_{(1)}Z_{(2)}G_{\rm R},\quad S=Z_{(1)}Z_{(2)}S_{\rm R},\quad K=(Z_{(1)}Z_{(2)})^{-1}K_{\rm R}, \tag{47}$$

where $Z_{(1)}$ and $Z_{(2)}$ are wave function renormalization constants for the two fermions and $G_{\rm R}$, $S_{\rm R}$, $K_{\rm R}$ are finite functions of the renormalized coupling constant and masses. (There is a subtlety in the renormalization of K in the fermion–antifermion case having to do with the one-photon-annihilation kernel. The vacuum polarization diagrams needed to renormalize K are two-particle-reducible, so they are not present in K and only come in through the perturbative expansion, but they do come in as needed to cancel all divergences [227].) We will not address the details of renormalization or the one-photon subtlety in this work. Instead we will drop the R notation and assume that G, S, and K in (45) and (46) are already finite renormalized functions of the physical coupling and masses.

The two-body Green function contains all information about two-body bound states and two-body scattering, including bound state energy levels. The energies E_n of the various bound states appear as poles $1/(P^0-E_n)$ of the total energy P^0. The poles can be displayed by inserting the identity operator in the form of a complete set of states between $\psi_1(x_1)\psi_2(x_2)$ and $\bar\psi_1(y_1)\bar\psi_2(y_2)$ of (44). The contributions from the two-body bound states contain the poles [226,228]:

$$G(P;p,q)=i\sum_{n,k}\frac{\Psi_{nk}(\vec P;p)\bar\Psi_{nk}(\vec P;q)}{P^0-\sqrt{\vec P^{\,2}+M_n^2}+i\epsilon}+\cdots, \tag{48}$$

where the bound states are labeled by indices n and k, k being a degeneracy index. The bound state energy is the position of the pole in the center-of-mass frame ($\vec P\to 0$): $P^0\to M_n$ where the bound state mass M_n is otherwise known as its energy. The functions $\Psi_{nk}(\vec P;p)$ are the Bethe–Salpeter "wave functions". They are analogous in some ways to standard quantum mechanical wave functions, but their dependence on the relative energy of the constituents represents a fundamental

difference. The wave functions satisfy the homogeneous Bethe–Salpeter equation

$$\Psi_{nk}(\vec{P};p)=S(P;p)\int\frac{d^4\ell}{(2\pi)^4}K(P;p,\ell)\Psi_{nk}(\vec{P};\ell), \tag{49}$$

obtained from the inhomogeneous equation (46) by identifying the residues of the bound-state poles on the two sides of (46). The normalization of Bethe–Salpeter wave functions follows from their origin as residues of poles in the Green function G which satisfies an inhomogeneous equation [229,230].

One question that must be addressed in bound state QED is the choice of gauge. QED is a gauge invariant theory, and in principal any gauge can be chosen for calculations, but the difficulty of a calculation can be strongly affected by the choice of gauge. While a covariant gauge is often optimal for scattering calculations in perturbation theory, the Coulomb gauge facilitates bound state calculations. The Coulomb gauge propagator

$$D_{00}(k)=\frac{1}{\vec{k}^{\,2}},\quad D_{ij}(k)=\frac{1}{k^2+i\epsilon}\left(\delta_{ij}-\frac{k^ik^j}{\vec{k}^{\,2}}\right) \tag{50}$$

with $D_{0i}=D_{i0}=0$ contains exactly the (Fourier transformed) Coulomb potential as its time–time piece, and the exchange of a transverse photon as its space–space part. Covariant gauges lead to contributions at anomalously low orders that are only seen to cancel when an infinite number of diagrams is summed [216,231]. In a covariant gauge, calculation even of the $O(\alpha^4)$ correction is a significant challenge.

The Bethe–Salpeter equation is much too complicated to solve exactly, so some approximation scheme must be developed. The first such scheme was due to Salpeter [216], who, as a first approximation, deleted all self-energy corrections in S, leaving the uncorrected Dirac propagators $S(P;p)\to S_0(P;p)$ where

$$S_0(P;p)=\left[\frac{i}{\xi_1\not{P}+\not{p}-m_1+i\epsilon}\right]_1\left[\frac{i}{\xi_2\not{P}-\not{p}-m_2+i\epsilon}\right]_2 \tag{51}$$

with $\xi_i=m_i/(m_1+m_2)$. He also truncated the interaction kernel to single photon exchange $K(P;p,q)\to K_0(P;p,q)$ where

$$K_0(P;p,q)=-4\pi iZ\alpha\left\{\frac{\gamma_1^0\gamma_2^0}{\vec{k}^{\,2}}+\frac{\gamma_1^i\gamma_2^j}{-\vec{k}^{\,2}}\left(\delta_{ij}-\frac{k_ik_j}{\vec{k}^{\,2}}\right)\right\}, \tag{52}$$

where Ze is the charge of the positive particle, $k=p-q$, and retardation has been neglected for the transverse photon. (For positronium $Z=1$, but it is useful to display Z so the effects of exchanged photons (which involve Z) can be distinguished from those of radiative photons that affect only one of the fermions.) The approximate Bethe–Salpeter equation has the form

$$\begin{aligned}\left(P^0-H_1-H_2\right)\psi_{nk}(\vec{p})&=\left(\Lambda_{++}-\Lambda_{--}\right)\int\frac{d^3\ell}{(2\pi)^3}\\&\times\frac{4\pi Z\alpha}{(\vec{p}-\vec{\ell}\,)^2}\left\{-1+\alpha_1^i\alpha_2^j\left(\delta_{ij}-\frac{(p-\ell)_i(p-\ell)_j}{(\vec{p}-\vec{\ell}\,)^2}\right)\right\}\psi_{nk}(\vec{\ell}).\end{aligned} \tag{53}$$

Here Λ_{++} and Λ_{--} are projection operators onto the large-large and small–small subspaces that are most easily written in momentum space, so the whole equation has been given in that form. Dependence on the relative energy has been eliminated through integration: the three-dimensional wave function here is $\psi_{nk}(\vec{p})=\int\frac{dp_0}{2\pi}\Psi_{nk}(\vec{P}=0;p_0,\vec{p})$. The one-particle Dirac Hamiltonians H_1 and H_2 are the same as in the Breit equation (37), but now in momentum space. This equation is identical to the Breit equation except for the projection operators, but their presence makes it a viable bound state equation with a proper treatment of negative energy states. A two-particle Foldy–Wouthuysen treatment of this equation is possible and gives the effective Hamiltonian as shown in (40) and the same energy levels correct through $O(\alpha^4)$ [213].

Building upon the Salpeter equation with a Coulomb kernel, whose approximate solutions are just the nonrelativistic Coulomb wave functions, a perturbative expansion can be developed that is sufficient for the calculation of all corrections at $O(\alpha^5)$. This was done for the positronium hfs in [78] and the 2S, 2P fine structure in [81], and could be used to get all energy levels at $O(\alpha^5)$. This basic formalism was used to obtain a number of corrections at $O(\alpha^2\ln\alpha)$ and $O(\alpha^2)$: see [85,87,89,92,101] for a sample of these works.

Over time, new and better ways were developed for extracting information from the Bethe–Salpeter equation. Early treatments suffered from several disadvantages. One challenge is that the two-to-two Green's function $G(P;p,q)$ contains more information than required when one is only interested in bound state energies. Specifically, details about the behavior of $G(P;p,q)$ as a function of relative energy (or relative time) is not required. Also, the usual ladder approximation to the Bethe–Salpeter equation does not have the correct one-particle limit as $m_1/m_2\to 0$. In fact, an infinite number of graphs involving crossed photons is required in order to obtain the correct limit. Perhaps the main difficulty with the early methods was the lack of an exact solution to the lowest order problem. On top of the usual perturbations arising from higher order terms in the kernel, the wave function itself had to be iterated to obtain a sufficient approximation (see especially [94,232] for a discussion).

A new phase of work on the Bethe–Salpeter equation was initiated by the development of approximation schemes for which an exact solution exists for the lowest order problem and which have a well-defined scheme of perturbative corrections. All of the new approaches start off with the choice of a simplified two-particle propagator S_0 to replace the fully corrected and renormalized two-particle propagator S of (45). Usually a constraint is placed on the relative energy variable as well, setting the relative energy to zero or using it to put the heavy particle on-shell, resulting in a three-dimensional bound state equation. These approaches are discussed in [233–236]. Use of a modified two-particle propagator results in additional kernel contributions that usually give rise to useful cancellations. With the proper choice of a lowest-order kernel (one that includes at least the Coulomb interaction) the new approaches lead to exact solutions to the lowest order problem and a well-behaved perturbative expansion. Many of the modified equations have the correct one-particle limit and are good options for heavy-light bound systems. Early uses of the new approach for QED bound states are discussed in [93–95,105,107,227,237]. Formalisms built on exactly soluble lowest order equations were used to compute all positronium energy contributions at $O(\alpha^6 \ln \alpha)$ [93–96], as well as most of the pure $O(\alpha^6)$ corrections. About the time the last of these were being completed, traditional Bethe–Salpeter based methods were overtaken and for the most part superseded by the effective quantum field theory approach.

2.2.3. Effective field theories and NRQED

The use of effective interactions has a long history in atomic physics. As we have seen, the Breit interaction [210] describing the exchange of a transverse photon gives correct energy levels at a certain level of approximation, but is not appropriate as a kernel of a bound-state equation and cannot be iterated. More sophisticated effective potential methods have been used by [11,118,130,238,239], among others, to good effect. With the advent of self-consistent effective quantum mechanics and effective quantum field theories, these methods have found a secure home.

The most powerful methods for two-body Coulombic bound state calculations are based on non-relativistic QED (NRQED) [13,240–242] and its variants. The explicit relativistic invariance built into QED is essential for particle physics but leads to unnecessary complications when QED is applied to Coulombic bound states, which are characterized by energy scales small compared to $m_e c^2$. NRQED is obtained by removing the high energy states ($m_e c^2$ and above) from the theory by including a cut-off of some sort, which could be an explicit cut-off on momentum and energy integrals or something more subtle, such as dimensional regularization. The resulting low-energy theory can be tuned to facilitate calculations of low energy properties such as bound state energy levels. However, the high energy states do affect the nonrelativistic physics. In order to account for this, additional interactions are added to the low energy theory to mimic the effect of the high energy states removed by the cut-off. The added complication of working with a theory augmented by the additional terms is more than made up for by the fact that the nonrelativistic theory can be optimized for low-energy calculations. In NRQED, two-component Pauli spinors are used to describe fermions instead of relativistic Dirac spinors. Instead of a covariant gauge such as Feynman gauge for photon propagation, in NRQED the advantages of the use of Coulomb gauge are not offset by disadvantages since the theory is not covariant in any case.

As a quantum field theory, NRQED is defined by the field variables involved (electron, positron, and photon fields for positronium), the cut-off chosen, and the Lagrangian. The NRQED Lagrangian has the form

$$\begin{aligned}\mathcal{L} = \sum_i \psi_i^\dagger \Big\{ & iD_t + \frac{\vec{D}^{\,2}}{2m_i} + \frac{\vec{D}^{\,4}}{8m_i^3} + c_F^{(i)} \frac{q_i}{2m_i} \vec{\sigma}^{(i)} \cdot \vec{B} \\ & + c_D^{(i)} \frac{q_i}{4m_i^2} \vec{D} \cdot \vec{E} + c_S^{(i)} \frac{iq_i}{4m_i^2} \vec{\sigma}^{(i)} \cdot \vec{D} \times \vec{E} + \cdots \Big\} \psi_i \\ & - \frac{1}{4} F_{\mu\nu} F^{\mu\nu} + \cdots , \end{aligned} \tag{54}$$

where the ψ_i are the two-component fermion fields of mass m_i and charge q_i, the $\vec{\sigma}^{(i)}$ are the Pauli matrices (for the ith fermion), A^μ is the photon field, $\vec{B} = \vec{\nabla} \times \vec{A}$, $\vec{E} = -\vec{\nabla} A^0 - \partial \vec{A}/\partial t$, $F_{\mu\nu} = \partial_\mu A_\nu - \partial_\nu A_\mu$, and $D_\mu = \partial_\mu + iq_i A_\mu$ is the gauge covariant derivative. Compared with standard QED, there are many additional interaction terms in NRQED, but the ones that are present have a more immediate physical interpretation. In principle, all interactions are included compatible with the symmetries of QED in the non-relativistic limit: rotational invariance, parity and time reversal invariance, and gauge invariance. However, as we will see, there are counting rules that allow one to estimate the order in α of any particular term such that only a finite number of terms contribute at any given order. The terms shown are adequate for the calculation of the fine structure up to $O(\alpha^4)$ for a system such as muonium. (Details of the construction of the NRQED Lagrangian are described in [243,244].) If we expand one of these terms, the $\vec{D}^{\,2}$ term for example, we find $\vec{D}^2/(2m) = -\vec{p}^{\,2}/(2m) + (q/(2m))(\vec{p} \cdot \vec{A} + \vec{A} \cdot \vec{p}) - (q^2/(2m))\vec{A}^{\,2}$, from which we identify a contribution to the nonrelativistic fermion propagator $-\vec{p}^{\,2}/(2m)$, the coupling of the fermion to a transverse photon proportional to the particle's velocity, and a "seagull" vertex coupling the fermion to two photons at a point. The complete set of NRQED Feynman rules sufficient to give all $O(\alpha^5)$ energy corrections is shown in Fig. 3.

The NRQED Lagrangian density has the form of an expansion in inverse powers of the fermion masses. Dimensional consistency implies that each additional power of mass in the denominator must be compensated by extra field derivatives, which translate into factors of the particle's momentum or energy in the numerator. Since the expectation value $\langle p \rangle / m_i \propto \alpha$, terms with more mass factors in their denominators give smaller contributions to energy levels.

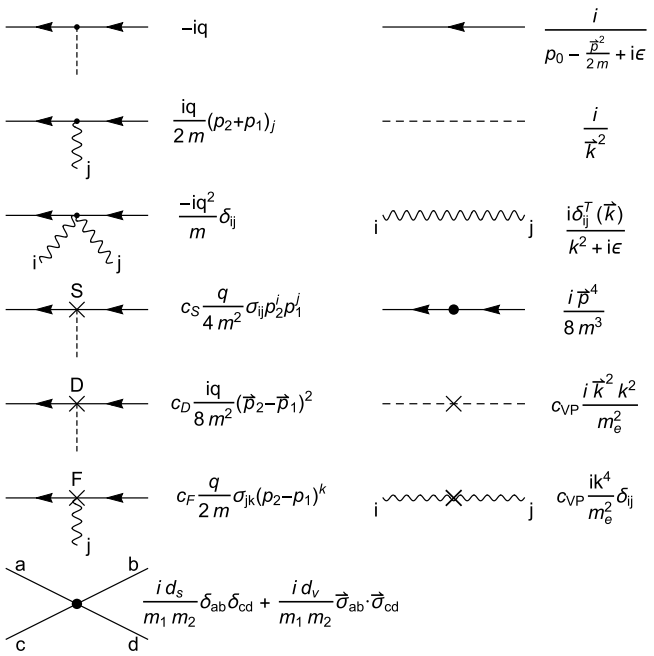

Fig. 3. The Feynman rules of NRQED. Solid lines represent the fermions (incoming momentum $\vec{p}_1$, outgoing momentum $\vec{p}_2$), dotted and wiggly lines represent Coulomb and transverse photons (momentum $\vec{k}$), q and m are the fermion charge and mass, and $\sigma_{ij} = \epsilon_{ijk}\sigma_k$ is a Pauli matrix. The transverse photon propagator contains the transverse delta function $\delta_{ij}^T(\vec{k}) = \delta_{ij} - \hat{k}^i\hat{k}^j$. The constants c_S, c_D, c_F are the spin–orbit, Darwin, and Fermi matching coefficients, c_{VP} is the vacuum polarization matching coefficient, and d_s and d_v are four-fermion contact term coefficients. (The rules shown here are sufficient for calculations at $O(\alpha^5)$. Additional vertices appear at higher orders.)

A perturbation theory can be developed for energy levels by analogy with the work done for the Bethe–Salpeter equation, except that now everything is simpler. In order to obtain our lowest order description, we choose the reference non-interacting two-to-two Green function to be the product of two non-relativistic fermion propagators

$$S_0(P;p) = \frac{i}{\xi_1 E + p_0 - \vec{p}^{\,2}/(2m_1) + i\epsilon}\,\frac{i}{\xi_2 E - p_0 - \vec{p}^{\,2}/(2m_2) + i\epsilon}, \tag{55}$$

(where $\xi_i = m_i/(m_1+m_2)$) and for the reference interaction we take simply the exchange of a single Coulomb photon

$$K_0(P;p,q) = -iV(\vec{p},\vec{q}), \quad V(\vec{p},\vec{q}) = \frac{-4\pi Z\alpha}{(\vec{p}-\vec{q})^2}. \tag{56}$$

The lowest-order homogeneous Bethe–Salpeter equation of NRQED takes the form

$$\psi_0(\vec{p}) = \frac{1}{E - \vec{p}^{\,2}/(2m_r)}\int\frac{d^3q}{(2\pi)^3}V(\vec{p},\vec{q})\psi_0(\vec{q}), \tag{57}$$

which is exactly the momentum space version of the standard Schrödinger–Coulomb equation. Contributions to the perturbation kernel $\delta K = K - K_0$ are shown in Fig. 4. NRQED has been used to reproduce all results for positronium energies at orders α^4 and α^5 (see Eqs. (4) and (7)) using the perturbations of Fig. 4. For the $O(\alpha^6)$ corrections we must take a number of additional kernels into account as well as the effects of second order perturbation theory. Results at $O(\alpha^6)$ are reported in Table 1 and the references given in Section 2.1.1. As a specific and distinctly non-trivial application of NRQED, we mention the calculation of Czarnecki, Melnikov, and Yelkhovsky of the positronium S state energy levels at order α^6 [25,126]. They used a dimensionally regularized version of NRQED to calculate all recoil and radiative recoil corrections at this order. At $O(\alpha^7)$ yet more kernels must be included in additional to further sub-leading contributions from kernels that contributed at lower orders. Furthermore, higher order corrections to the matching coefficients will be required, including four-photon annihilation, four-photon exchange, and light-by-light scattering contributions to the four-fermion matching coefficient of Fig. 4(k). Other contributions that have been studied include the two-loop Bethe log terms [140,141] and the numerically-important ultrasoft corrections [142]. References for the known corrections at $O(\alpha^7)$ are given in Section 2.1.1 but there are many that remain to be worked out.

Extensions of the effective field theory method have also been employed in positronium research. In NRQED, hard scale processes (with energies or momenta of order m_e) have been removed, leaving the soft (of order $m_e\alpha$) and ultrasoft (of order $m_e\alpha^2$) scales to be integrated over in the expectation values that give corrections to the energy levels. The

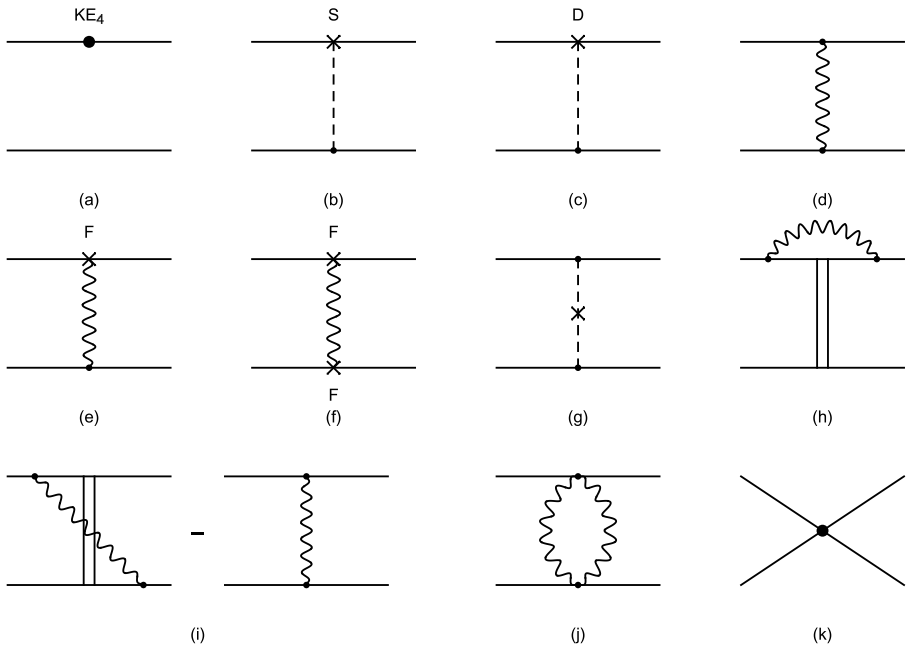

Fig. 4. Kernel perturbations that contribute to bound state energy levels at $O(\alpha^4)$ and $O(\alpha^5)$: (a) represents the relativistic correction to kinetic energy, (b) and (c) are the spin–orbit and Darwin corrections, (d) is the magnetic correction due to exchange of a transverse photon, (e) and (f) are the Fermi spin–orbit and spin–spin corrections, (g) is the vacuum polarization correction, (h) and (i) represent all diagrams having a transverse photon crossing any number of Coulomb ladder photons (the double line represents the nonrelativistic Coulomb Green's function—which is the sum of zero, one, etc. exchanged Coulomb photons in the ladder configuration. Graph (h) gives the traditional Lamb shift and (i) the "Salpeter term" [216]. Graph (j) is a "seagull" contribution, and (k) represents the contact potential that takes into account the effect of virtual annihilation and the hard contributions from multi-photon exchange.

presence of two scales in these integrals means that individual expectation values do not have a unique order in α but instead contain some lowest power of α plus a series of higher powers and logarithms. This complication can be removed by using instead a new effective field theory, called "potential NRQED" (pNRQED), in which the soft scale has been "integrated out", *i.e.* removed, from NRQED [14,84,245–247]. The effects of the soft scale processes are encoded in a number of additional interaction terms. When projected on the one-electron–one-positron subspace of the Fock space, the calculations of pNRQED can be done in a way that is similar to those of ordinary non-relativistic quantum mechanics where the interaction terms take the form of potentials. Matrix elements at the ultrasoft $m_e\alpha^2$ scale would not contain large logarithmic factors (such as $\ln\alpha$)—instead, the large logarithms are summed up using the renormalization group into the "Wilson" or "matching" coefficients that multiply the potential operators [248]. This, along with the fact that individual expectation values have unique orders in α, are advantages of the pNRQED version of the effective field theory approach. While pNRQED has been used to obtain all corrections to Ps energies at $O(m_e\alpha^5)$ [14], logarithmic corrections to the Ps hfs at $O(m_e\alpha^7\ln(1/\alpha))$ [137], and pure $O(m_e\alpha^7)$ corrections to the Ps hfs arising from one-photon-annihilation at $O(m_e\alpha^7)$ [143], it would be interesting to see a complete calculation of pure $O(m_e\alpha^6)$ energy level corrections done using pNRQED in order to assess the relative ease of pNRQED *vs.* traditional NRQED calculations.

Another extension of NRQED that has been used in positronium research is "velocity NRQED" (vNRQED) [246,249,250]. In vNRQED, separation of the effects of the low-energy scales is achieved by defining distinct fields to carry the soft and ultrasoft excitations. For example, the fermion field is written as a two-component spinor $\psi_{\vec{p}}(x)$ where $\vec{p}$ is a (discrete) soft momentum index and the continuous variable x is used to describe the ultrasoft fluctuations. The photon has a soft component $A^{\mu}_{\vec{q}}(x)$ and a separate field $A^{\mu}(x)$ to describe ultrasoft photons. Diagrams in vNRQED have well-defined orders because the scales were separated at the start by the definitions of the fields included in the theory. Two distinct regularization scales are introduced into the dimensionally regularized theory (instead of the usual one): μ_S for soft loops and μ_{US} for ultrasoft loops. For consistent power counting the scales must be correlated in terms of a "subtraction velocity" v according to $\mu_S = m_e v$ and $\mu_{US} = m_e v^2$. The "velocity renormalization group" is used to scale the matching coefficients of the theory from the matching scale $v = 1$ down to $v = \alpha$, which is a typical velocity of a bound state. Manohar and Stewart [155] used the velocity renormalization group to compute the logarithmic contributions to positronium energies at orders $m_e\alpha^7\ln^2(\alpha)$ and $m_e\alpha^8\ln^3(\alpha)$. Their results are consistent with other calculations and outline a systematic approach to the calculation of logarithmic contributions.

Due to the systematic treatment of logarithms and the fact that contributions from individual diagrams have unique orders in α, it seems to me likely that some version of NRQED with low-energy scales treated as in pNRQED or vNRQED

will become as important for positronium calculations as the analogous effective theories pNRQCD and vNRQCD are in the theory of heavy quark–antiquark physics [246,247,250,251].

2.3. Sensitivity to fundamental constants

The theoretical results for transitions energies of positronium all have the general form

$$\Delta E = \kappa m_e \alpha^r \left\{1 + f(\alpha)\right\} \tag{58}$$

where κ is a constant, $r \geq 2$, and $f(\alpha)$ is proportional to at least one power of α. Other constants, such as the muon mass and parameters of the strong and weak interactions, make negligible contributions. Decay rate predictions also have the same general form. Since the predictions depend on only two fundamental parameters, the comparison of any two measurements with theory would allow for the extraction of both m_e and α from purely positronium measurements. Unfortunately, measurements and the associated theory in positronium are generally not precise enough to compete with the best values of m_e and α, which are known to precisions of 0.30 ppb and 0.15 ppb, respectively [73]. Because all of the positronium results depend linearly on m_e, we can also express the predictions in terms of the Rydberg energy $R \equiv R_\infty = m_e\alpha^2/2$:

$$\Delta E = 2\kappa R \alpha^{r-2} \left\{1 + f(\alpha)\right\}. \tag{59}$$

and use the positronium measurements to extract values of R and α, from which a value for m_e can also be obtained. The 2018 CODATA value of the Rydberg has the amazingly small relative uncertainty 1.9 ppt [73].

The positronium transition with the best relative precision is $1^3S_1 - 2^3S_1$. The experimental precision is aided by the relatively small natural linewidths of the 1^3S_1 state (due to the relatively slow decay into three photons) and 2^3S_1 state (since it is metastable and cannot decay through single photon emission). The relative precision is strongly enhanced because the series in α for ΔE begins at $O(\alpha^2)$ rather than a higher power of α as is the case for the other measured transitions. Since $r = 2$ for this transition, the theoretical prediction simplifies to $\Delta E = 2\kappa R\{1 + f(\alpha)\}$. Because $f(\alpha) \approx -1.25\alpha^2 + O(\alpha^3 \ln(1/\alpha)) \ll 1$, the relative precision of R determined from a measurement of this transition is essentially the same as the relative precision of the comparison between experiment and theory. In this case, the measured [252] and calculated transition energies are

$$\Delta E_{\text{exp}} = 1\,233\,607\,216.4(3.2)\,\text{MHz}, \tag{60}$$

$$\Delta E_{\text{theor}} = 1\,233\,607\,222.12(58)\,\text{MHz}. \tag{61}$$

Since the actual difference between these two values is somewhat larger than the experimental uncertainty, we use the difference between them as the uncertainty for the comparison—this uncertainty amounts to 4.6 ppb. From the comparison we obtain a pure-positronium value for the Rydberg:

$$R_{\text{Ps}} = 3\,289\,841\,945(15)\,\text{MHz} \quad (4.6\,\text{ppb}). \tag{62}$$

(In this evaluation we used the 2018 CODATA value of α. The exact value for α used is not important since $1 + f(\alpha)$ is so close to one.) The positronium result for the Rydberg is within 1σ of the CODATA value.

There is a great deal of room for improvement in the $1^3S_1 - 2^3S_1$ measurement since the natural line-width of the $1^3S_1 - 2^3S_1$ triplet state transition is only 1.3 MHz. In the future, "one can expect an eventual measurement that splits the natural line width by a factor of 10^3" [49]. Such an experiment, of course, would be subject to numerous new systematic uncertainties, and theory would be hard-pressed to achieve the same level of precision. Work has already begun on a new set of experiments that should achieve uncertainties at the 0.10 MHz level [56,253]. The anticipated precision of theory, once the $O(\alpha^7)$ contributions are completed, is also at about this level, since the leading logarithmic contribution at $O(\alpha^8)$ is $21m\alpha^8L^3/(64\pi^2) \approx 0.004$ MHz [155], the next to leading term is of order $m_e\alpha^8L^2 \approx 0.024$ MHz (with an unknown coefficient), and $m_e\alpha^8 \approx 0.0010$ MHz. A successful comparison of experiment with theory for the $1^3S_1 - 2^3S_1$ transition at the 0.10 MHz level of precision would yield a pure-positronium Rydberg with a precision of ∼80 ppt.

It is interesting to compare the precision of the Rydberg obtainable through positronium measurements with the uncertainties in the Rydberg coming from discrepant values of the proton charge radius r_p. Consider the situation in the hydrogen atom. Given a hydrogen energy measurement and a value of the proton radius, by use of the theoretical formula for that energy one can deduce a value for the Rydberg. Because the value for the proton radius $r_p = 0.8751(61)$ fm coming from elastic electron–proton scattering and precision spectroscopy of normal (electronic) hydrogen [18] differs from the value $r_p = 0.84037(39)$ fm found by precision spectroscopy of muonic hydrogen [254], there is a "proton radius puzzle". The difference is significant, amounting to 5.7 σ (although more recent measurements in atomic hydrogen tend to lessen the discrepancy [255,256]). One can express the energy of the hydrogen state with quantum numbers n, ℓ, etc., as [2,82,235]

$$E(n, \ell, \ldots) = -\frac{R}{n^2} + \frac{2m_e^3\alpha^4}{3n^3} r_p^2\, \delta_{\ell=0} + \tilde{E}(n, \ell, \ldots), \tag{63}$$

where $-R/n^2$ is the leading Bohr term, the dependence on the proton radius r_p is displayed explicitly, and the remaining terms are combined into $\tilde{E}$. So, for $n = 1$ states, the uncertainty in energy $E(n, \ell, \ldots)$ due to an uncertainty δr_p in the value of the proton radius is given by

$$\delta E(n, \ell, \ldots) = \frac{8}{3} R m_e^2 \alpha^2 r_p \delta r_p. \tag{64}$$

Similarly, for $n = 1$ states, the uncertainty in energy due to an uncertainty in the Rydberg is $\delta E(n, \ell, \ldots) = \delta R$. The two types of uncertainty have the same effect on the energy when

$$\frac{\delta R}{R} = \frac{8}{3} \left(\frac{m_e c^2 \alpha}{\hbar c} \right)^2 r_p \, \delta r_p. \tag{65}$$

We have reinstated factors of $\hbar$ and c to make the numerical analysis more clear, and use $m_e c^2 = 0.5110\,\text{MeV}$, $\hbar c = 197.3$ MeV fm, $r_p = 0.84037\,\text{fm}$, and $\delta r_p = 0.034\,\text{fm}$. We see that the typical fractional uncertainty in the Rydberg due to the discrepant values for the proton radius is about $\delta R/R \sim 27 \times 10^{-12}$. This value is consistent with the conclusion that the revised proton radius from the muonic hydrogen experiment would imply a shift in the Rydberg of $-110\,\text{kHz}$, or a fractional amount -33×10^{-12} [20]. As discussed above, the positronium Rydberg that could be obtained from improved measurements and completion of the $O(\alpha^7)$ corrections has a fractional uncertainty of about 80×10^{-12}. A positronium result with this precision would give an indication of the correct value of the proton radius. Since the positronium Rydberg is based purely on QED with negligible or well understood strong and weak corrections, it would make a clean and independent contribution to the resolution of the proton radius puzzle. This would be especially true if the positronium precision could be further improved (beyond the amount considered above) by a factor of two or three through improved measurement and an understanding of the leading $O(\alpha^8)$ contributions.

Positronium measurements can also be used to constrain CPT violating differences between electron and positron charges and masses. The positronium Rydberg contains the positronium fine structure constant $\alpha_{\text{Ps}} = -4\pi q_{e^-} q_{e^+}$ and reduced mass $m_r = \frac{m_{e^-} m_{e^+}}{m_{e^-} + m_{e^+}}$. Small CPT-violating differences $\delta q = q_{e^+} + q_{e^-}$ and $\delta m = m_{e^+} - m_{e^-}$ lead to a change in the positronium Rydberg

$$\frac{\delta R}{R_{e^-}} = \frac{\delta m}{2 m_{e^-}} + 2 \frac{\delta q}{|q_{e^-}|}, \tag{66}$$

where R_{e^-} is the standard Rydberg $R_{e^-} = R_\infty = \frac{1}{2} m_{e^-} \alpha_{e^-}^2$. Possible simultaneous violations $\delta q \neq 0$, $\delta m \neq 0$ could be constrained by an independent measurement of the ratio of cyclotron frequencies $\frac{\omega_{e^+}}{\omega_{e^-}} = \frac{q_{e^+} B}{m_{e^+}} \left(\frac{|q_{e^-}| B}{m_{e^-}} \right)^{-1} = \frac{q_{e^+} m_{e^-}}{|q_{e^-}| m_{e^+}}$ [257]. If we for simplicity consider such violations independently, the positronium measurement of the Rydberg could constrain δq and δm according to $\frac{\delta m}{m_{e^-}} \approx 0$ at 9 ppb and $\frac{\delta q}{e} \approx 0$ at 2.3 ppb, with corresponding improvements expected when the new levels of precision for experiment and theory are obtained.

3. Experimental results

This section will briefly summarize the current experimental results for precision measurements of various Ps properties, where the definition of "precision" is subjective, and is in general simply the current state of the art. Certainly Ps spectroscopy experiments are much less precise than corresponding measurements using hydrogen or helium, and indeed are not yet comparable to the (estimated) precision of QED theory. Here the focus will be on the current results rather than an in-depth discussion of experimental techniques, although areas where systematic effects may impact results will be discussed, as well as possible modifications for future work that may allow for more precise measurements. We will, however, give some background description of the basic methods used to produce positron beams (Section 3.1.1) and briefly discuss some of the different ways in which Ps atoms may be produced (Section 3.1.2), since the resulting Ps properties strongly affect the way experiments have to be performed. The experimental methods used to perform different types of experiments are discussed in the relevant sections. This has been divided into optical (Section 3.3.1) measurements, ground state hyperfine (Section 3.3.2) and $n = 2$ fine structure (Section 3.3.3) microwave measurements. Decay rates (Section 3.4) and decay modes (Section 3.5) are discussed separately, although they employ some overlapping methodology.

3.1. Experimental methods

Ps was first produced in the laboratory by Martin Deutsch in 1951 [69]; in a series of ground-breaking experiments Deutsch and co-workers were able to demonstrate the existence of Ps, measure the triplet ground state annihilation lifetime [258] and the energy difference between the ground state singlet and triplet levels (i.e., the hyperfine structure [259,260]). This work was performed using Ps produced in a gas cell containing a β^+ emitting radioisotope (^{22}Na). Positrons emitted via beta-decay will have very high energies, ($\approx$200 keV on average for ^{22}Na), and must slow down to energies close to the 6.8 eV Ps binding energy before Ps atoms can be formed. If this takes place in a gas then the

density must be sufficiently high to ensure a reasonable fraction of the fast positrons will slow down, meaning that the created Ps is also likely to interact significantly with the source gas. This process is inefficient, and the resulting Ps is produced in a relatively large volume, and is not well-defined in terms of its velocity and angular distributions, making some measurements impossible; notable exceptions are the study of the Ps ground state hyperfine structure via microwave spectroscopy (Section 3.3.2 and early o-Ps lifetime measurements (Section 3.4).

As revolutionary as this approach was, the underlying technique is fundamentally limited, in that one has very little control over the properties of the produced Ps, and since the gas is necessary for Ps creation its effects must be taken into account in subsequent Ps–gas interactions [261,262]. The development of controlled positron beams [7] was a significant improvement in experimental capabilities, as was the development of positron traps [58] and new detection methods [263]. These advances opened the door for more efficient Ps production [264], the generation of intense (and high density) positron pulses [265], and the ability to observe changes in Ps decay rates using single-shot measurements (i.e., with multiple near-simultaneous events detected) [266].

3.1.1. Positron beams

The invention of slow positron beams in the early 1970s [267–269] made it possible to generate Ps atoms in a much more controlled manner than the gas cells used previously. The basic methodology of beam formation is that high energy (MeV scale) positrons (usually but not always emitted from a radioactive source) are thermalized in a solid material, known as a moderator, and then emitted with low energy (eV scale) to form a quasi mono-energetic beam. This can happen via several different processes involving work function or epithermal positron emission [270], but in general efficiencies, defined as the number of slow positrons in the final beam divided by the number of fast positrons emitted from the source, are low. Single crystal metals and insulating powders have been used with efficiencies on the order of 0.1% but the state of the art is the rare gas moderator, which can provide efficiencies up to $\approx$1% [271].

Most slow positron beams in use today are derived from the decay of ^{22}Na, which can be purchased in a capsule with activities up to 2 GBq. Thus, using neon moderators it is possible to generate a slow positron beam with up to 10^7 positrons/second (i.e., in the pA range), allowing for Ps atom sources to be generated with a few million atoms/second. This is not sufficient for various optical experiments in which the requirement of high laser power generally necessitates using ns pulsed lasers [57], which then require pulsed beams with a comparable pulse width. The obvious solution to this problem would be to employ a more intense positron beam. While this is possible, it is no easy task, and requires the use of large facilities. Some positron beams based on particle accelerators or reactors are in use, but they are not common. The most intense positron beam currently operational is generated via pair production following slow neutron capture in the pile of a nuclear reactor [272]; a previous world record holder used a high energy (120 MeV) electron Linac to generate positrons, also via pair production [273]. Despite the large scale of such facilities, they nevertheless have been limited to the production of positron beams with intensities of less than 10^{10} slow positrons per second (i.e., below 1 nA). In reality the available flux at such facilities may be far less than the maximum advertised [274].

A more practical (and cost-effective) approach is to employ a buffer gas positron trap [58,275,276] to convert a DC beam into a pulsed beam. Although this does not, of course, increase the total number of positrons available, it does make it possible to accumulate positrons and generate intense pulses [265]. These pulses can be used to generate a low-density Ps "gas" that can be probed with pulsed laser systems. The development of various trapping and non-neutral plasma manipulation techniques [58] has driven advances in Ps-laser physics over the last decade or so [57] and will continue to be important for the next generation precision measurements.

3.1.2. Ps production

Ps atoms may be produced following positron implantation into a wide variety of target materials, which are in this context sometimes referred to as Ps converters. For materials that rely on positrons diffusing to the surface (metals and semiconductors) the use of slow positron beams with controllable energies is essential [264]. Positrons rapidly thermalize when implanted at keV energies into solid bulk matter, usually within a few 10's of pico seconds [277]. Low energy positrons may then go on to form Ps via several distinct processes. For the present purposes it is not necessary to consider these mechanisms in great detail, since the end result is invariably that Ps atoms are generated with useful efficiencies (ranging from $\approx$10 to 100% [278]) and with energies ranging from 10's of meV to several eV. Ps production at low energies (which we arbitrarily define as energies below 10 meV), remains elusive, in part because the usual formation processes rely on the physical properties of various converters, which cannot be easily controlled. Some methods to generate cold Ps have been demonstrated, but are either too inefficient [279] or unreliable [280] for many applications. An efficient and robust source of low energy Ps atoms is urgently needed for future experiments in precision spectroscopy [57].

Different Ps formation processes occur according to the nature of the Ps converter:

- *Gas targets:* Positron production in gasses results in energetic Ps atoms since it generally occurs within a broad energy window known as the Ore gap [54]. This method was used extensively with β^+ sources in early experiments. With a slow positron beam as the positron source gas interactions may be used for the production of energetic (5–500 eV) positronium beams [281,282] which are used for measuring Ps scattering cross sections with atoms and molecules. Using this method it is possible to tune the positron beam energy to generate a significant fraction of excited state ($n = 2$) Ps atoms [283,284] with eV energies. This approach may be useful for Ps $n = 2$ microwave spectroscopy using separated oscillatory fields [285] generated by spatially separated waveguides.

- *Metals:* Ps cannot be produced inside metals because the Coulomb interaction between a positron and any particular electron is screened by the large number of free electrons present [286,287]. However, Ps formation may occur in the surface or near surface region, where the electron density is reduced. This can happen directly, or via an intermediate positron surface state, resulting in different energies and emission profiles in accordance with the energetics [278,288]. In the latter case Ps atoms are emitted through a thermal desorption process and so have (beam) Maxwell–Boltzmann distributions corresponding to the sample temperature required for activation (typically between 500–1000 K) [289]. In general only ground state atoms are produced in this way, however a small fraction of positrons that are not fully thermalized may have sufficient energy to form $n = 2$ Ps atoms via the direct formation process [290]. Although it is extremely inefficient (on the order of 0.1%), this process was successfully used in several measurements of the $n = 2$ Ps fine structure, as described in Section 3.3.3.
- *Semiconductors:* For many years Ps formation in semiconductors was thought to be essentially the same as it is in metals. This is a reasonable assumption since the observed Ps emission properties are similar [278], and Ps is again restricted to formation only in the near surface regions, for the same reasons as in metals. However, it has now been shown that other processes also occur, at least in the case of Si and Ge [291–295]. This was discovered when the energy of Ps was measured via Doppler broadening spectroscopy and found not to vary with the sample temperature, ruling out a thermal desorption process, even though the production efficiency followed an Arrhenius-type activation curve, which is very suggestive of a thermal desorption process, and rules out the direct Ps formation mechanism seen in metals (this process is largely insensitive to temperature). This observation was attributed to "excitonic" Ps emission, wherein the thermal profile was in fact due to the excitation of electrons to surface states that can subsequently form Ps atoms. This type of Ps emission typically occurs with energies of a few hundred meV, and shows no significant difference in the emission properties even for samples at cryogenic temperatures [296]. Thus, while it may be of value for low temperature applications, it does not seem to offer a route towards the formation of cold Ps atoms.
- *Insulators:* Since there are no free electrons in insulating materials Ps formation in the bulk material is possible [297]. If this occurs within a diffusion length of a surface Ps may then be emitted into vacuum, with an energy that depends on the Ps "work function", which is typically on the order of an eV (e.g., [298]). Ps formation in various oxide powders has been studied for many years [299,300]. As these materials often exist as powders with grain sizes on the nm scale Ps can be emitted from grains into inter-granular spaces, where collisions can occur, cooling the atoms to near thermal energies [301]. A similar process can take place in mesoporous insulating materials, such as silica [302–305], allowing for useful Ps production materials. The model of energetic Ps emission followed by collisional cooling [306] has been assumed to apply in a general sense (e.g., [307]), and does indeed seem to be the case for Ps emitted from mesoporous silica films, as evidenced by a dependence of the Ps energy on the positron implantation depth [308,309]. However, recent experiments using MgO powder have shown that this is not always true, and that additional Ps formation mechanisms can be supported [310]. Using reflection and transmission geometries it was shown that Ps was emitted from MgO smoke powder with a fixed energy of $\approx$ 350 meV, regardless of the positron implantation depth. This was attributed to surface Ps formation at this energy, with minimal subsequent energy loss while passing through the internal MgO spaces. As with the excitonic emission observed from Si and Ge, this new process, while potentially useful for specific applications (in this case, long range Ps atom transfer from the formation site), does not appear to be suitable for producing cold Ps. It may be the case that powder samples with a smaller and more uniform crystal size distribution would support efficient collisional cooling to lower temperatures.
- *Special materials:* Some complex materials have particular properties arising by virtue of their structures, which can have a significant impact on Ps formation. Mesoporous films also fit into this category since the cooling of Ps can be affected by the structure, and if they were to be engineered with particular patterns or void structures one could envisage better cooling or controlled emission as a result. Another prominent example is Metal Organic Framework (MOF) materials, which actually comprise a large number of different compounds (e.g., [311]). The periodic structures of some MOF crystals allow Ps to exist as a delocalized (Bloch) wave [312,313], which allows Ps atoms to be emitted into vacuum with much lower energy spreads (but not necessarily lower energies) than are typically observed using other materials [314]. This is potentially useful for many experiments where broad velocity distributions lead to difficulties (e.g., Rydberg deceleration [315]). The production of suitable macroscopic single crystals remains to be demonstrated, however, and it is not yet clear if these or similar materials can be utilized to obtain useful Ps sources.

The choice of Ps converter may in practice be dictated by experimental conditions. For example, if one requires operation in a cryogenic environment then surface-based formation processes may be compromised, unless the vacuum is under good control. Similarly, porous materials may absorb a lot of gas and become low efficiency converters unless they can be cooled down under ultra high vacuum conditions [296]. Most metal and semiconductor Ps converters require atomically clean surfaces, which tend to degrade with a time scale of many hours, even when a good vacuum is maintained [316]. Moreover, surface cleaning and analysis systems (such as sputter ion guns and Auger spectrometers) may not be compatible with other experimental requirements (eg insertion in a cold bore superconducting magnet). For these reasons much recent work has been done using mesoporous silica films as Ps converters [302–305]. These materials are extremely convenient to work with in that in general they do not require any treatment after insertion into the vacuum system. The energy of Ps emitted from these samples is comparable to what can be obtained from other converters; it

is generally limited by the zero-point energy of the mesoporous voids [308,309] which for available samples amounts to ≈50 meV. One disadvantage, however, is that the random nature of the porous network, and the mechanism by which quantum confined Ps atoms [317] are emitted from the samples into vacuum, result in broad angular distributions. They are also susceptible to the formation of para-magnetic centers when exposed to ultra violet radiation, especially at low temperatures [318–321].

3.1.3. Ps detection

One of the experimental challenges associated with Ps is the fact that the atoms will eventually self-annihilate, typically into two or three gamma rays having total energy of $2m_ec^2 = 1022$ keV. This radiation can be used as a signal that is not available in other atomic systems. Significant information is encoded in the annihilation gamma radiation, and ideally one would like to record all information contained therein. That is, the number of annihilation photons, their angular distribution, energy, and polarization, and the time spectrum of the radiation can all be used. In practice, however, no single detection system can provide all of this information. In particular, photon polarization is not usually measured as this is technically difficult for the relevant (order of 100 keV) energy range.

For experiments that change Ps decay rates it may be sufficient to measure only the time spectrum of annihilation radiation, correlated with experimental parameters that cause the difference lifetimes, such as positron beam density [322] or laser wavelength [57]. This approach has been useful when used with pulsed beams because it allows many decay events to be detected almost simultaneously [263]. This is important since previous methods relied on single event counting [323], which meant that the full intensity of the pulsed beam used could not be exploited. Thus much weaker beams were later able to provide stronger signals [34].

Ps atoms can be detected in other ways: if excited atoms are ionized the liberated positrons and/or electrons can be detected using conventional micro channel plate (MCP) detectors [324,325]. Since experiments usually involve relatively small numbers of atoms (typically in the range 10^5–10^7), methods that rely on directly detecting the absorption of emission of light (e.g., [326]) are not generally used in Ps experiments [57], although some early experiments, conducted without laser excitation, have used the detection of Lyman alpha emission in coincidence with annihilation radiation to observe excited state ($n = 2$) Ps production [290] and to conduct precision microwave spectroscopy (see Section 3.3.3).

3.2. Ps spectroscopy

Precision spectroscopic studies of Ps properties can be divided into three categories: namely, measurements of Ps energy levels (Section 3.3), decay rates (Section 3.4), and decay modes (Section 3.5). The former are easily understood as the energies of different sublevels, which are not observed directly, but are measured as the intervals corresponding to transitions between levels. Experiments performed so far include optical and microwave transitions. Ps annihilation decay rates (or, equivalently, lifetimes) are measured by time-tagging the formation of Ps and its subsequent annihilation radiation. The decay modes of Ps are characterized by the number and properties of photons emitted when a Ps atom annihilates. These are dictated by conservation laws and fundamental symmetries, which can therefore be tested by searching for forbidden decays (for example, the wrong number of decay photons for a particular state). Such measurements can also test QED theory, which offers well-defined predictions of the probability of rare (but allowed) decay modes, such as the emission of more photons than the primary decay mode. The Standard Model allows for an extremely small probability of decay modes involving neutrinos (mediated by the weak interaction) which would manifest as forbidden decay modes, since neutrinos would not be observed. However the rates for these processes are extremely small [15,178,179], and it remains possible to use invisible decay modes to test for and set meaningful limits on other processes, such as decay into mirror particles, or other new particles not included in the SM [327] (see Section 2.1.2).

The measurements performed to date with the highest *relative precision* are two-photon optical transitions between the $1\,^3S_1$ ground state and the $2\,^3S_1$ excited state [252]. By relative precision we refer to the measurement uncertainty as a fraction of the measured interval. Thus the 3.2 MHz uncertainty of the $1\,^3S_1 \rightarrow 2\,^3S_1$ interval represents a relative precision of 2.6 parts per billion (ppb). This measurement is consistent with QED calculations (to within 1.6 standard deviations). It should be remembered that the relative precision is not necessarily the most important consideration; what really matters is how well experimental data compare with calculations. A very precise measurement of a quantity that has not been calculated to comparable precision, for example, is of limited value (and *vice versa*) [16].

Microwave spectroscopy of the ground state hyperfine interval has been performed with higher absolute precision (0.74 MHz) but much lower relative precision (3.6 ppm). New measurements of the $n = 2$ fine structure have been made with highest absolute precision of any Ps spectroscopic measurement, reaching 0.66 MHz for the $2\,^3S_1 \rightarrow 2\,^3P_0$ transition [328]. However, there is a disagreement with the calculated interval (which is known to 0.08 kHz). A measurement of the $2\,^3S_1 \rightarrow 2\,^3P_2$ was performed reaching 0.37 kHz, but asymmetric lineshapes again limited the accuracy. Presently discrepancies with theory exist for both ground state and excited state fine structure measurements, and are actively being checked [29,328].

Ps decay rates have been measured numerous times since the first experiments performed by Deutsch [69]. Even with more modern beam experiments there was a persistent discrepancy observed between measured and calculated Ps decay rates (specifically the triplet ground state decay rate) [334]. However, this has since been traced to a problem related to incomplete Ps thermalization, and there is now good agreement between experiment and theory [203]. No anomalous decay processes have been observed and obtained limits on various branching ratios are all consistent with theory. Similarly, bounds on new particle masses and coupling constants have been set that are consistent with other bounds, such as those obtained from astrophysical sources (see Section 4.4).

Table 5
List of the most precise optical and microwave spectroscopy measurements of Ps performed to date. Where available both the systematic and statistical errors are quoted. The quoted precision refers to the relative precision (i.e., the measurement uncertainty divided by the interval). Note that in the $1\,^3S_1 \rightarrow 2\,^3P_J$ measurement [329], the individual $2\,^3P_J$ levels were not resolved. See Table 2 for corresponding theory values.

Transition	Measurement (MHz)	Precision	Ref.
$1\,^3S_1 \rightarrow 1\,^1S_0$	203 387.5 ± 1.6	7.9 ppm	[330]
$1\,^3S_1 \rightarrow 1\,^1S_0$	203 389.10 ± 0.74	3.6 ppm	[331]
$1\,^3S_1 \rightarrow 1\,^1S_0$	$203\ 394.2 \pm 1.6_{stat} \pm 1.3_{sys}$	10.2 ppm	[29]
$1\,^3S_1 \rightarrow 2\,^3S_1$	1 233 607 216.4 ± 3.2	2.6 ppb	[252]
$1\,^3S_1 \rightarrow 2\,^3P_J$	1 233 603 150 ± 2538	2.1 ppm	[329]
$2\,^3S_1 \rightarrow 2\,^1P_1$	$11\ 180.0 \pm 5.0_{stat} \pm 4.0_{sys}$	600 ppm	[332]
$2\,^3S_1 \rightarrow 2\,^3P_0$	$18\ 499.65 \pm 1.20_{stat} \pm 4.00_{sys}$	230 ppm	[333]
$2\,^3S_1 \rightarrow 2\,^3P_0$	$18\ 501.02 \pm 0.57_{stat} \pm 0.32_{sys}$	36 ppm	[328]
$2\,^3S_1 \rightarrow 2\,^3P_1$	$13\ 012.42 \pm 0.67_{stat} \pm 1.54_{sys}$	130 ppm	[333]
$2\,^3S_1 \rightarrow 2\,^3P_2$	$8\ 624.38 \pm 0.54_{stat} \pm 1.40_{sys}$	170 ppm	[333]

3.3. Ps energy levels

Measurements of Ps energy levels are performed by using radiation to induce transitions between different sublevels of the atom. The transitions can be observed in different ways. For example, the atoms may be photoionised [48] from a resonantly excited state. Alternatively, since different Ps levels may have very different lifetimes (which may be determined by radiative decay rates or by annihilation decay rates [335]), one may use lifetime spectra to observe transitions between short-lived and long-lived states [336]. In some experiments coincidences between optical emission and annihilation radiation have been used as signatures of excited state decays [290,337].

The current best experimental energy spectroscopy results for Ps are listed in Table 5. This is not an exhaustive list of all measurements performed to date, but rather the presumed state of the art. In some cases discrepancies exist, and multiple entries are shown. Thus, there are three entries for the ground state hyperfine interval (i.e., the $1\,^3S_1 \rightarrow 1\,^1S_0$ transition), since the 2014 experiment [29], which is currently less precise than the previous measurements, may with improvements address a 3.5 standard deviation disagreement with theory arising from the previous measurements (see Section 3.3.2).

There are also two entries for the $2\,^3S_1 \rightarrow 2\,^3P_0$ interval. The 1993 measurement [333] is in agreement with theory, with an uncertainty of 4 MHz. However a recent measurement with an overall uncertainty of 0.61 MHz disagrees with theory by more than 4 standard deviations [328]. The two results are not in conflict owing to the large uncertainty of the 1993 measurement, but the apparent discrepancy with theory is currently unexplained. Other recent Ps fine structure measurements have been performed. In these measurements asymmetric lineshapes were observed, precluding accurate determination of the relevant intervals, despite the improved precision [338].

3.3.1. Optical spectroscopy

The first experimental production of Ps in 1951 [69] predates the invention of the laser. Attempts to drive $1\,^3S_1 \rightarrow 2\,^3P_J$ optical transitions in Ps were made using lamps were not unambiguously successful [339,340]. The first optical excitation of Ps was performed using pulsed lasers by Chu and Mills in 1982 [48]. This was a two-photon $1\,^3S_1 \rightarrow 2\,^3S_1$ excitation, used because it allows Doppler-free excitation [341–343]. This scheme uses two counter-propagating photons ($\lambda = 486$ nm) to excite the transition, which for a single photon is forbidden by electric dipole selection rules. This approach is particularly advantageous for Ps experiments owing to the very large first-order Doppler effects one typically observes in single-photon transitions [308]. Two-photon single color transitions of this kind are used to perform very precise measurements in atomic hydrogen, which have a natural width on the order of 1 Hz [344]. After many years of improvements [345], the hydrogen spectroscopy has now reached a fractional frequency uncertainty of 4.2×10^{-15} [346]. Unfortunately the same precision can never be achieved using Ps, owing to the much broader natural linewidth of 1.3 MHz, arising primarily from the finite lifetime of the Ps ground state [57]. An optimistic experimenter might believe that a broad line can be split by a factor of 10,000 [21], which would yield $\approx$ 130 Hz, or a fractional uncertainty of a part in 10^{13}. However, Ps experiments do not simply mirror what can be done with hydrogen. In addition to broader lines one has to deal also with faster atoms, and fewer of them, meaning that this level of precision is most likely not achievable.

The initial $1\,^3S_1 \rightarrow 2\,^3S_1$ measurements of Chu and Mills [48] were improved (with the help of Hall) by using better laser stabilization and metrology, allowing a more precise measurement to be performed a few years later [347]. In this work a transition frequency of $1,233,607,185 \pm 15$ MHz was obtained, which amounts to 12 ppb relative uncertainty. Using pulsed lasers for precision spectroscopy, however, is not ideal because the exact excitation process is less well defined than is the case for CW lasers, making it more difficult to model the lineshape, for example [348]. For this reason, several improvements were made to the experiments [349], including using a much more intense positron beam [350] and a CW laser [351] in a build-up cavity. The result of this work was a measured transition frequency of $1,233,607,216.4 \pm 3.2$ MHz [252,324]. The current theory value for this transition is (see Table 2)

1, 233, 607, 211.12 $\pm$ 0.58 MHz, meaning that there is a small difference of 5.28 MHz, which amounts to 1.6 standard deviations. With the exception of the initial pulsed measurements [347] there have been no other measurements of the Ps $1\,^3S_1 \rightarrow 2\,^3S_1$ interval, although new experiments have been reported [56,253]. The new experiments have the goal of reaching an uncertainty of 100 kHz, an improvement of a factor of $\approx$30 that would make the experimental uncertainty 6 times smaller than that of the current theory.

The two-photon $1\,^3S_1 \rightarrow 2\,^3S_1$ excitation of Ps constitutes the only high-precision optical measurement of this system. The factor of $\approx$5 reduction in the experimental uncertainty obtained in revised measurement [324] is fairly modest when one considers the extent to which the experiments were improved. Ultimately this is due to the nature of Ps atoms available for experiments: they are invariably fast, essentially uncontrolled, and few in number. This also explains why the first example of Ps excitation by laser light remains the only precision measurement, despite being a more complex two-photon process. Single photon excitation is easier to implement, but it is susceptible to Doppler broadening, which makes it necessary to use high power pulsed lasers in order to cover a useful fraction of the bandwidth [57]; this methodology is not compatible with precision measurements.

The first single-photon excitation of Ps was the $1\,^3S_1 \rightarrow 2\,^3P_J$ excitation ($\lambda = 243$ nm) reported by Ziock and co-workers in 1990 [323]. The natural linewidth of this transition is $\approx$ 50MHz, primarily because of the 3.2 ns radiative lifetime of the $2\,^3P_J$ levels. However, typical Doppler broadening results in linewidths closer to 500 GHz, essentially precluding precision measurements, and making the use of broad band lasers necessary. This experiment was performed using an intense pulsed linac beam [273] and a broad band dye-laser system. A similar approach has since been adopted in subsequent work (e.g., [308,352,353]), with the main difference being that Surko-type buffer gas traps are now used to provide pulsed positrons [58].

The production of highly excited Rydberg [354] Ps atoms was also achieved by Ziock and co-workers [355] using a two-color two-photon excitation scheme. This process is not the same as the Doppler-free two-photon excitation used for earlier Ps measurements [324], and was therefore not amenable to high precision measurements. The same excitation scheme has been used more recently with an improved signal [34,353,356,357]. However, this process is also limited by Doppler effects and the need to use broad band lasers, and high precision has not been achieved. The availability of Rydberg atoms may allow future experiments to be performed with high precision since these states do not annihilate and possess radiative lifetimes comparable to (twice) those of the corresponding states in hydrogen [358]. These atoms may allow an alternative two-photon optical measurement, namely $nS \rightarrow 2\,^3S_1$, where the principal quantum number n may be in the range 20–40 [359]. The reason for using Rydberg states is that one can control them using electric fields [315] so it may be possible to decelerate and focus the Ps beam [360]. This is useful because a limiting factor in two-photon spectroscopy of Ps is the speed of the atoms and their large angular spread, which lead to inefficient interactions with the (typically physically narrow, on the order of mm waist sizes) CW beam in a cavity, large transit time broadening, and even significant second order Doppler shifts [324]. A disadvantage of this approach is that Rydberg atoms are highly sensitive to electric fields [361], which must therefore be controlled. One can study field effects by performing measurements for a range of n states, but it may nevertheless limit the obtainable precision.

Single photon experiments can be performed using several different Doppler correction techniques [326]; for example, saturated absorption spectroscopy (SAS) has been used to measure the Ps $1\,^3S_1 \rightarrow 2\,^3P_J$ transition (where the $2\,^3P_J$ levels were unresolved) [329]. The experiment yielded 1,233,603,150 $\pm$ 2538 MHz, although some systematic errors were not accounted for, primarily because the experiment was designed to measure the Ps hyperfine interval via a crossover resonance [326]. High precision was not achieved because a broad band laser was used, but future improvements are possible.

Recently a Doppler free single-photon excitation method (not SAS) has been used to obtain remarkable precision (2.3 kHz) in measurements of $2S_{1/2}^{F=1} \rightarrow 4P_J^{F=1}$ transitions ($J = 1/2, 3/2$) in atomic hydrogen [21,362]. In this work a retro-reflected laser was used to excite a beam of metastable $2S_{1/2}^{F=1}$ hydrogen atoms to levels with $n = 4$; by careful alignment of the laser light (including precisely matching the phase and amplitude of the two beams) it was possible to obtain equal and opposite Doppler shifts, which average to zero, providing a Doppler-free measurement (to first order). The natural width of this transition is $\approx$13 MHz, and in Ps the equivalent would be half of this value. In principle, therefore, it may be possible to perform a similar experiment using Ps, although there are considerable challenges arising from the quality of the Ps sources obtainable.

A slow Ps beam can be produced using existing sources via extreme collimation, which is undesirable given the already low count rates typical of such measurements. Improved detection efficiency is the most direct way to (partially) mitigate this problem. A significant improvement would be to directly detect Ps atoms using a multi channel plate (MCP) detector. This may be achieved by exciting atoms to Rydberg levels and then efficiently detecting positrons (or electrons) after electric field ionization [325], or it may be possible to directly detect excited state atoms on the MCP by virtue of their $\approx$6 eV internal energy. The latter process has not yet been explicitly demonstrated.

3.3.2. Microwave spectroscopy of the Ps ground state hyperfine interval

The hyperfine structure of hydrogen (especially the Lamb shift [363,364]) has been extensively studied using microwave spectroscopy, and the structure of Ps has also been studied in this way. The interaction between a positron and an electron differs significantly from the electron–proton interaction (see Section 2.1.1), and as a result the Ps fine and hyperfine structures (as defined for electron–proton interactions) are both on the same order. Thus the Ps energy

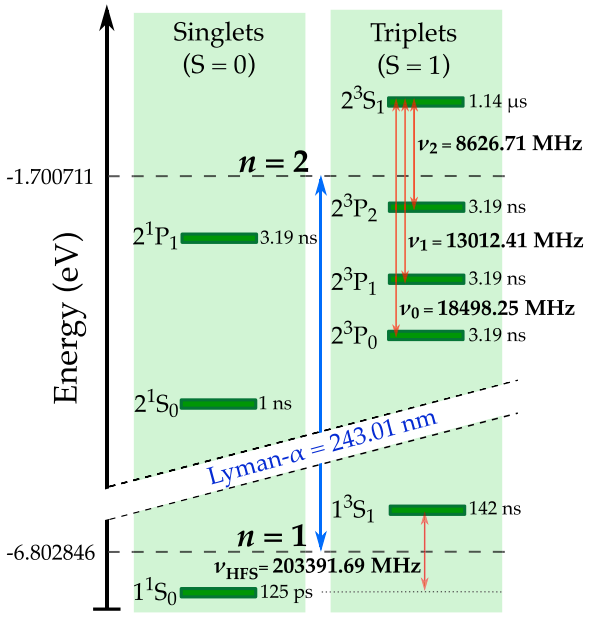

Fig. 5. Energy level diagram of the $n = 1$ and $n = 2$ levels in positronium. The energies of the $\mathcal{O}(m\alpha^2)$ (Bohr) levels are indicted by the dashed horizontal lines. The calculated transition frequencies for the $n = 1$ hyperfine interval ($\nu_{\rm HFS}$) and the $2\,^3{\rm S}_1 \to 2\,^3{\rm P}_J$ ($J = 0, 1, 2$) intervals (ν_J), are also shown [126]. Radiative or annihilation lifetimes for all levels are also indicated, according to the primary decay mode.
Source: From [338] with permission.

level structure differs from that of hydrogen and measurements thereof can be used as unique tests of the methodology of QED calculations [16].

Of particular significance is the ground state singlet–triplet energy splitting (i.e., the hyperfine interval), which is 1.4 GHz in hydrogen and 203 GHz in Ps (see Fig. 1). This difference is predominantly due to the stronger spin–spin interactions and annihilation channels in Ps. A practical consequence of this is that it is not possible to perform direct microwave spectroscopy of the Ps hyperfine structure (as it is known) in the same way that has been done for hydrogen. This interval, which gives rise to the 21 cm line used extensively in radio astronomy and cosmology [365], is well measured in hydrogen and is the basis of the hydrogen maser frequency standard [366]. Unfortunately, owing to the much larger Ps hyperfine interval, among other difficulties, there will be no positronium maser.

The energy levels of the ground and first excited states of Ps are shown in Fig. 5. The $n = 2$ fine structure intervals are all in a range easily accessible using commercially available signal generators (i.e., 0–20 GHz). The large ground state hyperfine interval, however, is not. Since $1\,^3{\rm S}_1 \to 1\,^1{\rm S}_0$ transitions are magnetic (M1) transitions, very high power is required to drive them, on the order of kW for practical experimental conditions. Radiation sources and amplifiers in this power regime are not widely available in the THz frequency range, but an experiment has been carried out using a high power gyrotron [367] in which the transition was observed [368]. Because of the high power required, this methodology is not generally compatible with precision measurements.

The approach used to measure the Ps ground state hyperfine interval $\Delta_{\rm hfs}$, was first employed by Deutsch [260], and remains the only technique used so far to provide a precision measurement. In the experiments Ps atoms were produced directly from a radioactive source in a gas cell, and measurements had to be performed at different gas pressures and the results extrapolated to zero pressure. Since 203 GHz radiation with sufficient power is technically inaccessible, measurements were instead made in a magnetic field B, such that the substates with $M_J = 0$ were shifted relative to the substates with $|M_J| = 1$ via the Zeeman effect [217,369,370]. The separation $\Delta_{\rm mix}$ is approximately given by [371]

$$\Delta_{\rm mix} = \frac{\Delta_{\rm hfs}}{2}[(1+x)^{1/2} - 1] \tag{67}$$

where $x = 2g_e\mu_B B/h\Delta_{\rm hfs}$, g_e is the electron g factor, and μ_B is the Bohr magneton. NB: in this expression the Planck constant h is included so that $\Delta_{\rm hfs}$ is given as a frequency. The Zeeman shifts are shown in Fig. 6, from which it can be seen that relatively small magnetic fields will separate the $1\,^3{\rm S}_1(0)$ level from the $1\,^3{\rm S}_1(\pm 1)$ levels by small intervals ($\Delta_{\rm mix}$) with frequencies that can easily be generated with the required high power. Thus, by measuring the Zeeman shift in a known magnetic field, the hyperfine interval $\Delta_{\rm hfs}$ can be obtained. This obviously means that one needs to know the magnetic field with a precision at least as good as the precision with which the measurement is to be made, and that the field must be very uniform in the region where the Ps atoms are probed.

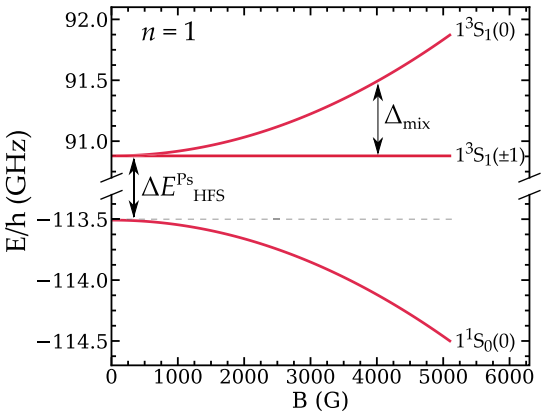

Fig. 6. Zeeman shifted ground state Ps energy levels.

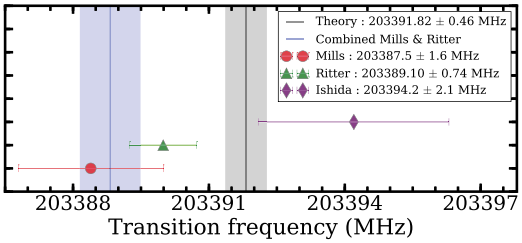

Fig. 7. Comparison of measurements of the Ps ground state hyperfine interval with current theory. The combined value of the older experiments (Mills [330] and Ritter [331]) is shown as a shaded (blue) band. The statistical and systematic errors of the more recent measurement by Ishida et al. [29] have been added in quadrature.

The ground state Ps hyperfine interval was measured via this technique in a series of precision experiments spanning almost three decades by Hughes and co-workers at Yale [331,372–378] and also by Mills and Bearman at Brandeis [379]. These experiments were later re-evaluated to account for lineshape effects in the measurement [330,331,380]. Note that Eq. (67) is not strictly valid for high precision (ppm) as it does not include annihilation effects that perturb the lineshape.

The combined results from the two most precise measurements (using the corrected lineshape) is $\Delta^{\rm exp}_{\rm hfs}$ = 203,388.82 ± 0.67 MHz. The current theory value is (see Table 2) $\Delta^{\rm th}_{\rm hfs}$ = 203,391.69 ± 0.46 MHz. This means there is a discrepancy of 2.87 MHz, which corresponds to 3.5 standard deviations. NB: the combined experimental value is the weighted mean, obtained using the squares of the uncertainty; slightly different values can be found in the literature (e.g., [29]).

There is evidence that this discrepancy may be at least partially due to a pressure shift arising from Ps collisions with the gas in which it is formed [261,262,381]. A new measurement has been performed in which this effect is taken into account by performing cuts (based on energy selection) to the data to isolate stronger collisional perturbations for non-thermal atoms [29]. Unfortunately this reduces the signal by a considerable amount, and introduces a relatively large statistical error. The result obtained from this measurement is $\Delta^{\rm exp}_{\rm hfs}$ = 203,394.2 ± $1.6_{\rm stat}$ ± $1.3_{\rm sys}$ MHz. While the total uncertainty here is almost three times higher than that of the previous experiments, it is consistent with theory, and less consistent with those measurements, as indicated in Fig. 7. This suggests that the observed discrepancy may well be caused by Ps–gas interactions, and offers hope that theory and experiment will converge when the new measurements are improved.

We note briefly that the Ps ground state hyperfine interval has been measured using several different alternative methods, including an all-optical measurement [329], observations of quantum beats (that is, oscillations in the Ps decay rate due to singlet–triplet mixing in a magnetic field [382–384]), and a motion induced transition, driven when fast Ps atoms fly through a static, spatially varying, magnetic field at a speed that gives rise to an effective 203 GHz oscillating field [385]. For a variety of technical reasons, none of these methods are currently able to operate with high precision, although it is possible that optical measurements can be improved to the ppm level.

3.3.3. Microwave spectroscopy of $n = 2$ fine structure intervals

The $n = 2$ fine structure has also been measured in several experiments, with the most recent results shown in Table 5. These experiments have been conducted by four different groups, starting with Mills, Berko and Canter at Brandeis in 1975 [337], followed by researchers in Michigan in 1987 [386] and Mainz in 1993 [333], and more recently at University

College London (UCL) in 2020 [328,338]. Measurements of the $2\,^3S_1 \rightarrow 2\,^1P_1$ transition have also been performed (in Michigan) as a test of C violation [387].

The Brandeis, Michigan, and Mainz experiments were all conducted using $n = 2$ excited state Ps produced following positron bombardment of various metal surfaces; this process has been observed by several groups [290,388–392]. It relies on Ps formed from unthermalised positrons, and produces $n = 2$ atoms approximately equally distributed among all 16 of the $n = 2$ sublevels, with reported overall efficiencies varying from 0.1 to 2%. Thus the efficiency for $2\,^3S_1$ production is, at most 0.4%, and more likely much lower. Owing to the energetics of the formation process, excited state atoms produced in this way have kinetic energies of several eV. The formation of more highly excited atoms (i.e., those with $n \geq 3$) via this process has not been observed.

In these experiments $2\,^3S_1 \rightarrow 2\,^3P_J$ transitions were driven with microwave radiation and were detected via coincidence measurements of the Ps Lyman alpha photons emitted in the radiative decay of the produced $2\,^3P_J$ atoms and the corresponding ground state annihilation photons. However, because many $2\,^3P_J$ atoms are generated using this method there is an unavoidable and large background component. Moreover, the high energies of the Ps atoms mean that high microwave power has to be used, resulting in significant broadening of the lineshapes (from both power broadening and transit time broadening [326]).

The new UCL experiments were performed using different methods, the principal changes being that ground state atoms were excited (indirectly) to the $2\,^3S_1$ level using a laser, and that microwave transitions were observed via the time spectrum of Ps annihilation radiation only. By producing $2\,^3S_1$ atoms from relatively slow ground state atoms [28] lower microwave power could be employed, reducing line broadening effects. Avoiding Lyman-alpha detection in coincidence with annihilation radiation also increases the overall detection efficiency. This new approach was facilitated by technological developments in positron trapping and manipulation [58] as well as Ps production and optical excitation [57]. While offering a significant advantage in terms of pulsed beam production, the use of a positron trap meant that the experiments were conducted in a magnetic field.

In these measurements lineshapes with sub-MHz uncertainties on the inferred line centers were obtained. However, it was found that some of the lineshapes were asymmetric, precluding a precise determination of the transition frequencies [338]. Examples of both symmetric and asymmetric lineshapes obtained in these measurements are shown in Fig. 8. Here it may be seen that there is good agreement between Lorentz and Fano fits for the ν_0 transition [Fig. 8(a)], indicating a symmetric lineshape. However, this is not the case for the ν_1 and ν_2 transitions [Fig. 8(b) and (c)], indicating that these lineshapes are asymmetric. The source of the asymmetry has not yet been identified: quantum interference effects arising from nearby off-resonant transitions [393] do not seem to be capable of causing such large shifts [338].

In order to empirically characterize the asymmetries, Fano profiles were used to fit the data [394]. The particular Fano profiles used reduce to Lorentzians for large values of an asymmetry parameter q, which can therefore be used as a metric of the extent to which lineshapes are non-Lorentzian. The Fano profiles were able to fit the data well, and the peak positions (as opposed to the resonance positions as defined by the fitting function) were found to be closer to theory, possibly indicating that the fitting errors caused by applying symmetric functions to asymmetric data can be partially mitigated in this way. Other asymmetric line shape functions gave similar results (e.g., [395]). However, for precision experiments a full lineshape model is required.

The physical reason for the asymmetries has not been conclusively identified, precluding the development of a useful model. Recent numerical simulations have indicated that the asymmetries may be caused by frequency dependent reflections of microwave radiation in the vacuum chamber surrounding the waveguides [396]. If this is confirmed then it should be possible to re-design the apparatus to eliminate this effect and perform improved experiments.

Previous $n = 2$ fine structure measurements are summarized in Fig. 9. The asymmetric lineshapes discussed above cannot presently be used to obtain accurate intervals, and hence these data have not been included in Table 5. Once the asymmetries are understood and accounted for (or eliminated), however, it is likely that experimental values will be obtained with uncertainties less than five times larger than the current theory values. With better understanding of systematic errors improved measurement techniques can be used (e.g., [285]) which are expected to reduce the uncertainties to levels below the current theory values, and therefore to be sensitive to the $n = 2$ ultrafine splittings [156] (see Table 2) and may even provide a test of the noncommutativity of space [397].

Fast atoms are generally detrimental to precision measurements [57] but for measurements using the separated oscillatory fields (SOF) method [285] they may be advantageous since one can produce spatially separated fields using the same radiation source, eliminating unwanted phase differences between the excitation regions. This methodology mitigates some of the problems associated with fast atoms because it is not necessary to know the exact lineshape for a transition, but the divergent Ps beams typically generated [57] will require severe collimation, and concomitant loss of signal.

A modified SOF measurement called frequency offset separated oscillatory fields (FOSOF) [398] was recently used to perform a precision measurement of the hydrogen Lamb shift using a 55 keV beam [399]. This corresponds to atoms with speeds of $\approx 3 \times 10^8$ cm/s, which is more than an order of magnitude faster than Ps emitted from mesoporous films [308]. Thus, it may be possible to take advantage of some Ps sources that would otherwise not be considered useful for spectroscopic measurements, such as gas-cell excited state beam production [284] to perform similar measurements; so far this has not been attempted.

In summary, the precision of $n = 2$ fine structure measurements has been improved [328] and is expected to improve further [338], with a reasonable chance of approaching the QED uncertainties in the next few years. Some apparent

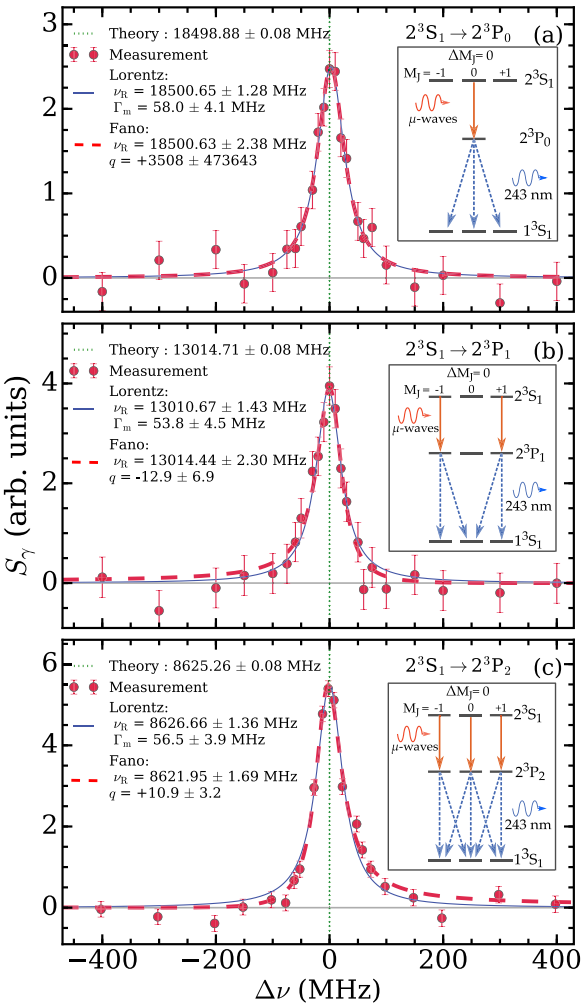

Fig. 8. Example lineshapes of the ν_0 (a), ν_1 (b), and ν_2 (c) transitions, measured in a magnetic field of 32 G. Both Lorentzian and Fano fits were applied to all lineshapes. The green vertical lines at $\Delta\nu = 0$ indicate the (Zeeman shifted) theoretical transition frequencies, shown in the legends. The insets show the allowed $\Delta M_J = 0$ transitions (solid arrows) to the $2\,^3P_J$ states, followed by $\Delta M_J = 0, \pm 1$ radiative decay pathways (dashed arrows) to the ground state.
Source: From Ref. [338] with permission.

discrepancies have been observed and are the focus of new measurements. The ground state hyperfine interval is currently being re-measured using energy selection techniques that can account for incomplete Ps thermalization, and results so far [29] indicate that the long-standing discrepancy with theory is an experimental artefact and will be resolved. A new experiment designed to measure the $2\,^3S_1 \rightarrow 2\,^1S_0$ interval has been proposed [400], but no data have been reported so far.

3.4. Decay rates

As discussed in Section 2.1.2, Ps self-annihilation rates can be measured and compared to QED calculations in order to test them. The decay rate of o-Ps was the first measurement made [258] with Ps after its discovery [69]. This measurement yielded a decay rate $\Gamma_{\rm exp} = 6.8 \pm 0.7$ MHz. With the large error this is consistent with the modern (theory) value of $\Gamma_{\rm th} = 7.039\,979 \pm 0.000\,019$ MHz, and was sufficient to resolve a disagreement between three different calculations, confirming the result of Ore and Powell [8] (see Eq. (26)).

Since 1951 Ps decay rates have been measured many times (see [46,47,401] for some older reviews and [51] for a more recent discussion). The p-Ps decay rate is harder to measure than the o-Ps decay rate because it is much faster. However, it is also less susceptible to controversy because the atoms do not have enough time to react to their surroundings in the same way that o-Ps atoms do, and hence different types of measurements are less likely to yield different results. This is

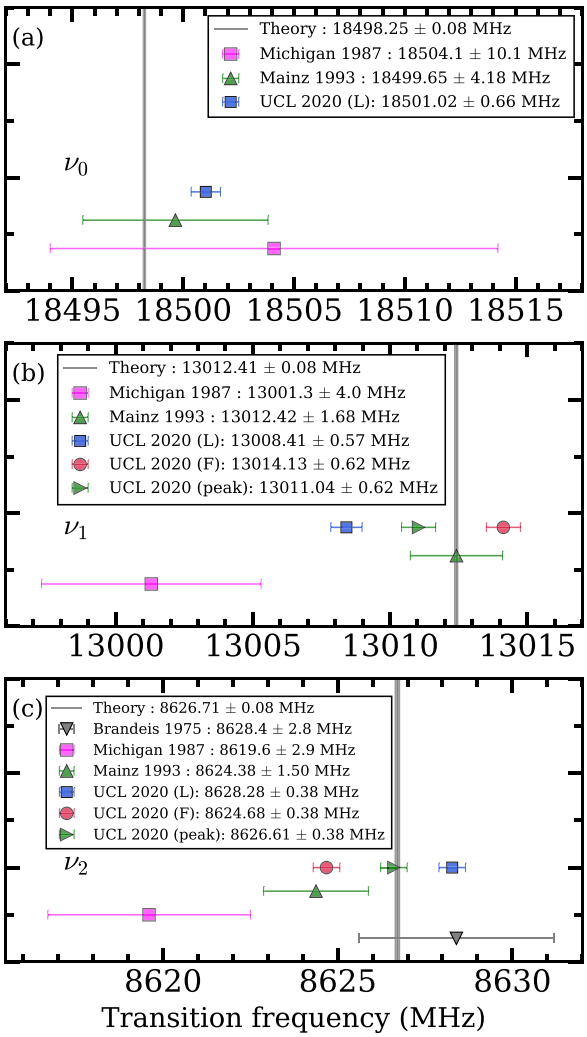

Fig. 9. Comparison of measurements with theory for the (a) ν_0, (b) ν_1, and (c) ν_2 transitions. Results from Lorentz (L) and Fano (F) line profile fits are shown for recent measurements of ν_1 and ν_2 intervals owing to asymmetric lineshapes. Also shown are the peak positions of the Fano fits (peak), as explained in Ref. [338]. The theoretical values with uncertainties are indicated by the vertical solid lines [126]. Statistical and systematic uncertainties for the experimental data have been added in quadrature.
Source: From Ref. [338] with permission.

essentially the same problem encountered in all precision measurements, namely that, as precision increases, more and more small systematic effects arise that must be taken into account.

The annihilation process necessarily requires that the electron and positron wavefunctions overlap, which means that only states with orbital angular momentum $\ell = 0$ have any experimentally relevant annihilation decay rates [402,403]. Most excited atoms predominantly decay radiatively to the ground state before annihilation, and it is necessary to consider both radiative and self-annihilation decay rates for these atoms [335,358,404]. The only excited states for which self annihilation is likely are the $2\,^1S_0$ and $2\,^3S_1$ levels, since they are radiatively metastable. These levels annihilate at rates 8 times slower than their $n = 1$ counterparts, making this process difficult to measure because the excited state atoms may travel a considerable distance before they decay. The decay of $2\,^1S_0$ atoms has not yet been directly observed. The decay of $2\,^3S_1$ atoms has been observed [253], and the decay rate has been measured [405]. However, the 8.5% precision obtained in this measurement is not sufficient to test any QED corrections to the lowest order decay rate.

The current best individual measurements of Ps decay rates are listed in Table 6. Note that both p-Ps and o-Ps decays include contributions from all allowed higher order decay modes (that is, decays to more than 2 or 3 photons) such that

$$\Gamma_{\text{p-Ps}} = \Gamma_2 + \Gamma_4 + \Gamma_6 + \cdots \tag{68}$$

and

$$\Gamma_{\text{o-Ps}} = \Gamma_3 + \Gamma_5 + \Gamma_7 + \cdots \tag{69}$$

Table 6
List of the most precise Ps decay rate measurements performed to date. The quoted precision refers to the relative precision (i.e., the measurement uncertainty divided by the interval). See Table 3 and Table 4 for corresponding ground state singlet and triplet theory values, respectively. We note that the theoretical $n = 2$ decay rates are a factor of 8 larger than the corresponding ground state rates, and that the measurement of the $2\,^3S_1$ decay rate was performed in a 50 G axial magnetic field that shifted the theoretical decay rate from ≈880 to 890 kHz.

Decay mode	Measurement	Precision	Ref	year
$1\,^1S_0 \to 2\gamma$	7.9909 ± 0.0017 GHz	213 ppm	[160]	1994
$1\,^3S_1 \to 3\gamma$	7.0401 ± 0.0011 MHz	156 ppm	[161]	2009
$2\,^1S_0 \to 2\gamma$	Not measured	N/A	N/A	N/A
$2\,^3S_1 \to 3\gamma$	843 ± 72 kHz	8.5%	[405]	2020

but that at the current level of precision the higher order contributions are negligible (see e.g., Eqs. (23) and (27)) and Section 3.5. We note also that measurements may not in any case be sensitive to the higher order decay modes as the detection efficiency of the lower energy photons may well be reduced.

3.4.1. Singlet decay rates

There are very few measurements of $\Gamma_{\text{p-Ps}}$ because it is very fast; the corresponding lifetime of ≈125 ps is just about at the limit of standard timing systems, and measurements have only been performed using indirect methods. The first such measurement was essentially a by-product of ground state hyperfine measurements [373,374]; in this work a resonant transition between Zeeman shifted Ps states with $m = 0$ (see Section 3.3.2) was obtained using a fixed microwave frequency and a variable applied magnetic field strength. The width of observed lineshape depends in part on the singlet decay rate, which is the basis of the measurement. However, the decay rate must be derived from several experimental parameters, and the method is not well suited to high precision (Theriot and co-workers obtained $\Gamma_{\text{p-Ps}} = 7.99 \pm 0.11$ GHz [374]).

Other measurements have been performed [160,406] that also rely on Zeeman mixing between the $m = 0$ singlet and triplet ground states in an applied magnetic field. In this case the perturbed state decay rate Γ_{mix} is measured, which is given by

$$\Gamma_{\text{mix}} = (1 - b^2)\Gamma_{\text{o-Ps}} + b^2\Gamma_{\text{p-Ps}} \tag{70}$$

where $\Gamma_{\text{o-Ps}}$ and $\Gamma_{\text{p-Ps}}$ are the unperturbed triplet and singlet decay rates, respectively, and b depends on the magnetic field and the hyperfine interval (see [160] for details). For typical experimental parameters the mixed state decay rate Γ_{mix} is generally much higher than the field-free triplet rate (≈30 MHz for a 4 kG magnetic field, compared to ≈7 MHz in zero field), but is still much slower than $\Gamma_{\text{p-Ps}}$ and is therefore measurable; thus, $\Gamma_{\text{p-Ps}}$ is obtained by measuring $\Gamma_{\text{o-Ps}}$ and also Γ_{mix} in a known magnetic field. Systematic effects can be explored by performing measurements at different fields; as with the hyperfine measurements discussed in Section 3.3.2, this requires knowledge of the magnetic field experienced by the atoms. This is usually measured with an NMR probe, although some form of atomic magnetometry or Rydberg spectroscopy may be a viable alternative [57]. This measurement also requires knowledge of the hyperfine interval.

The most precise measurement of $\Gamma^{\text{exp}}_{\text{p-Ps}}$ yielded 7.9909 ± 0.0017 GHz [160], where the theory value $\Gamma^{\text{th}}_{\text{p-Ps}} = 7.989\,618 \pm 0.000\,018$ GHz (see Eq. (25)). This means that the experimental uncertainty is ≈100 times larger than the theory uncertainty estimate (and not a factor of 10,000 as reported in Ref. [51]). It is therefore unlikely that parity between theory and experiment for $\Gamma_{\text{p-Ps}}$ will be achieved in the foreseeable future.

Digital timing systems have improved considerably since these measurements were performed. However, apart from achieving sufficient time resolution, performing a direct measurement of the singlet ground state decay rate is complicated by the need to uniquely identify the Ps formation time (a problem similar to the measurement of sub-ns positron surface-state lifetimes on metals [407]). One could envision using a short-pulsed (pico-second) laser to rapidly populate $1\,^1S_0$ levels from an ensemble of long-lived atoms, but this nevertheless remains a challenging prospect: no new experiments aimed at measuring the $1\,^1S_0$ decay rate appear to have been proposed in recent years.

3.4.2. Triplet decay rates

Measurements of $\Gamma_{\text{o-Ps}}$, the o-Ps decay rate, have been performed many times. The first generation of such measurements (starting with Deutsch [258]) pre-date the development of positron beams, and were performed using the gas cell method of producing Ps atoms directly from β-emitting radioactive sources. Even after positron beams became available this method continued to be widely used. In these experiments lifetime spectra were generated using a start signal derived from the positron emission following nuclear decay (usually via an almost simultaneously emitted gamma ray, or by allowing the fast positrons to pass through a thin scintillator), and a stop signal obtained from the Ps annihilation radiation. Any delays in Ps formation would then be included in the spectrum, but these are generally negligible owing to very fast positron cooling and Ps formation rates in gases [54]. As with the hyperfine interval experiments, such measurements are susceptible to complications arising from Ps–gas interactions, which can reduce the Ps lifetime.

Table 7
Selection of different o-Ps decay rate measurements. The quoted precision refers to the relative precision (i.e., the measurement uncertainty divided by the interval). Most source/gas experiments used freon-isobutane mixtures, although other gases were also used. Beam experiments used slow positron beams incident on SiO_2 or MgO films or powder targets. Source/SiO_2 refers to radioactive sources that emit positrons into SiO_2 powder or aerogel targets. For comparison, the theory value is $\Gamma_{\rm th} = 7.039\,979 \pm 0.000\,019$ MHz.

Measurement (MHz)	Precision	Ref	Year	Method
7.104 ± 0.006	845 ppm	[408]	1976	Source/gas
7.09 ± 0.02	2821 ppm	[409]	1976	Beam/MgO
7.056 ± 0.007	992 ppm	[410]	1978	Source/gas
7.045 ± 0.006	852 ppm	[411]	1978	Source/gas
7.051 ± 0.005	709 ppm	[406]	1982	Source/gas
7.0516 ± 0.0013	184 ppm	[334]	1987	Source/gas
7.0482 ± 0.0016	227 ppm	[412]	1990	Beam/MgO
7.0398 ± 0.0029	412 ppm	[413]	1995	Source/SiO_2
7.0404 ± 0.0013	185 ppm	[203]	2003	Beam/SiO_2
7.0396 ± 0.0016	227 ppm	[202]	2003	Source/SiO_2
7.0401 ± 0.0011	156 ppm	[414]	2009	Source/SiO_2

In some experiments solid materials are used to stop the positrons instead of a gas; various porous materials, such as silica aerogels, have been used for this purpose. Then, radioactive material is covered by layers of material thick enough to stop energetic positrons and produce Ps atoms in a much smaller volume than a gas cell (typically a few cm^3). Experiments using the same types of materials can also be performed with a mono-energetic positron beam. In this case individual positrons are usually time-tagged via secondary electrons emitted from a remoderator or from the Ps formation target itself [264] to generate the start signal for lifetime spectroscopy [9]. In either case, the produced Ps atoms will continue to interact with the porous material in which they are created, which affects subsequent lifetime measurements.

A selection of o-Ps decay rate measurements made using various techniques is shown in Table 7. Other measurements exist; these data were (arbitrarily) selected to highlight a long-standing discrepancy between experiment and theory. During the course of many measurements a persistent discrepancy of up to ten standard deviations was observed. Experiments performed using different methods and in several different laboratories served only to reinforce the discrepancy, as did advances in the theory. This became known as the positronium lifetime puzzle, where the puzzling nature of the problem was reinforced by the fact that Ps is expected to be a very well understood system, not easily admitting to such a large disagreement with QED.

The lifetime puzzle was eventually solved by performing experiments that either minimized Ps interactions with surrounding material [203], or by explicitly taking such interactions into account [202,413]. The former was accomplished by using thin silica films that produced slow o-Ps atoms emitted into vacuum, where they were largely free of perturbing interactions. In the latter case, energy selection methods were used to identify and remove two-photon decay events, which is the dominant decay mode for o-Ps atoms that do not decay via self-annihilation. The last four entries in Table 7 refer to experiments that were performed in this way, and they are in good agreement with each other, and with theory. Evidently extrapolating to zero gas pressure was insufficient, and did not properly account for some Ps–gas interactions; the exact nature of these interaction has not yet been elucidated.

The *combined* value of the decay rates believed to be free of thermalization effects (i.e., the results in Refs. [161,202,203, 413]) is $\Gamma^{\rm exp}_{\text{o-Ps}} = 7.0401 \pm 0.0007$ MHz. This is in agreement with the theory value of $\Gamma^{\rm th}_{\text{o-Ps}} = 7.039\,979 \pm 0.000\,019$ MHz, and the positronium lifetime puzzle can therefore be considered to be resolved. One can regard this exercise as an example of the scientific method at work. The extent to which Ps thermalization rates may affect measurements is not necessarily obvious. It was only through a series of careful experiments and advances in theory that the problem was, eventually, solved.

We note that the discrepancy observed between theory and measurements of the Ps ground state hyperfine interval discussed in Section 3.3.2 did not quite rise to the level of a “puzzle", probably because the disagreement was not as large (3–4 standard deviations) and was based on only two measurements. In light of the subsequent resolution of the o-Ps lifetime puzzle, it does now seem likely that what may be called the “hyperfine vexation" will also be resolved by experiments that can isolate non-thermalized Ps [29].

3.5. Decay modes

The fact that Ps is composed of a leptonic particle–antiparticle pair means that Ps is an eigenstate of the charge conjugation operator C, the Parity operator P and the combined CP operator. It should be remembered that this is a rather unusual situation, and that most atoms are definitely *not* C eigenstates. Photons are eigenstates of C with eigenvalue -1 (if you change the sign of electric charges electromagnetic fields are reversed). Atoms and molecules are of course eigenstates of P, having even or odd parity depending on the electronic configuration.

In general Ps states with orbital angular momentum ℓ and total spin quantum numbers s are eigenstates of the C, P and CP operators with eigenvalues of $(-1)^{(\ell+s)}$, $(-1)^{(\ell+1)}$, and $(-1)^{(s+1)}$, respectively [71]. As discussed in Section 2, the

Table 8
A selection of experimental measurements of the branching ratio (BR) or upper limit (UL) for various electron–positron decay modes. C.L refers to the confidence limit quoted in the various experiments, and all branching ratios are given with respect to the corresponding highest order decay process (i.e., $2(3)\gamma$ decays for spin singlet (triplet) states). Where available, systematic and statistical errors have been added in quadrature. In some cases the $1\,^1S_0$ decays may in fact be relative spin singlet electron–positron configurations rather than bound-state singlet Ps atoms.

Decay mode	C allowed?	BR/UL	C.L	Ref.	Year
$1\,^1S_0 \to 3\gamma$	No	2.8×10^{-6}	68%	[423]	1967
$1\,^3S_1 \to 4\gamma$	No	8×10^{-6}	68%	[424]	1974
$1\,^1S_0 \to 4\gamma$	Yes	$1.3 \pm 0.3 \times 10^{-6}$	68%	[425]	1990
$1\,^3S_1 \to 4\gamma$	No	2.6×10^{-6}	90%	[426]	1996
$1\,^3S_1 \to 5\gamma$	Yes	$2.2^{+2.6}_{-1.7} \times 10^{-6}$	90%	[427]	1996
$1\,^1S_0 \to 4\gamma$	Yes	$1.14 \pm 0.39 \times 10^{-6}$	68%	[428]	2002
$1\,^3S_1 \to 5\gamma$	Yes	$1.67 \pm 1.1 \times 10^{-6}$	68%	[428]	2002
$1\,^3S_1 \to 4\gamma$	No	3.7×10^{-6}	90%	[428]	2002
$1\,^1S_0 \to 5\gamma$	No	2.7×10^{-7}	90%	[428]	2002

number of photons emitted in Ps self-annihilation is governed by *C* invariance, meaning that singlet (triplet) ground states decay into an even (odd) number of photons (see Eq. (2)), with rapidly decreasing probability as the number of photons increases (see Section 2.1.2). It is challenging even to observe these higher order processes, and in most experiments, including precision decay rate measurements, they can be neglected.

Since the number of annihilation photons emitted in Ps decay is fundamentally dictated by *C* invariance, this symmetry can be tested by searches for Ps atoms that decay into the "wrong" number of photons (that is to say, decay modes forbidden by the selection rule given by Eq. (2)). Similarly, the momentum and polarization of the emitted photons in the decay of triplet Ps is governed by *CP*, and *CPT* invariance, and hence observation of various properties of these photons can be used to test these symmetries (singlet decays are less informative as they are constrained into a smaller phase space region). The restrictions on the allowed angular correlations between decay photons has been described in detail by Bernreuther and co-workers [39]. We note that this treatment does not include the photon polarizations, since these cannot be easily measured; if they could be measured this could provide stronger constraints on symmetry violation tests. Recently the JPET detector [415] has demonstrated the potential to perform polarization sensitive measurements based on Compton scattering of gamma rays between detector elements, opening up the possibility of new symmetry tests [416].

3.5.1. Higher order decay modes and C invariance tests

In addition to the much-studied two and three-photon decay modes of singlet and triplet Ps, it is of course possible for Ps atoms to decay into more photons and still respect *C* invariance, as long as the number of decay photons is appropriately even or odd. Searches for the decay of a singlet (triplet) state to an odd (even) number of photons can, therefore, be used to directly test Charge conjugation invariance, and searches for decays into more than two or three photons can be used to test QED theory

How might *C* violating decays occur? Either the symmetry is not observed by nature, or they may proceed via a decay process other than electromagnetic interactions. This could be mediated by the weak interaction (e.g., [71,177–179]) or via an unknown particle (e.g., [417–422]). The rate for weak interaction mediated events can be calculated, and is extremely small and entirely negligible. No new particles have been identified in this way, and no evidence for *C* violation has been found so far, but several searches have been conducted, some of which being motivated by the positronium lifetime puzzle. The first was performed in an experiment in 1967 by Mills and Berko [423] that was designed to look for the decay of singlet Ps into three photons (i.e., $1\,^1S_0 \to 3\gamma$), which is forbidden by *C* invariance. Since this work many other measurements setting limits on higher order or forbidden decay modes have been performed, some of which are listed in Table 8.

Such experiments are designed to measure Ps annihilation radiation emission angles and energies over a wide range, generally via an array of detectors (e.g., [429]). In addition to low count rates for the processes of interest, the main difficulties to be overcome are related to large backgrounds arising from allowed decay processes, Compton scattering of radiation in the apparatus, bremsstrahlung from radiation emitted from the source and so on. Each detector arrangement will have specific background signals. Several large detector arrays have been constructed, based on different types of detectors, for example plastic scintillators in the JPET detector [415], high purity germanium (HPGe) in the GAMMASPHERE [430], thallium doped sodium iodide (NaI(Tl)) in the APEX detector [431], and bismuth germanate (BGO) crystals in the KAPAE detector [432]. The type of detector used as well as the geometry of the device allows for particular properties to be optimized, so, for example, the JPET detector has good time resolution but low detection efficiency, whereas the GAMMASPHERE detector has excellent energy resolution, but essentially no time resolution.

These kinds of large detector arrays are more akin to those used in high energy physics, or medical imaging, and are not widely used in Ps physics, largely owing to their cost and complexity. However, they have great potential for cutting edge experimentation, and precise measurements of Ps decay processes using large area or multi-component detectors with good spatial and time resolution is an obvious next step for this research. Because the detector response is

Table 9
Selection of different invisible o-Ps decay measurements. C.L is the confidence limit. Other experiments exist that rule out bosons in different mass ranges. Only a selection of results are shown here. Where applicable ΔE refers to the energy range of the unobserved particle(s) X^0 corresponding to the quoted upper limit. Here o-Ps^{mir} refers to mirror o-Ps, which subsequently decay to unobserved mirror gamma photons.

Decay mode	UL	C.L	ΔE (keV)	Ref.	Year
o-Ps $\rightarrow$ γX^0	2.8×10^{-6}	90%	0-800	[417]	1991
o-Ps $\rightarrow$ invisible	2.8×10^{-6}	90%	N/A	[433]	1993
o-Ps $\rightarrow \gamma X^0$	3×10^{-4}	90%	0–500	[418]	1994
o-Ps $\rightarrow \gamma X^0$	2×10^{-4}	90%	847–1013	[419]	1995
o-Ps $\rightarrow \gamma\gamma X^0$	6.2×10^{-6}	90%	0–200	[420]	1996
o-Ps $\rightarrow$ $\gamma X_1^0 X_2^0$	4.4×10^{-5}	90%	40–900	[434]	2002
o-Ps $\rightarrow$ invisible	4.2×10^{-7}	90%	0–80	[435]	2007
p-Ps $\rightarrow$ invisible	4.3×10^{-7}	90%	0–80	[435]	2007
o-Ps $\rightarrow$ o-Ps^{mir}	3×10^{-5}	90%	N/A	[327]	2020

a critical aspect of data interpretation these experiments generally require sophisticated simulations, as well as complex data acquisition systems, as is also the case in particle physics experiments. Given the possibilities for searches for New Physics (see Section 4), more collaborations between atomic and particle physicists in the future may be advantageous.

3.5.2. Invisible decays

In addition to Ps atoms decaying into forbidden numbers of photons, violating *C* invariance, some models have been proposed in which Ps atoms may decay into particles that are not observed, such as neutrinos, or unknown particles not included in the Standard Model (see Section 4). Ps decay processes mediated by the weak interaction are clearly allowed in the Standard Model, and the rates for such processes can be precisely calculated. One might expect that such mechanisms could provide a route to a determination of the neutrino mass, for example via exotic decay modes that depend on the mass distributions of different neutrino species [71]; in principle this is true but in reality the rates of such processes are highly suppressed by the exchange of heavy Z and $W^{\pm}$ bosons, as expected for electro-weak interactions. It is therefore not experimentally realistic to determine the neutrino mass via Ps decay processes. However, this approach can be used to test the existence of light Dark Matter via the virtual single-photon decay channel of Ps [422].

Invisible decays may also occur through the coupling of "regular" matter to mirror matter. Mirror matter was originally developed as a way to restore Parity conservation [436] by invoking a set of mirror particles that correspond to known particles, and interact predominantly via gravity (see Ref. [437] for a review). Mirror particles are strong Dark Matter candidates whose existence can be probed via Ps decays [438]. This is possible because neutral particles can mix with their mirror counterparts (charged particles cannot without violating charge conservation), so that o-Ps atoms can couple to mirror o-Ps atoms via a virtual single-photon annihilation process [439]. This would manifest as an apparent invisible decay, and was suggested as a possible solution to the (now resolved) ortho-positroniun lifetime puzzle [440], as were invisible decays to hypothetical light bosons in various mass ranges (see Table 9). These processes were already excluded from contributing to the puzzle (before it was resolved).

Searching for rare invisible decays involves recording a large number of events, and knowing with some accuracy when events are not being detected. This approach therefore requires a hermetic detector (i.e., a detector with very high overall detection efficiency, including the solid angle coverage) [432,438]. Detectors that have lower coverage must make use of extensive modeling.

3.5.3. CP and CPT invariance tests

The observation of Parity violation in weak interactions [441–443] proved that discrete symmetries are not necessarily respected by nature. However, it was believed that various combinations of symmetries would be, until *CP* violation was observed [444]. It is still widely believed that the combined operation of *CPT* is a true symmetry of nature that is strictly observed, partly because its violation would seriously undermine the quantum field theories upon which the Standard Model is based [445]. There is some interest in *CP* violating processes because (1) the lack of *CP* violation in strong interactions is not well understood (this is known as the strong *CP* problem [446]) and (2) it relates to a possible explanation for the apparent matter–antimatter imbalance in the Universe [447]; CP violation has been observed in the quark sector, and can be explained within the Standard Model, but this mechanism is too weak to explain the observed baryon asymmetry [448]. Therefore, *CP* tests in the lepton sector are potentially able to address this problem (i.e., Baryogenesis through leptogenesis [449]). Tests of *CPT* invariance may be performed based on comparisons between particles and antiparticles (which under *CPT* transformation should be exactly identical). For example, precision spectroscopy of antihydrogen is performed as a *CPT* test [5]. This symmetry is the only discrete symmetry that has never been observed to be violated.

The three photon decay of o-Ps can be used to test *CP* and *CPT* symmetries because correlations between the emitted photon momenta are governed by these symmetries. Some correlations are allowed according to QED, while others are forbidden [39,450]. Thus experiments designed to observe forbidden correlations can be used to test whether or not the

Table 10
Selection of different measurements of CP and CPT violating processes in Ps decay, as defined by the coefficients C_{CP} and C_{CPT} (see text). Note that the C_{CPT} value quoted for REF [451] was obtained from the analysis of [452]. Non-zero values of C_{CP} or C_{CPT} indicate violation of the corresponding symmetry.

Correlation	Result	Reference	Year
$\langle(\hat{S}\cdot\hat{k}_1)(\hat{S}\cdot\hat{k}_1\times\hat{k}_2)\rangle$	$C_{CP} = -0.0056 \pm 0.0154$	[453]	1991
$\langle(\hat{S}\cdot\hat{k}_1)(\hat{S}\cdot\hat{k}_1\times\hat{k}_2)\rangle$	$C_{CP} = 0.0013 \pm 0.0.0022$	[454]	2010
$\langle\vec{S}\cdot\hat{k}_1\times\hat{k}_2\rangle$	$C_{CPT} = 0.020 \pm 0.023$	[455]	1988
$\langle\vec{S}\cdot\hat{k}_1\times\hat{k}_2\rangle$	$C_{CPT} = 0.0140 \pm 0.0190$	[451]	2000
$\langle\vec{S}\cdot\hat{k}_1\times\hat{k}_2\rangle$	$C_{CPT} = 0.0071 \pm 0.0062$	[452]	2003

symmetries are respected in Ps decay. Given the usual convention $|\vec{k}_1| \geq |\vec{k}_2| \geq |\vec{k}_2|$, where $\vec{k}_i$ represents the ith decay photon momentum vector, *CP* and *CPT* forbidden angular correlations are [39,450] $\langle(\hat{S}\cdot\hat{k}_1)(\hat{S}\cdot\hat{k}_1\times\hat{k}_2)\rangle$ and $\langle\vec{S}\cdot\hat{k}_1\times\hat{k}_2\rangle$, respectively, where $\hat{S}$ is the spin of the Ps atom. Other forbidden correlations exist, but these are the only ones to have been tested.

Measurements are performed using multiple coincident gamma ray detectors with sufficient energy resolution to identify the $\vec{k}_i$ photons. In the case of the CPT forbidden correlation $\langle\vec{S}\cdot\hat{k}_1\times\hat{k}_2\rangle$, a non-zero correlation implies a difference between the number of decays with the normal to the decay plane parallel (N_+) to the spin direction and the number with the normal antiparallel (N_-) to the spin direction, since the quantity $\hat{k}_1\times\hat{k}_2$ defines a vector normal to the plane in which all three decay photons are emitted. The measured quantity is then [456]

$$A = \frac{N_+ - N_-}{N_+ + N_-}. \tag{71}$$

The asymmetry parameter A is converted to the correlation coefficient C_{CPT} taking into account the exact properties of the experimental arrangement. It is also critical to take into account the polarization of the Ps and various background effects that could lead to false signals. Similar considerations apply to the *CP* forbidden correlation $\langle(\hat{S}\cdot\hat{k}_1)(\hat{S}\cdot\hat{k}_1\times\hat{k}_2)\rangle$.

Only two *CP* tests using Ps decays have been performed to date [453,454,457], along with three *CPT* tests [451,452,455]. The results of these tests are shown in Table 10, in terms of correlation coefficients C_{CP} or C_{CPT}, where non-zero values indicate violation of the corresponding symmetry. As is evident from Table 10, no significant symmetry violations have been observed.

4. New Physics with positronium

In this section, we review the limitations of the Standard Model of particle physics and the mainstream physics beyond the Standard Model that potentially affect the spectroscopy of Ps. Similarly, the physics beyond the SM will impact different systems apart from Ps, and some of them are also covered here. In particular, we explain how astrophysical observations can be used to establish stringent constraints on the existence of novel particles interacting with SM leptons.

4.1. The Standard Model of particle physics

The Standard Model (SM) of particle physics is the most comprehensive theory of three of the four fundamental forces of nature, namely, the electromagnetic, weak, and strong nuclear forces. Within the SM, matter is constituted by six quarks and six leptons, as shown in the left panel of Fig. 11. Quarks are the fundamental constituents of neutrons and protons in the atomic nucleus. Quarks show a fractional charge and come in three different generations (columns of Fig. 11). Similarly, leptons appear in three generations, but they show an integral charge, and some are neutrals, such as neutrinos. Indeed, Ps is a leptonic atom constituted by an electron and a positron, as explained in Section 2.1.1.

The SM, more than a first-principle theory, may be considered an effective theory of the interaction between fundamental particles [458–460]. The SM has been developed as a hybrid framework of beautiful theoretical models and intriguing experimental results. The SM describes the strong nuclear force through quantum chromodynamics, which is mainly a Yang–Mills theory with SU(3) symmetry, in which the carrier of the color force is the gluon, g. The electromagnetic interaction through QED has a $U(1)$ symmetry, and its carrier is the photon, γ. The weak nuclear force is described within the same framework as electromagnetism in the so-called electro-weak interaction showing a SU(2) symmetry. As a result, the weak force carriers are three massive vector gauge bosons: one neutral, Z, and two charged $W^{\pm}$. Last but not least, we find the Higgs boson, H, the particle that explains the mass of the vector gauge bosons via the Higgs mechanism [461,462]. Even though it may look that the discovery of the Higgs boson was the last piece of the SM, still there is a lot of fundamental questions regarding the nature of the Higgs potential. For instance, the SM may be a proper description of nature up to the Planck scale depending on the Higgs self-coupling [463–465].

4.1.1. Limitations of the standard model

The SM of particle physics is the most elegant and comprehensive theory of nature and it has successfully explained some of the most intriguing phenomena of modern physics in the XX and XXI centuries. However and despite its success, the SM faces limitations regarding new and unexplained phenomena and crucial questions in modern cosmology and particle physics. In this section, we review the most relevant phenomenology, based on the scope of this review, not properly interpreted within the SM.

- The neutrino sector. In the SM, neutrinos are massless particles since they do not couple to the Higgs. However, it is an empirical fact that neutrinos change flavor as they travel long distances, the so-called neutrino oscillations [466], meaning that neutrinos have a small mass. Furthermore, this opens up a debate about the inherent nature of neutrinos as Majorana or Dirac fermions.
- The strong CP problem. Quantum chromodynamics preserves the CP (charge conjugation-parity) symmetry although, *a priori*, there is no reason for it. This surprising fine-tuning problem can be solved by invoking the existence of a new particle: the axion [446,467], which is not included in the SM. Indeed, we will discuss further in this section about axion-like particles motivated by the pioneering work of Peccei and Quinn.
- Dark Matter (DM). From the rotation curves of galaxies to the large-structure of the universe, there are strong evidences of the existence of Dark Matter, which constitutes around 85% of the matter of the universe [468–470]. However, despite its ubiquitousness, its nature remains a mystery due to the large mass range in which one may expect signals from SM-Dark Matter particles interactions. Nowadays, it is necessary for a collaborative effort between the high energy physics with the condensed matter physics and atomic, molecular, and optical physics communities to explore different avenues to detect light Dark Matter (Dark Matter with a mass below the proton mass) [471–474], which is of interest for the scope of this review.
- Dark energy. It is an observational fact that 74% of the energy budget of the universe is in the form of unknown energy called dark energy [469,470]. Dark energy is a global energy that accelerates the expansion of the universe, although its nature is unknown. We know very little about this energy, and indeed, elucidating its nature is one of the fascinating fundamental questions in modern physics.
- Baryogenesis. The SM predicts that matter and antimatter should be created equally in almost any process. However, the baryonic matter of the universe, i.e., excluding DM, appears to be constituted of fundamental particles instead of anti-particles. The conditions for an asymmetry between baryonic and anti-baryonic matter are known as the Sakharov conditions [475]: (1) A mechanism that does not conserve the baryon number. (2) C and CP symmetries must be violated, implying that the early universe should not show time-reversal symmetry. (3) It is necessary for a system out of equilibrium. However, the SM predicts a very small CP violation to explain matter-antimatter asymmetry. Therefore, new models and theories are still to come to elucidate this fascinating mystery.

4.2. New Physics

New physics (NP) refers to the study of theoretical models aimed to extend the SM or to propose alternative frameworks to explain observed phenomena. The field of NP is vast, and often it requires a collaborative effort across distinct disciplines of physics. A prime example is the interplay between atomic, molecular, and optical (AMO) physics and high energy physics, leading to unique findings complementing the phenomenology in the high energy front, as sketched in Fig. 10. The AMO physics contribution to NP is mainly based on high-precision spectroscopy studies of atoms and molecules to check the SM predictions' accuracy and elucidate the role of new interactions and forces. Surprisingly enough, with the same observables it is possible to place stringent constraints on the electric dipole moment (EDM) of the electron [41,476,477], study the existence of extra dimension through the Arkani-Hamed, Dimopoulos, and Dvali model of gravity [478–483], establish new limits on the time variation of the electron-to-proton mass ratio [483–486] and the fine structure constant [487], and the quest of the fifth force [488,489]. In addition, recently it has been shown that atomic and molecular systems are good candidates for direct detection of light Dark Matter particles [422,472–474,490].

In this section, we focus on the most relevant models for the study of new physics with Ps. We introduce a well-motivated model in which a vector mediator bridges SM leptons with scalar Dark Matter particles known as the vector portal within the set of hidden sector models. Based on such a model, Ps could be a good candidate for detecting Dark Matter particles [422]. Similarly, we analyze the relevance of hypothetical scalar and pseudo-scalar particles on the spectroscopy of Ps by looking at the electronic states' energy shifts in Ps through novel spin-independent and spin-dependent interactions.

4.3. Natural units and atomic units

Atomic units are the standard units in atomic, molecular, and optical physics, i.e., $\hbar = 1$. However, in high energy physics, it is preferable to work in natural units, i.e., $\hbar = c = 1$. As a result, it is necessary to interpret the results based on natural units into atomic units, which usually induces some difficulties. Independently of the confusion to change between these two sets of units, it is essential to develop a specific intuition about characteristic scales in natural units. This is very important to correctly identify the mass range of novel particles susceptible to affect spectroscopic observables

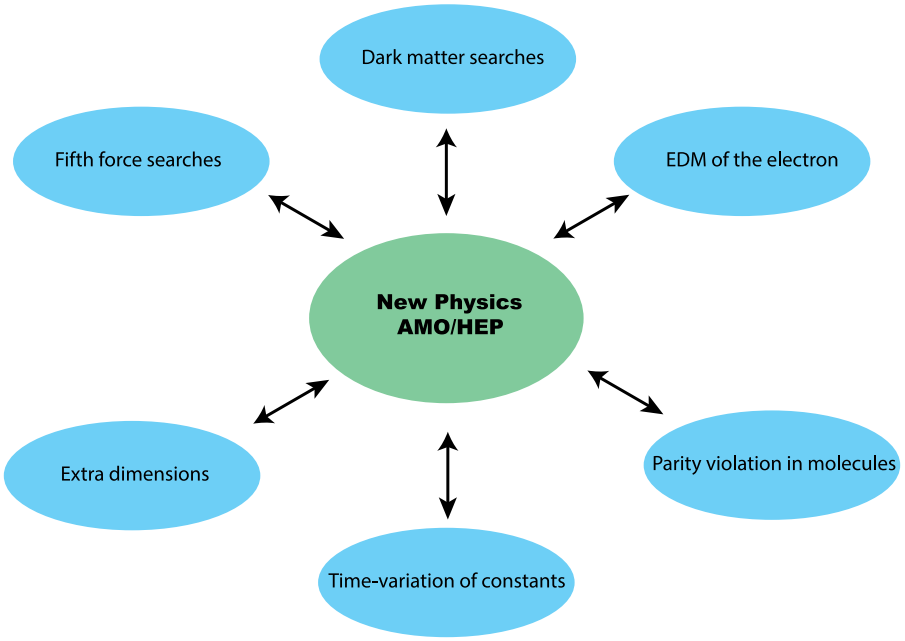

Fig. 10. New physics at the interplay between atomic, molecular and optical (AMO) physics and high energy physics (HEP). Atoms and molecules are a valuable probe of new physics, shown as the blue shapes in the diagram.

in atomic and molecular systems. Therefore, we believe that it is worth introducing the basics of natural units and how they relate to atomic units.

In natural units, mass M using the celebrated Einstein's relation, $E = mc^2$, is equivalent to energy, which implies that the unit of mass is GeV/c^2. For instance, the mass of the electron is 511×10^{-6} GeV/c^2. In natural units, length L and time T have the same units, and taking into account $\hbar c = 1$ leads to $L \equiv T = 1/E$, and their units are c^2/GeV. Consequently, in natural units, the cross section has units of $(\text{GeV/c}^2)^{-2}$, and the rate of a process has units of GeV/c^2.

To transform from natural units to atomic units is essential to keep in mind that $L = \hbar c/E$, and in atomic units c$=$ 137. As a result, one finds

$$\frac{1}{\text{GeV/c}^2} \equiv \frac{511 \times 10^{-6}}{137} a_0 = 3.73 \times 10^{-6} a_0, \tag{72}$$

where a_0 is the Bohr radius ($a_0 \equiv 0.529177 \times 10^{-10}$ m). Therefore, the unit of length in natural units is tiny in comparison with the typical extension of atomic and molecular systems. Similarly, it is possible to invert such expression to find that $a_0 = 1/3.73\ (\text{keV/c}^2)^{-1}$. In this section, when analyzing the existence of new particles we explore a mass range between 10 MeV/c^2 and 0.1 keV/c^2, which corresponds to a length of 3.73×10^{-4} a_0 and 37.3 a_0, respectively.

4.3.1. Vector portal to Dark Matter and its relevance on Ps

There are many theoretical models that, in principle, accommodate some of the phenomenology that the SM cannot explain regarding Dark Matter and the existence of novel particles. One well-motivated framework is the hidden sector, in which one assumes that a set of fields and symmetries are hidden in nature. In particular, it is assumed that there are more symmetries that the ones contemplated on the SM, however these are unnoticed, although under given circumstances they may manifest due to its effects on the SM particles [491–501], as it is sketched in Fig. 11. Within this model, one finds the well-known SM sector, i.e., the set of particles and interactions within the SM, and the hidden sector, which represents new particles that do not directly interact with SM particles, as may be the case of DM. These two independent sectors interact through portals, i.e., new particles that mediate between the SM and hidden sectors.

Here, we focus on the vector portal in which the mediator is the dark photon [502–506], opening up the possibility of milli-charged DM particles [491,492,494]. The dark photon is a vector mediator, A'_μ, that shows a hidden $U_D(1)$ symmetry (not contemplated in the SM) similar to the charge of the electromagnetic interaction and it couples with the hypercharge $U_Y(1)$ symmetry as

$$\frac{\epsilon}{2\cos\theta_W} B^{\mu\nu} F'_{\mu\nu}, \tag{73}$$

where $F'_{\mu\nu} = \partial_\mu A'_\nu - \partial_\nu A'_\mu$, $B^{\mu\nu}$ is the hypercharge field strength, θ_W is the weak mixing angle, and ϵ is a parameter that specifies the strength of the coupling between the $U(1)$'s symmetries [501]. After the electroweak symmetry breaking

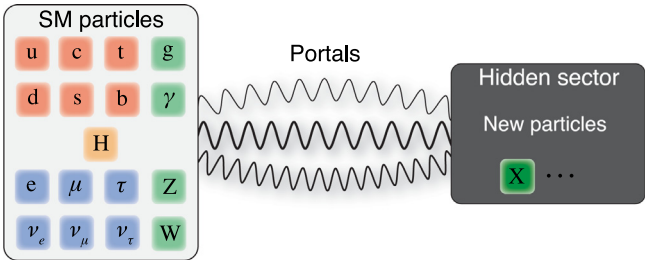

Fig. 11. A sketch of the hidden sector framework for physics beyond the standard model. Within this approach, on the one hand, one finds the SM of particle physics composed of three generations of quarks (fermions), three generations of leptons (fermions), four carriers (bosons) regarding electromagnetism, weak interaction and color, and one scalar boson, the Higgs, H, giving mass to the quarks through the Higgs mechanism. On the other hand, one finds the hidden sector containing new particles like new scalars X (e.g., constituting Dark Matter) that couple to the standard model of particles through portals. These portals contain mediators between new particles and the SM model ones. One kind of portal is the vector portal, which is explained in the text.

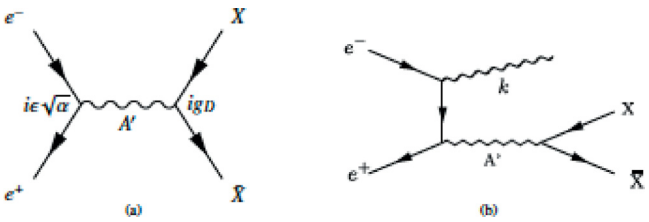

Fig. 12. Production of scalar Dark Matter via a dark photon in e^-–e^+ collisions. Panel (a), off-shell production: a dark photon A' couples the SM sector and the dark sector particle X and its antiparticle $\bar{X}$. Panel (b) shows the on-shell production of scalar Dark Matter via a dark photon in e^-–e^+ collisions. There is a second contributing diagram in which the photon is emitted from the positron's leg.

Eq. (73) translates into a kinetic mixing with the photon, and the full Lagrangian reads as

$$\mathcal{L} \supset -\frac{1}{4}F_{\mu\nu}F^{\mu\nu} - \frac{1}{4}F'_{\mu\nu}F'^{\mu\nu} + \frac{\epsilon}{2}F_{\mu\nu}F'^{\mu\nu} + \frac{1}{2}m^2_{A'}A'_\mu A'^\mu + eA_\mu J^\mu_{EM} + g_D A'_\mu J^\mu_D, \tag{74}$$

where the kinetic mixing term $\frac{\epsilon}{2}F_{\mu\nu}F'^{\mu\nu}$ shows the coupling between the dark photon and the SM photon explicitly and ϵ defines its strength. The mass of the dark photon can be explained via a dark Higgs mechanism in which a massive dark Higgs boson is integrated out of the theory [507]. In Eq. (74), the dark photon field does not couple directly to the SM charged particles since it does not couple to the SM current J^μ_{EM}. However, it does with the dark current J^μ_D through a gauge coupling g_D. By introducing a vector field as

$$\tilde{A}_\mu = A_\mu - \epsilon A'_\mu, \tag{75}$$

Eq. (74) yields

$$\mathcal{L} \supset -\frac{1}{4}\tilde{F}_{\mu\nu}\tilde{F}^{\mu\nu} - \frac{1-\epsilon^2}{4}F'_{\mu\nu}F'^{\mu\nu} + \frac{1}{2}m^2_{A'}A'_\mu A'^\mu + e\left(\tilde{A}_\mu + \epsilon A'_\mu\right)J^\mu_{EM} + g_D A'_\mu J^\mu_D, \tag{76}$$

where it is clear that the dark photon couples with the SM charged particles via ϵ. Therefore, the kinetic mixing of the dark photon with the photon translates into a coupling of the dark photon to SM charged particles, and at the same time to the dark current. In other words, the dark photon bridges the SM charged particles and particles in the hidden sector.

Let us assume that DM belongs to a hidden sector and the dark current is given by

$$J^\mu_D = \bar{X}\gamma^\mu X, \tag{77}$$

which in virtue of Eq. (76) denotes a vertex in which the dark photon field is coupled to a DM fermionic particle X and its antiparticle $\bar{X}$ with a coupling strength g_D. As a consequence, the scattering of SM-charged particles could potentially produce DM particles, or the existence of DM may affect the scattering properties between charged particles. In particular, electron–positron scattering may produce DM particles through an off-shell dark photon mediator [491,508], as shown in panel (a) of Fig. 12, or via an on-shell dark photon mediator with the emission of a photon [491,508], as sketched in panel (b) of the same Figure. At low collision energies, it would be possible to constrain the existence of sub-GeV DM, as Essig et al. have suggested [491], and the results are shown in Fig. 13, where it also appears the constraints coming from the value of the muon anomalous magnetic dipole moment [509] depicted as the shaded region. This figure suggests that performing electron–positron collision experiments at a relatively low center of mass-energy can be a sensitive tool to explore the existence of dark photons and the production of fermionic DM particles beyond the constraint due to the anomalous magnetic dipole moment of the muon.

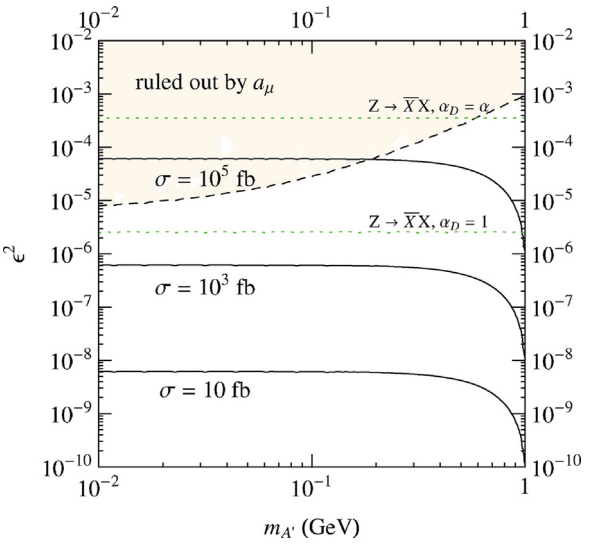

Fig. 13. Cross section (center-of-mass energy of 10.58 GeV) for production of on-shell dark photons [see panel (b) of Fig. 12] at a as a function of the mass of the dark photon $m_{A'}$ and ϵ^2. Solid lines correspond to a contour showing the same value of the cross section. The cross section is given in fb $\equiv 10^{-39}$ cm^2. Also shown are the constraints on the couplings from measurements of the muon anomalous magnetic dipole moment (shaded regions) [509]. The dashed lines denote the lower bounds for DM production in rare Z-decays. In the notation of this figure $\alpha_D \equiv g_D$.
Source: Figure reproduced with permission from Ref. [491].

The kinetic mixing between $U_D(1)$ and $U_Y(1)$ also induces a coupling between the Z boson and particles in the hidden sector. Therefore, the direct decay $Z \to X\bar{X}$ is another possible decay process in which DM particles could be detected. The results of using this decay process appear as green-dashed lines in Fig. 13. However, this decay channel is not a good candidate for sensitive DM production and further detection.

Electron–positron scattering can be used to explore the existence of dark photons and the nature of DM particles. Thus, it seems natural to extend the validity of that statement to Ps. However, in the case of Ps, the transition matrix elements differ from the ones associated with collision experiments since Ps is a bound state. Furthermore, Ps shows an SM single-photon decay mode competing with the production of on-shell dark photons. However, luckily enough, the SM decay rate for such a process is extremely slow $\approx 10^{-13}$ s^{-1} [178,179,422] due to the largely suppressed exchange of heavy Z and W bosons in Ps. Therefore, in principle, it would be possible to look at the single-photon decay of Ps as a signal for DM detection [422].

The decay rate of Ps into a single photon mediated by a dark photon is given by

$$\Gamma_{\mathrm{Ps}\to\gamma} = 4 v_{\mathrm{rel}} |\psi_{\mathrm{Ps}}(0)|^2 \sigma_{e^+e^-\to\gamma X\bar{X}}, \tag{78}$$

where v_{rel} stands for the relative velocity of the leptons, X and $\bar{X}$ can be a fermionic particle and anti-particle or a couple of complex scalar fields, for instance. The decay rate is weighted by the probability to find the electron and the position at the same position

$$|\psi_{\mathrm{Ps}}(0)|^2 = \frac{m_e \alpha^3}{8\pi}. \tag{79}$$

The cross section for electron–positron scattering decaying into a pair particle–antiparticle and emitting a photon is given by

$$\sigma_{e^+e^-\to\gamma X\bar{X}} = \frac{1}{4 m_e v_{\mathrm{rel}}} \int \frac{d^3\mathbf{p}_3}{2(2\pi)^3 E_3} \int \frac{d^3\mathbf{k}}{2(2\pi)^3 |\mathbf{k}|} \int \frac{d^3\mathbf{p}_4}{2(2\pi)^3 E_4} (2\pi)^4 \delta^{(4)}(P - p_3 - p_4 - k) \langle |\mathcal{T}|^2 \rangle, \tag{80}$$

where $\delta^{(4)}(x)$ represents a four-dimensional Dirac delta function guaranteeing the momentum–energy conservation during the scattering process, $\mathbf{k}$ is the wave vector for the emitted photon, $p_3^\mu = (E_3, \mathbf{p}_3)$ and $p_4^\mu = (E_4, \mathbf{p}_4)$ represent the energy–momentum vectors of the DM particles and $P^\mu = p_1^\mu + p_2^\mu \simeq (2m_e, \mathbf{0})$ is the total energy–momentum in the center of mass. p_1^μ and p_2^μ stand for the energy–momentum vector of the leptons and $\langle |\mathcal{T}|^2 \rangle$ is the spin and polarization averaged transition matrix [422].

Assuming that DM is a complex scalar field, the transition matrix associated with the Feynman diagram of the panel (b) of Fig. 12 is given by

$$\mathcal{T} = \frac{g_D \sqrt{4\pi\alpha}\epsilon}{p_{A'}^2 - m_{A'}^2} \left[\bar{v}(p_2) \left\{ (\not{p}_3 - \not{p}_4) \left(\frac{\not{p}_1 - \not{k} + m_e}{(p_1 - k)^2 - m_e^2} \right) \gamma \cdot \epsilon(k) \right.\right.$$

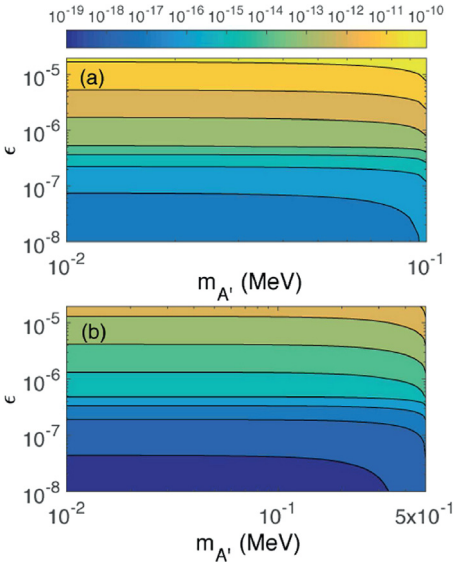

Fig. 14. Branching ratio of Ps $\to X\bar{X}\gamma$ with respect to SM prediction for the two-photon decay mode p-Ps as a function of the dark photon mass, $m_{A'}$, and the kinetic mixing parameter ϵ. Panel (a) $m_X = 50$ keV and for panel (b) $m_X = 250$ keV. $g_D = e$ and the values of ϵ shown are consistent with the latest constrains from the NA64 collaboration at CERN [510,511]. The range of mass for the dark-photon in panel (a) is different than in panel (b) since one needs to impose that $m'_A \leq 2m_X$ to ensure the stability with respect to the $X\bar{X}$ channel.
Source: Figure reproduced with permission from Ref. [422].

$$+\gamma\cdot\epsilon(k)\left(\frac{\not{k}-\not{p}_2+m_e}{(k-p_2)^2-m_e^2}\right)(\not{p}_3-\not{p}_4)\Big\}u(p_1)\Big], \tag{81}$$

where the contribution of a second diagram where the photon emerges from the positron leg has been included. Using the result of Eq. (81) into Eqs. (80) and (78) it is possible to predict the single-photon emission rate mediated by dark photons. And with it, the branching ratio between p-Ps$\to X\bar{X}\gamma$ and the two-photon decay mode of p-Ps as

$$B(\text{p-Ps}\to X\bar{X}\gamma)=\frac{\Gamma_{p-Ps\to X\bar{X}\gamma}}{\Gamma_{p-Ps\to\gamma\gamma}}=\frac{1}{m_e c^2\alpha^5/2}\Gamma_{p-Ps\to X\bar{X}\gamma}, \tag{82}$$

which is shown in Fig. 14 as a function of the mass of the dark photon, $m_{A'}$, and ϵ, for a given DM particle mass, m_X. Assuming that a branching ratio up to 10^{-12} may be detectable in future experiments, the single-photon decay process mediated by a dark photon in Ps could be sensitive to $\epsilon \lesssim 10^{-6}$. Thus, expanding the actual constraints for the range of masses of the dark-photon under consideration. To summarize: the single-photon decay mode of p-Ps helps to search for dark light photons and slightly expands the dark photon's constraints in the studied mass range.

4.3.2. Constraints on new scalar from Ps spectroscopy

A hypothetical new scalar particle after the electroweak symmetry breaking is coupled with SM fermions by the following interaction term

$$\mathcal{L}_\phi^{\text{int}}=-\imath g_e\bar{\Psi}(x)\Psi(x)\phi(x), \tag{83}$$

where Ψ denotes a fermionic SM field, ϕ is the field associated with the new scalar and g_e is the coupling strength of the interaction. As a result, the electron–positron interaction will have an additional contribution as it is shown in Fig. 15. In the non-relativistic limit, such a diagram translates into a Yukawa potential given in natural units by [31–33,497]

$$V(r)=\frac{g_e^2}{4\pi}\frac{e^{-m_\phi r}}{r}, \tag{84}$$

where m_ϕ is the mass of the new scalar and r stands for the electron–positron relative distance.[2]

Let us consider two different levels of the spectra of a Ps atom, labeled by $|i\rangle$ and $|f\rangle$, respectively, as depicted in Fig. 16. We are going to assume that the energy spacing between these two levels is determined experimentally as $E^{\text{exp}}_{i\to f}$, with an accuracy $\Delta E^{\text{exp}}_{i\to f}$. Similarly, we assume that the energy difference between those two states can be determined

2 The same potential appears when assuming a vector coupling through a new gauge boson.

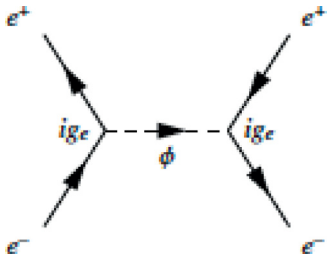

Fig. 15. Contribution of a new scalar ϕ into electron–positron scattering. A new scalar particle couples with the SM leptons via the Yukawa potential given in Eq. (84). As a result, the energy levels of Ps will experience a shift that, in principle, may be experimentally observed.

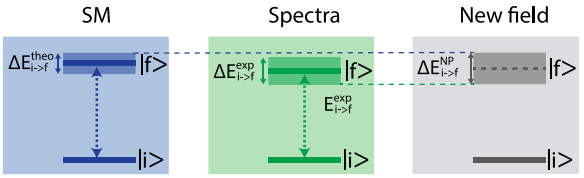

Fig. 16. Schematic representation of the impact of a new particle on the energy levels of Ps. The energy spacing between two levels in Ps ($|i\rangle$ and $|f\rangle$) is calculated through the SM $E^{\text{theo}}_{i\to f}$ with a precision $\Delta E^{\text{theo}}_{i\to f}$. Similarly, the same observable can be measured experimentally: $E^{\text{exp}}_{i\to f}$ for the energy difference, and $\Delta E^{\text{theo}}_{i\to f}$ for the accuracy. The effect of a new particle will cause a shift on the energy difference between the two states labeled as $\Delta E^{\text{NP}}_{i\to f}$, which has to lie within the limits set by the dashed lines [Eq. (85)].

theoretically based on the Standard Model (QED in this case) $E^{\text{theo}}_{i\to f}$ with a precision $\Delta E^{\text{theo}}_{i\to f}$, and both results agree within the uncertainties. In this scenario, the existence of new physics is constraint by

$$|\Delta E^{\text{NP}}_{i\to f}| < |\Delta E^{\text{exp}}_{i\to f} - \Delta E^{\text{theo}}_{i\to f}| \lesssim 2\text{Max}\left(\Delta E^{\text{exp}}_{i\to f}, \Delta E^{\text{theo}}_{i\to f}\right), \tag{85}$$

where $\Delta E^{\text{NP}}_{i\to f}$ is the energy shift of the levels caused by the interaction between the new particle and leptons. In other words, the effect of a new interaction over leptons cannot induce a shift of the energy levels larger than the accuracy of the experimental measurements plus the precision of the theoretically predicted value. The energy shift caused by a new particle is calculated as

$$\Delta E^{\text{NP}}_{i\to f} = \langle\psi_{\text{f}}|V(r)|\psi_{\text{f}}\rangle - \langle\psi_{\text{i}}|V(r)|\psi_{\text{i}}\rangle, \tag{86}$$

where $V(r)$ is the effective potential as a result of the interaction between the novel scalar and SM leptons.

For a scalar mediator, $V(r)$ depends on two parameters: the coupling strength and the mass of the mediator. Using spectroscopy data of Ps and QED calculations it is possible to constrain the relevant coupling strength of the interaction as a function of the mass of the mediator, as it is shown in Fig. 17. This figure shows that the most stringent constraint over the parameter space relevant for a new scalar comes from the $1\,^3S_1 \to 2\,^3S_1$ transition. These results are obtained using the most accurate experimental measurement for the $1\,^3S_1 \to 2\,^3S_1$ transition in Ps [252]

$$E^{\text{exp}}_{1S\to 2S} = 1233607216.4 \pm 3.2 \text{ MHz}, \tag{87}$$

and the most precise theoretical prediction [126,155]

$$E^{\text{theory}}_{1S\to 2S} = 1233607222.12 \pm 0.58 \text{ MHz}. \tag{88}$$

In the same figure, it is shown the constraint assuming that a new scalar induces a shift equal to 2.77 MHz for the 2S→2P transition. Indeed, it corresponds with the observed discrepancy between QED prediction and the measurement for the $2\,^3S_1 \to 2\,^3P_0$ transition [328,338] (see Section 3.3.1). It is conspicuous that a new scalar field could not explain such discrepancy because the relevant parameter space has been ruled out by previous spectroscopic studies in Ps [252]. Indeed, it is further constrained by measurements of the gyromagnetic factor of the electron, a_e, [35] and even a more drastic bound is due to astrophysical observations (shaded gray region), as we explain in Section 4.4. In addition, we have calculated the expected reach for the 1S→2S and 2S→2P transitions assuming that the experimental precision matches the theoretical accuracy, and the results are shown as the dashed lines in Fig. 17. The orange-dashed line refers to bounds based on the $1S-20S$ transition assuming an accuracy ∼500 kHz, which surpasses at low scalar masses the reach based on the electron gyromagnetic factor. Therefore, Rydberg states in Ps may be more efficient in constraining the existence of new scalar particles for masses $m_\phi \lesssim 1$ keV/c^2.

It is worth noticing that the transitions show their maximum reach at $m_\phi \sim 2$ keV/c^2, which corresponds with the typical atomic size of Ps $\sim 2a_0$. Similarly, for low scalar masses, transitions involving states with different electronic

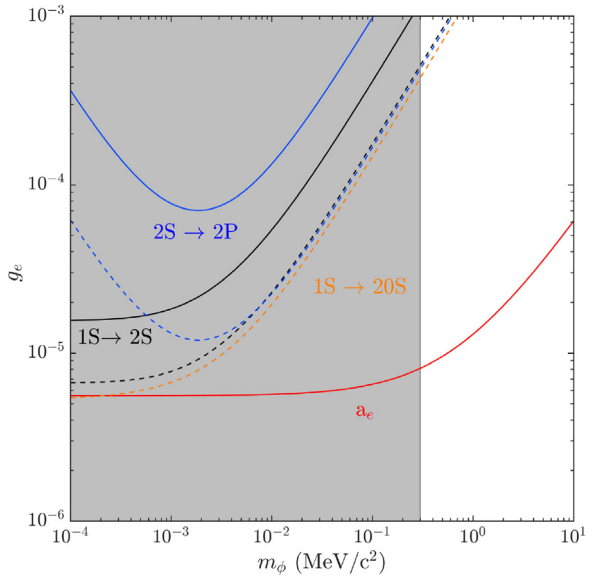

Fig. 17. Coupling strength of a hypothetical scalar mediator with the leptons as a function of the mediator's mass. The black line stands for the bound regarding for the Ps 1S → 2S transition [252], whereas the black-dashed curve stands for the reach assuming that the experimental accuracy matches the theoretical precision of 0.58 MHz. The blue line denotes the lower bound for a shift of 2.77 MHz for $2^3S_1 \rightarrow 2^3P_0$, and the dashed blue line represents the same observable assuming that the experimental accuracy matches the theoretical one. The dashed-orange line corresponds to a Rydberg excitation 1S→ 20S assuming a precision of 500 kHz. The red line is the bound coming from electron gyromagnetic factor [35], a_e, using the most precise value for the fine structure constant [512]. The shaded gray region represents parameter space constrained by astrophysical observations explained in Section 4.4 [36].

angular momentum show a more steep behavior due to the faster decay of the electronic wave function for $l > 1$ at long distances. Therefore, the large mass region is dominated by the S-states since they show a certain probability of finding the two leptons very close, whereas the low-mass region is dominated by P-states showing a faster decay with large distances.

4.3.3. Constraints on axion-like particles from Ps spectroscopy

A hypothetical pseudoscalar or axion-like particle, after the electroweak spontaneous symmetry breaking, interacts with the leptons of the SM with the following Lagrangian [513]

$$\mathcal{L}_{\rm ALP}^{\rm int} = -ig_e^{\rm ALP}\bar{\Psi}(x)\gamma^5\Psi(x)\phi(x), \tag{89}$$

leading to a similar contributing diagram to the electron–positron scattering as the one depicted in Fig. 15. In the non-relativistic limit, the interaction of a pseudoscalar of mass $m_{\rm ALP}$ with electrons and positrons translates into a potential that reads as [32,513,514].

$$V^{\rm ALP}(r) = -\frac{\left(g_e^{\rm ALP}\right)^2}{12\pi m_e^2}\left[\boldsymbol{S}_1\cdot\boldsymbol{S}_2\left(4\pi\delta^3(\mathbf{r}) - \frac{m_{\rm ALP}^2 e^{-rm_{\rm ALP}}}{r}\right) - \frac{S_{12}(\hat{r})}{4}\left(\frac{m_{\rm ALP}^2}{r} + \frac{3m_{\rm ALP}}{r^2} + \frac{3}{r^3}\right)e^{-rm_{\rm ALP}}\right], \tag{90}$$

where m_e is the electron mass, r is the electron–positron distance, $\boldsymbol{S}_i$ is the spin operator of the ith lepton, $\delta^3(\mathbf{r})$ represents the three-dimensional Dirac delta function and

$$S_{12}(\hat{r}) = 4\left[3\left(\boldsymbol{S}_1\cdot\hat{r}\right)\left(\boldsymbol{S}_2\cdot\hat{r}\right) - \boldsymbol{S}_1\cdot\boldsymbol{S}_2\right], \tag{91}$$

is a tensor operator.

The structure of Eq. (90) makes clear that the interaction with an axion-like particle only affects electronic states with $l \neq 0$ and leads to a spin-dependent energy shift. The bounds over the parameter space for axion-like particles are based on the most accurate observations and most precise calculations for the hyperfine splitting (HFS)

$$\Delta E_{\rm HFS} = E(1^1S_0) - E(1^3S_1), \tag{92}$$

and the ultrafine splitting given by Eq. (19) with $n = 2$ of Ps are shown in Fig. 18. In this figure, it is noticed that the constraint from the HFS (black line) is surpassed by the ultrafine splitting, assuming an accuracy equal to the theoretical

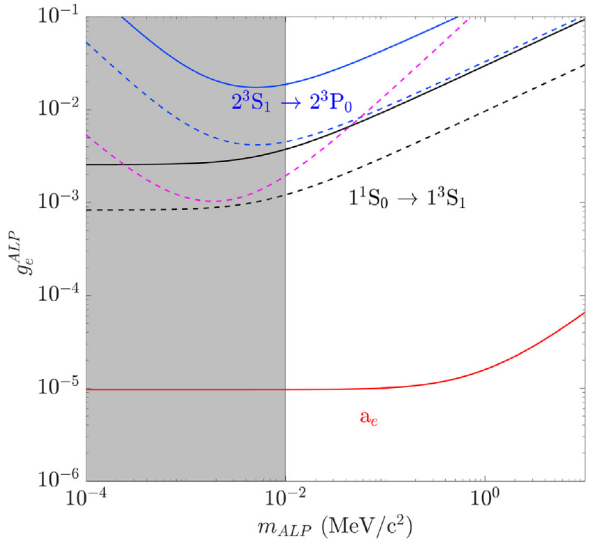

Fig. 18. Constraint on the coupling strength as a function of the axion-like particle mass. The black line represents the bound for the HFS in Ps, whereas it dashed version represents the bound, assuming that the experimental accuracy matches the theoretical one. The blue line denotes the lower bound for a shift of 2.77 MHz for $2^3S_1 \rightarrow 2^3P_0$, and the dashed blue line represents the same observable assuming that the experimental accuracy matches the theoretical one. The dashed-magenta line corresponds to the ultrafine splitting in Ps, assuming that the experimental accuracy matches the theoretical precision. The red line is the bound coming from electron gyromagnetic factor [35], a_e, using the most precise value for the fine structure constant [512]. The shaded gray region represents parameter space constrained by astrophysical observations explained in Section 4.4 [36].

one of 2.6 kHz [126] (dashed-magenta line). However, the most stringent constraints are obtained for the HFS, assuming that the experimental precision matches the theoretical one of 0.22 MHz [126]. The blue line is for a particular shift of 2.77 MHz that corresponds with the deviation between the QED prediction and the latest measurements [338] and a projection assuming that the experimental accuracy matches the theoretical one of 0.08 MHz. As a result, the mentioned discrepancy cannot be explained by axion-like particles since the observation of other spectroscopic lines in Ps rules out the relevant region of the parameter space. Furthermore, a more strict constraint comes from the electron's gyromagnetic factor measurements, as in the scalar mediator's case shown above. In addition to this striking result, it is interesting to notice that, transitions involving P-states show the same trend for low masses: a power-law behavior as a function of the mass of the mediator. This observation indicates that the low-mass limit is readily controlled by the decay of the electronic wave function at long distances.

4.4. Astrophysical constraints on new physics competing with positronium bounds

A new particle beyond the Standard Model has an impact on the energy transfer mechanisms of a star. In particular, a fraction of the energy produced by nuclear reactions in the core, $\epsilon_{\rm Nuc}$, is transformed into the emission of new particles ϵ_ϕ that freely stream (potentially) through the star [515]. However, the effect of a novel particle depends on the kind of star under consideration. For instance, the duration of the different stages on the evolution of a star is sensitive to the existence of novel interactions and particles [36,516–526].

The most relevant observable for constraining the existence of new fields is the helium-burning lifetime. This is determined by measuring the ratio, R, between stars on the horizontal branch stage with respect to stars in the red giant phase within the same globular cluster.[3] The size of globular clusters is much smaller than the distance from us. Therefore it is safe to assume that all the stars in a globular cluster are at the same distance from us. After comparing observations with state-of-the-art simulations, R is determined within 10% of accuracy. As a result, the impact that a novel particle will have is limited by such an error bar. In particular, the 10% accuracy on R leads to

$$\epsilon_\phi = 0.1 \times \epsilon_{\rm He}, \tag{93}$$

where $\epsilon_{\rm He} \approx 80$ erg g^{-1} s^{-1} (1 erg $\equiv 10^{-7}$ J $\equiv 0.62$ TeV/c^2) and stands for the energy generation rate in the star's core assuming a typical core mass of 0.5 $M_\odot$. Therefore, the existence of a novel particle may induce an energy loss rate $\epsilon_\phi \lesssim 10$ erg g^{-1} s^{-1}.

[3] These are gravitationally bound systems of several thousand to 10^6 stars presenting a roughly spherical shape, and its typical density can exceed 10^6 of solar masses per cubic parsec ($\approx 4 \times 10^7$ hydrogen atoms per cubic centimeter) [527–529].

In the core of horizontal-branch stars a novel particle interacting with leptons induces an energy loss rate based on the following processes:

- Compton scattering. A photon scatters off an electron leading to the emission of a new scalar or pseudoscalar particle, ϕ, i.e.,

$$\gamma + e \to e + \phi. \tag{94}$$

- Bremsstrahlung. An electron scatters off an alpha particle leading to the formation of a novel particle

$$e + {}^4\mathrm{He} \to e + {}^4\mathrm{He} + \phi. \tag{95}$$

Each process's relevance depends on the nature of the novel particle under consideration and the media's physical conditions, i.e., density and temperature. For horizontal-branch stars, $\rho \sim 10^4$ g cm^{-3} and $T \sim 10^8$ K, and the plasma is mainly non-degenerate.

Novel scalars. For a novel scalar particle the main contribution to the energy loss of a star is through bremsstrahlung and after imposing $\epsilon_\phi \lesssim 10$ erg g^{-1} s^{-1} one finds a coupling constant $g_e \geq 1.3 \times 10^{-14}$ valid in a range of $m_\phi \lesssim 30$ keV [521,530,531]. Indeed, a stringent constraint appears when plasma mixing effects are included [36] displayed as the shaded region in Fig. 17.

Novel pseudoscalars. The Compton scattering process dominates the contribution of pseudoscalars or axion-like particles to the energy loss of a star. In this case, a constraint comes from Compton processes when the helium ignites into carbon on a red giant star to become a horizontal branch star. In this case, it can be shown that $\epsilon_\phi \lesssim 10$ erg g^{-1} s^{-1} is a good constraint on the energy loss rate [521] which leads to $g_e^{\mathrm{ALP}} \leq 4.5 \times 10^{-13}$ for $m_\phi \lesssim 10$ keV [521,532–538]. Indeed, this constraint appears as the shaded region in Fig. 18.

5. Prospects for the future

The major theoretical goal is the completion of energy corrections at $O(m_e\alpha^7)$. Theory at the $O(m_e\alpha^7)$ level combined with anticipated experimental advances would allow for a stringent test of our understanding of bound-state QED in the regime where recoil and virtual annihilation play a prominent role and would also enable the extraction of a precise value for the pure-QED Rydberg. There is no reason to doubt that current methods of calculation based on effective field theories will prove adequate to the calculation of all $O(m_e\alpha^7)$ corrections. Many of these corrections have already been obtained: some of them come from the "hard", *i.e.* high energy, region of internal loops, but others depend crucially on the lower energy "soft" and "ultrasoft" regions and require precise control of the bound-state aspects of the problem. The challenges in this work are related to the sheer number of terms involved, the algebraic complexity of the individual terms, disentangling contributions coming from the various regions, the delicate cancellation of ultraviolet and infrared divergences, and the intricacies of the binding problem at this high order of approximation. It is difficult to predict when future results might be available but there seems to be no reason why the all-important S-state energies might not be completed within the next five or ten years.

Experimentally there is much room for improvement and, as discussed above, the immediate and essential task is to get all measured properties of Ps in line with the corresponding uncertainties in theory. If the anomalous microwave measurement [328] stands then explaining this will be of great importance. More likely this problem will be resolved by performing further experiments, in which case the gap between theory and experiment for the $n = 2$ fine structure will soon be closed, at least until the next theoretical advances. New $1\,^3S_1 \to 2\,^3S_1$ measurements are expected within 5 years: however, this was also true 5 years ago, so we must await data in that area. There are several developments in methodology that may inform the next generation of experiments: these include the application of Ramsey-type separated oscillatory field (SOF) experiments [285] (especially variants such as frequency offset versions (FOSOF) [398]) for microwave spectroscopy, and interferometric techniques in general. Virtually all experiments would benefit from improved Ps sources. These could arise from new Ps production materials, or from the development of Rydberg–Stark manipulation methods [360]. Some advances have been made regarding Rydberg Ps production [34,358] and manipulation [315,539] but more work is needed before these methods can be applied in a way that will directly benefit Ps spectroscopic measurements. The use of Surko-type buffer gas positron traps [58] has already been highly advantageous [57], and these methods will continue to enable the development of new techniques. It is therefore reasonable to expect significant developments in experimental Ps physics in the near future.

Thanks to advances in the control and spectroscopy of atomic and molecular systems we live a fruitful age for the study of physics beyond the Standard Model, and Ps is a prime example of it. We have shown here that Ps presents a unique arena in which to test QED to increased levels of precision, and to explore the existence of hypothetical new particles. However, there is still much to be done on this front. For instance, there is a 4.2σ discrepancy between the experimentally measured energy difference and the QED prediction for the $2\,^3S \to 2\,^3P_0$ interval. This observation cannot be explained by the existence of a new scalar or axion-like particle, but there are other interesting possibilities, such as the Chameleon model, in which a new scalar interacts with SM leptons with a strength depending on the environment's density [540]. Another model is the Arkani-Hamed, Dimopoulos, Dvali model [478], in which it is assumed that gravity operates in a higher-dimensional space. In contrast, the rest of the fundamental forces exist only in a four-dimensional

brane embedded in this space, thereby diluting gravity in more dimensions and making it much weaker than the rest of the fundamental forces in our brane. It may be the case that more precise measurements remove the disagreement with theory (as discussed in 3.4, this has happened before in Ps physics), but this does not reduce the importance of performing measurements in a wide range of systems, covering as much parameter space as possible in the search for new physics. Finally, it is worth emphasizing that the study of physics beyond the Standard Model requires a collaborative effort across disciplines of physics and chemistry, and we hope that this review will provide a broad enough platform to help facilitate this goal.

Declaration of competing interest

The authors declare that they have no known competing financial interests or personal relationships that could have appeared to influence the work reported in this paper.

Acknowledgments

We gratefully acknowledge A. P. Mills, Jr., P Crivelli, S. D. Hogan, S. T. Love and R. Pohl for useful discussions and R. E. Sheldon and L. Gurung for assistance with preparing some of the figures. GSA was supported by the National Science Foundation under Grant No. PHY-2011762. DBC was supported by the EPSRC under Grant No. EP/R006474/1.

References

[1] H.A. Bethe, E.E. Salpeter, Quantum Mechanics of One- and Two-Electron Atoms, Springer, Berlin, 1957.
[2] S.G. Karshenboim, Precision physics of simple atoms: QED tests, nuclear structure and fundamental constants, Phys. Rep. 422 (2005) 1–63, http://dx.doi.org/10.1016/j.physrep.2005.08.008, URL http://www.sciencedirect.com/science/article/pii/S0370157305003637.
[3] S. Chu, A.P. Mills, Jr., A.G. Yodh, K. Nagamine, Y. Miyake, T. Kuga, Laser excitation of the muonium $1S-2S$ transition, Phys. Rev. Lett. 60 (1988) 101–104, http://dx.doi.org/10.1103/PhysRevLett.60.101, URL http://link.aps.org/doi/10.1103/PhysRevLett.60.101.
[4] R. Pohl, H. Daniel, F.J. Hartmann, P. Hauser, F. Kottmann, V.E. Markushin, M. Mühlbauer, C. Petitjean, W. Schott, D. Taqqu, P. Wojciechowski-Grosshauser, Observation of long-lived muonic hydrogen in the $2S$ state, Phys. Rev. Lett. 97 (2006) 193402, http://dx.doi.org/10.1103/PhysRevLett.97.193402, URL https://link.aps.org/doi/10.1103/PhysRevLett.97.193402.
[5] M. Ahmadi, B.X.R. Alves, C.J. Baker, W. Bertsche, A. Capra, C. Carruth, C.L. Cesar, M. Charlton, S. Cohen, R. Collister, S. Eriksson, A. Evans, N. Evetts, J. Fajans, T. Friesen, M.C. Fujiwara, D.R. Gill, J.S. Hangst, W.N. Hardy, M.E. Hayden, C.A. Isaac, M.A. Johnson, J.M. Jones, S.A. Jones, S. Jonsell, A. Khramov, P. Knapp, L. Kurchaninov, N. Madsen, D. Maxwell, J.T.K. McKenna, S. Menary, T. Momose, J.J. Munich, K. Olchanski, A. Olin, P. Pusa, C.Ø. Rasmussen, F. Robicheaux, R.L. Sacramento, M. Sameed, E. Sarid, D.M. Silveira, G. Stutter, C. So, T.D. Tharp, R.I. Thompson, D.P. van der Werf, J.S. Wurtele, Characterization of the 1S-2S transition in antihydrogen, Nature 557 (7703) (2018) 71–75, http://dx.doi.org/10.1038/s41586-018-0017-2.
[6] J.A. Wheeler, Polyelectrons, Ann. New York Acad. Sci. 48 (3) (1946) 219–238, http://dx.doi.org/10.1111/j.1749-6632.1946.tb31764.x.
[7] P.G. Coleman, Positron Beams and their Applications, first, World Scientific Publishing Co. Singapore, 2000, http://dx.doi.org/10.1142/3719.
[8] A. Ore, J.L. Powell, Three-photon annihilation of an electron-positron pair, Phys. Rev. 75 (1949) 1696–1699, http://dx.doi.org/10.1103/PhysRev.75.1696, URL http://link.aps.org/doi/10.1103/PhysRev.75.1696.
[9] R. Krause-Rehberg, H. Leipner, Positron Annihilation in Semiconductors: Defect Studies, in: Springer Series in Solid-State Sciences, Springer Berlin Heidelberg, 2010.
[10] C.G. Darwin, The wave equations of the electron, Proc. R. Soc. London, Ser. A 118 (1928) 654–680, URL https://www.jstor.org/stable/94929.
[11] S.N. Gupta, W.W. Repko, C.J. Suchyta, Jr., Muonium and positronium potentials, Phys. Rev. D 40 (12) (1989) 4100–4104, http://dx.doi.org/10.1103/PhysRevD.40.4100.
[12] E.E. Salpeter, H.A. Bethe, A relativistic equation for bound-state problems, Phys. Rev. 84 (1951) 1232–1242, http://dx.doi.org/10.1103/PhysRev.84.1232.
[13] W.E. Caswell, G.P. Lepage, Effective Lagrangians for bound state problems in QED, QCD, and other field theories, Phys. Lett. B 167 (4) (1986) 437–442, http://dx.doi.org/10.1016/0370-2693(86)91297-9.
[14] A. Pineda, J. Soto, Potential NRQED: The positronium case, Phys. Rev. D 59 (1) (1998) 016005, http://dx.doi.org/10.1103/PhysRevD.59.016005, URL http://link.aps.org/doi/10.1103/PhysRevD.59.016005.
[15] J. Govaerts, M.V. Caillie, Neutrino decay of positronium in the standard model and beyond, Phys. Lett. B 381 (4) (1996) 451–457, http://dx.doi.org/10.1016/0370-2693(96)00623-5, URL http://www.sciencedirect.com/science/article/pii/0370269396006235.
[16] S.G. Karshenboim, Precision study of positronium: Testing bound state QED theory, Internat. J. Modern Phys. A 19 (23) (2004) 3879–3896, http://dx.doi.org/10.1142/S0217751X04020142.
[17] T. Aoyama, M. Hayakawa, T. Kinoshita, M. Nio, Tenth-order QED contribution to the electron $g-2$ and an improved value of the fine structure constant, Phys. Rev. Lett. 109 (2012) 111807, http://dx.doi.org/10.1103/PhysRevLett.109.111807, URL https://link.aps.org/doi/10.1103/PhysRevLett.109.111807.
[18] P.J. Mohr, D.B. Newell, B.N. Taylor, CODATA recommended values of the fundamental physical constants: 2014, Rev. Modern Phys. 88 (2016) 035009, http://dx.doi.org/10.1103/RevModPhys.88.035009, URL https://link.aps.org/doi/10.1103/RevModPhys.88.035009.
[19] C. Alexandrou, Novel applications of lattice QCD: Parton distributions, proton charge radius and neutron electric dipole moment, EPJ Web Conf. 137 (2017) 01004, http://dx.doi.org/10.1051/epjconf/201713701004.
[20] R. Pohl, A. Antognini, F. Nez, F.D. Amaro, F. Biraben, J.M.R. Cardoso, D.S. Covita, A. Dax, S. Dhawan, L.M.P. Fernandes, A. Giesen, T. Graf, T.W. Hänsch, P. Indelicato, L. Julien, C.-Y. Kao, P. Knowles, E.-O. Le Bigot, Y.-W. Liu, A.M. Lopes, L. Ludhova, C.M.B. Monteiro, F. Mulhauser, T. Nebel, P. Rabinowitz, J.M.F. dos Santos, L.A. Schaller, K. Schuhmann, C. Schwob, D. Taqqu, J.F.C.A. Veloso, F. Kottmann, The size of the proton, Nature 466 (7303) (2010) 213–216, http://dx.doi.org/10.1038/nature09250.
[21] A. Beyer, L. Maisenbacher, A. Matveev, R. Pohl, K. Khabarova, A. Grinin, T. Lamour, D.C. Yost, T.W. Hänsch, N. Kolachevsky, T. Udem, The Rydberg constant and proton size from atomic hydrogen, Science 358 (6359) (2017) 79–85, http://dx.doi.org/10.1126/science.aah6677.
[22] H. Fleurbaey, S. Galtier, S. Thomas, M. Bonnaud, L. Julien, F.m.c. Biraben, F.m.c. Nez, M. Abgrall, J. Guéna, New measurement of the $1S-3S$ transition frequency of hydrogen: Contribution to the proton charge radius puzzle, Phys. Rev. Lett. 120 (2018) 183001, http://dx.doi.org/10.1103/PhysRevLett.120.183001, URL https://link.aps.org/doi/10.1103/PhysRevLett.120.183001.

[23] ATLAS Collaboration and CMS Collaboration, ATLAS Collaboration and CMS Collaboration Collaboration Collaboration, Combined measurement of the higgs boson mass in pp collisions at $\sqrt{s} = 7$ and 8 TeV with the ATLAS and CMS experiments, Phys. Rev. Lett. 114 (2015) 191803, http://dx.doi.org/10.1103/PhysRevLett.114.191803, URL https://link.aps.org/doi/10.1103/PhysRevLett.114.191803.

[24] M.S. Safronova, D. Budker, D. DeMille, D.F.J. Kimball, A. Derevianko, C.W. Clark, Search for new physics with atoms and molecules, Rev. Modern Phys. 90 (2018) 025008, http://dx.doi.org/10.1103/RevModPhys.90.025008, URL https://link.aps.org/doi/10.1103/RevModPhys.90.025008.

[25] A. Czarnecki, K. Melnikov, A. Yelkhovsky, Positronium hyperfine splitting: Analytical value at $O(m\alpha^6)$, Phys. Rev. Lett. 82 (1999) 311–314, http://dx.doi.org/10.1103/PhysRevLett.82.311, URL http://link.aps.org/doi/10.1103/PhysRevLett.82.311.

[26] P. Crivelli, C.L. Cesar, U. Gendotti, Advances towards a new measurement of the 1S-2S transition of positronium, Can. J. Phys. 89 (1) (2011) 29–35, http://dx.doi.org/10.1139/P10-101.

[27] G.S. Adkins, Higher order corrections to positronium energy levels, J. Phys. Conf. Ser. 1138 (2018) 012005, http://dx.doi.org/10.1088/1742-6596/1138/1/012005.

[28] A.M. Alonso, S.D. Hogan, D.B. Cassidy, Production of 2^3S_1 positronium atoms by single-photon excitation in an electric field, Phys. Rev. A 95 (2017) 033408, http://dx.doi.org/10.1103/PhysRevA.95.033408, URL https://link.aps.org/doi/10.1103/PhysRevA.95.033408.

[29] A. Ishida, T. Namba, S. Asai, T. Kobayashi, H. Saito, M. Yoshida, K. Tanaka, A. Yamamoto, New precision measurement of hyperfine splitting of positronium, Phys. Lett. B 734 (2014) 338–344, http://dx.doi.org/10.1016/j.physletb.2014.05.083.

[30] S.G. Karshenboim, Precision physics of simple atoms and constraints on a light boson with ultraweak coupling, Phys. Rev. Lett. 104 (2010) 220406, http://dx.doi.org/10.1103/PhysRevLett.104.220406, URL https://link.aps.org/doi/10.1103/PhysRevLett.104.220406.

[31] C. Delaunay, C. Frugiuele, E. Fuchs, Y. Soreq, Probing new spin-independent interactions through precision spectroscopy in atoms with few electrons, Phys. Rev. D 96 (2017) 115002, http://dx.doi.org/10.1103/PhysRevD.96.115002, URL https://link.aps.org/doi/10.1103/PhysRevD.96.115002.

[32] C. Frugiuele, J. Pérez-Ríos, C. Peset, Current and future perspectives of positronium and muonium spectroscopy as dark sectors probe, Phys. Rev. D 100 (2019) 015010, http://dx.doi.org/10.1103/PhysRevD.100.015010, URL https://link.aps.org/doi/10.1103/PhysRevD.100.015010.

[33] P.W. Graham, D.E. Kaplan, S. Rajendran, Cosmological relaxation of the electroweak scale, Phys. Rev. Lett. 115 (22) (2015) 221801, http://dx.doi.org/10.1103/PhysRevLett.115.221801.

[34] T.E. Wall, A.M. Alonso, B.S. Cooper, A. Deller, S.D. Hogan, D.B. Cassidy, Selective production of rydberg-stark states of positronium, Phys. Rev. Lett. 114 (2015) 173001, http://dx.doi.org/10.1103/PhysRevLett.114.173001, URL http://link.aps.org/doi/10.1103/PhysRevLett.114.173001.

[35] D. Hanneke, S. Fogwell, G. Gabrielse, New measurement of the electron magnetic moment and the fine structure constant, Phys. Rev. Lett. 100 (2008) 120801, http://dx.doi.org/10.1103/PhysRevLett.100.120801, URL http://link.aps.org/doi/10.1103/PhysRevLett.100.120801.

[36] E. Hardy, R. Lasenby, Stellar cooling bounds on new light particles: plasma mixing effects, J. High Energy Phys. 2017 (2) (2017) 33, http://dx.doi.org/10.1007/JHEP02(2017)033.

[37] A. Joyce, B. Jain, J. Khoury, M. Trodden, Beyond the cosmological standard model, Phys. Rep. 568 (2015) 1–98, http://dx.doi.org/10.1016/j.physrep.2014.12.002.

[38] P.F. De Salas, S. Gariazzo, O. Mena, C.A. Ternes, M. Tórtola, Neutrino mass ordering from oscillations and beyond: 2018 status and future prospects, Front. Astron. Space Sci. 5 (2018) 36, http://dx.doi.org/10.3389/fspas.2018.00036, arXiv:1806.11051.

[39] W. Bernreuther, U. Löw, J.P. Ma, O. Nachtmann, How to test CP, T, and CPT invariance in the three photon decay of polarized $^3S_1$ positronium, Z. Phys. C Part. Fields 41 (1) (1988) 143–158, http://dx.doi.org/10.1007/BF01412589.

[40] M. Ahmadi, B.X.R. Alves, C.J. Baker, W. Bertsche, E. Butler, A. Capra, C. Carruth, C.L. Cesar, M. Charlton, S. Cohen, R. Collister, S. Eriksson, A. Evans, N. Evetts, J. Fajans, T. Friesen, M.C. Fujiwara, D.R. Gill, A. Gutierrez, J.S. Hangst, W.N. Hardy, M.E. Hayden, C.A. Isaac, A. Ishida, M.A. Johnson, S.A. Jones, S. Jonsell, L. Kurchaninov, N. Madsen, M. Mathers, D. Maxwell, J.T.K. McKenna, S. Menary, J.M. Michan, T. Momose, J.J. Munich, P. Nolan, K. Olchanski, A. Olin, P. Pusa, C.Ø. Rasmussen, F. Robicheaux, R.L. Sacramento, M. Sameed, E. Sarid, D.M. Silveira, S. Stracka, G. Stutter, C. So, T.D. Tharp, J.E. Thompson, R.I. Thompson, D.P. van der Werf, J.S. Wurtele, Observation of the 1S-2S transition in trapped antihydrogen, Nature 541 (2016) 506, http://dx.doi.org/10.1038/nature21040.

[41] V. Andreev, et al., ACME Collaboration Collaboration, Improved limit on the electric dipole moment of the electron, Nature 562 (7727) (2018) 355–360, http://dx.doi.org/10.1038/s41586-018-0599-8.

[42] S. DeBenedetti, H.C. Corben, Positronium, Annu. Rev. Nucl. Sci. 4 (1954) 191–218, http://dx.doi.org/10.1146/annurev.ns.04.120154.001203.

[43] B. Maglich, Discovery of positronium, Adventures Expt. Phys. 4 (1973) 63–127.

[44] M.A. Stroscio, Positronium: A review of the theory, Phys. Rep. 22 (1975) http://dx.doi.org/10.1016/0370-1573(75)90029-0, 215–177.

[45] T. Murota, Hyperfine structure of positronium, Progr. Theoret. Phys. Suppl. 95 (1988) 46–77, http://dx.doi.org/10.1143/PTPS.95.46.

[46] S. Berko, H.N. Pendleton, Positronium, Annu. Rev. Nucl. Part. Sci. 30 (1980) 543–581, http://dx.doi.org/10.1146/annurev.ns.30.120180.002551.

[47] A. Rich, Recent experimental advances in positronium research, Rev. Modern Phys. 53 (1) (1981) 127, http://dx.doi.org/10.1103/RevModPhys.53.127.

[48] S. Chu, A.P. Mills, Jr., Excitation of the positronium $1\,^3S_1 \rightarrow 2\,^3S_1$ two-photon transition, Phys. Rev. Lett. 48 (1982) 1333–1337, http://dx.doi.org/10.1103/PhysRevLett.48.1333, URL http://link.aps.org/doi/10.1103/PhysRevLett.48.1333.

[49] A.P. Mills, Jr., S. Chu, Precision measurements in positronium, in: T. Kinoshita (Ed.), Quantum Electrodynamics, in: Advanced Series on Directions in High Energy Physics–Vol. 7, World Scientific, Singapore, 1990, pp. 774–821.

[50] A. Rich, R.S. Condi, D.W. Gidley, M. Skalsey, P.W. Zitzewitz, Tests of QED and related symmetry principles using positrons and positronium, in: S. Haroche, J.C. Gay, G. Grynberg (Eds.), Atomic Physics, Vol. 11, World Scientific, Singapore, 1988, pp. 337–353.

[51] S. Bass, QED and fundamental symmetries in positronium decays, Acta Phys. Polon. B 50 (7) (2019) 1319, http://dx.doi.org/10.5506/aphyspolb.50.1319.

[52] A. Rubbia, Positronium as a probe for new physics beyond the standard model, Internat. J. Modern Phys. A 19 (23) (2004) 3961–3985, http://dx.doi.org/10.1142/S0217751X0402021X.

[53] S.N. Gninenko, N.V. Krasnikov, V.A. Matveev, A. Rubbia, Some aspects of positronium physics, Phys. Part. Nucl. 37 (2006) 321–346, http://dx.doi.org/10.1134/S1063779606030038.

[54] M. Charlton, J.W. Humberston, Positron Physics, first, in: Cambridge Monographs on Atomic, Molecular and Chemical Physics, vol. II, Cambridge University Press, Cambridge, 2001.

[55] A.P. Mills, Jr., Physics with many positrons, Riv. Nuovo Cimento 34 (4) (2011) 151–252, http://dx.doi.org/10.1393/ncr/i2011-10064-5.

[56] A.P. Mills, Jr., Chapter five - experiments with dense low-energy positrons and positronium, in: C.C.L. Ennio Arimondo, S.F. Yelin (Eds.), Advances in Atomic, Molecular, and Optical Physics, in: Advances In Atomic, Molecular, and Optical Physics, vol. 65, Academic Press, 2016, pp. 265–290, http://dx.doi.org/10.1016/bs.aamop.2016.04.003.

[57] D.B. Cassidy, Experimental progress in positronium laser physics, Eur. Phys. J. D 72 (3) (2018) 53, http://dx.doi.org/10.1140/epjd/e2018-80721-y.

[58] J.R. Danielson, D.H.E. Dubin, R.G. Greaves, C.M. Surko, Plasma and trap-based techniques for science with positrons, Rev. Modern Phys. 87 (2015) 247–306, http://dx.doi.org/10.1103/RevModPhys.87.247, URL http://link.aps.org/doi/10.1103/RevModPhys.87.247.

[59] P.A.M. Dirac, Quantised singularities in the electromagnetic field, Proc. R. Soc. London A: Math. Phys. Eng. Sci. 133 (821) (1931) 60–72, http://dx.doi.org/10.1098/rspa.1931.0130, URL http://rspa.royalsocietypublishing.org/content/133/821/60.

[60] C.D. Anderson, The positive electron, Phys. Rev. 43 (1933) 491–494, http://dx.doi.org/10.1103/PhysRev.43.491, URL http://link.aps.org/doi/10.1103/PhysRev.43.491.
[61] S. Mohorovičić, Möglichkeit neuer Elemente und ihre Bedeutung für Die astrophysik, Astron. Nachr. 253 (4) (1934) 93–108, http://dx.doi.org/10.1002/asna.19342530402.
[62] H. Kragh, From "electrum" to positronium, J. Chem. Educ. 67 (3) (1990) 196–197, http://dx.doi.org/10.1021/ed067p196.
[63] M. Randić, Positronium — hydrogen like and unlike, Croatica Chemica Acta 82 (2009) 791–800, URL https://hrcak.srce.hr/index.php?show=clanak&id_clanak_jezik=70552.
[64] A.E. Ruark, Positronium, Phys. Rev. 68 (11–12) (1945) 278, http://dx.doi.org/10.1103/PhysRev.68.278.
[65] J. Pirenne, Le champ propre et l'interaction des particules de Dirac suivant l'êlectrodynamique quantique, Arch. Sci. Phys. Naturelles 28 (1946) 233–272, http://dx.doi.org/10.5169/seals-742869.
[66] J. Pirenne, Le champ propre et l'interaction des particules de Dirac suivant l'êlectrodynamique quantique (continued), Arch. Sci. Phys. Naturelles 29 (1947) 121–150, http://dx.doi.org/10.5169/seals-742257.
[67] J. Pirenne, Le champ propre et l'interaction des particules de Dirac suivant l'êlectrodynamique quantique. II. L'interaction de deux particules de Dirac, Arch. Sci. Phys. Naturelles 29 (1947) 207–238, http://dx.doi.org/10.5169/seals-742259.
[68] J. Pirenne, Le champ propre et l'interaction des particules de Dirac suivant l'êlectrodynamique quantique. III. Le systèm électron-positron, Arch. Sci. Phys. Naturelles 29 (1947) 265–300, http://dx.doi.org/10.5169/seals-742261.
[69] M. Deutsch, Evidence for the formation of positronium in gases, Phys. Rev. 82 (1951) 455–456, http://dx.doi.org/10.1103/PhysRev.82.455, URL http://link.aps.org/doi/10.1103/PhysRev.82.455.
[70] J. Zatorski, $O(m\alpha^6)$ Corrections to energy levels of positronium with nonvanishing orbital angular momentum, Phys. Rev. A 78 (3) (2008) 032103, http://dx.doi.org/10.1103/PhysRevA.78.032103.
[71] W. Bernreuther, O. Nachtmann, Weak interaction effects in positronium, Z. Phys. C Part. Fields 11 (3) (1981) 235–245, http://dx.doi.org/10.1007/BF01545680.
[72] R. Alcorta, J.A. Grifols, Electro-weak corrections to the hyperfine structure of positronium, Ann. Physics 229 (1994) 109–159, http://dx.doi.org/10.1006/aphy.1994.1004.
[73] 2018 CODATA recommended values, URL https://physics.nist.gov/cuu/Constants/index.html.
[74] V.B. Berestetski, L.D. Landau, On the interaction between electrons and positrons, Zh. Eksp. Teor. Fiz. 19 (1949) 673–679.
[75] V.B. Berestetski, On the spectrum of positronium, Zh. Eksp. Teor. Fiz. 19 (1949) 1130–1135.
[76] R.A. Ferrell, The positronium fine structure, Phys. Rev. 84 (1951) 858–859, http://dx.doi.org/10.1103/PhysRev.84.858.
[77] R.A. Ferrell, The Fine Structure of Positronium, (Ph.D. thesis), Princeton University, 1951, Department of Physics, Adviser A. S. Wightman.
[78] R. Karplus, A. Klein, Electrodynamic displacement of atomic energy levels. III. The hyperfine structure of positronium, Phys. Rev. 87 (1952) 848–858, http://dx.doi.org/10.1103/PhysRev.87.848.
[79] T. Fulton, R. Karplus, Bound state correction in two-body systems, Phys. Rev. 93 (5) (1954) 1109–1116, http://dx.doi.org/10.1103/PhysRev.93.1109.
[80] T. Fulton, P.C. Martin, Radiative corrections in positronium, Phys. Rev. 93 (1954) 903–904, http://dx.doi.org/10.1103/PhysRev.93.903.
[81] T. Fulton, P.C. Martin, Two-body system in quantum electrodynamics. energy levels of positronium, Phys. Rev. 95 (1954) 811–822, http://dx.doi.org/10.1103/PhysRev.95.811.
[82] M.I. Eides, H. Grotch, V.A. Shelyuto, Theory of Light Hydrogenic Bound States, in: Springer Tracts in Modern Physics, vol. 222, Springer, Berlin, 2007.
[83] P. Labelle, S.M. Zebarjad, Derivation of the lamb shift using an effective field theory, Can. J. Phys. 77 (4) (1999) 267–278, http://dx.doi.org/10.1139/cjp-77-4-267, URL https://www.nrcresearchpress.com/doi/10.1139/p98-056#.XyKxyC3MxsY.
[84] A. Pineda, J. Soto, Effective field theory for ultrasoft momenta in NRQCD and NRQED, Nucl. Phys. B (Proc. Suppl.) 64 (1–3) (1998) 428–432, http://dx.doi.org/10.1016/S0920-5632(97)01102-X.
[85] T. Fulton, D.A. Owen, W.W. Repko, Corrections to the positronium hyperfine structure of order $\alpha^2 \ln \alpha^{-1}$, Phys. Rev. Lett. 24 (19) (1970) 1035–1037, http://dx.doi.org/10.1103/PhysRevLett.24.1035.
[86] T. Fulton, D.A. Owen, W.W. Repko, Hyperfine structure of positronium, Phys. Rev. A 4 (5) (1971) 1802–1811, http://dx.doi.org/10.1103/PhysRevA.4.1802.
[87] R. Barbieri, P. Christillin, E. Remiddi, On the theoretical value of positronium ground state splitting, Phys. Lett. B 43 (1973) 411–412, http://dx.doi.org/10.1016/0370-2693(73)90386-9.
[88] R. Barbieri, P. Christillin, E. Remiddi, Vacuum polarization and positronium-ground-state splitting, Phys. Rev. A 8 (5) (1973) 2266–2271, http://dx.doi.org/10.1103/PhysRevA.8.2266.
[89] D.A. Owen, Fourth-order vacuum polarization correction to the positronium hyperfine structure, Phys. Rev. Lett. 30 (19) (1973) 887–888, http://dx.doi.org/10.1103/PhysRevLett.30.887.
[90] Y.J. Ng, Electron-Electron Scattering and Hyperfine Structure of Positronium, (Ph.D. thesis), Harvard University, Cambridge, Massachusetts, 1974.
[91] V.K. Cung, T. Fulton, W.W. Repko, D. Schnitzler, Complete reduction of fermion-antifermion bethe-salpeter equation with static kernel, Ann. Phys. (N.Y.) 96 (1976) 261–285, URL http://www.sciencedirect.com/science/article/pii/0003491676901925.
[92] R. Barbieri, E. Remiddi, More $\alpha^6 \ln \alpha$ terms in positronium ground state splitting, Phys. Lett. B 65 (3) (1976) 258–262, http://dx.doi.org/10.1016/0370-2693(76)90177-5.
[93] G.P. Lepage, Analytic bound-state solutions in a relativistic two-body formalism with applications in muonium and positronium, Phys. Rev. A 16 (3) (1977) 863–876, http://dx.doi.org/10.1103/PhysRevA.16.863.
[94] G.T. Bodwin, D.R. Yennie, Hyperfine splitting in positronium and muonium, Phys. Rep. 43 (1978) 267–303, http://dx.doi.org/10.1016/0370-1573(78)90151-5.
[95] W.E. Caswell, G.P. Lepage, $O(\alpha^2 \ln(\alpha^{-1}))$ Corrections in positronium: Hyperfine splitting and decay rate, Phys. Rev. A 20 (1) (1979) 36–43, http://dx.doi.org/10.1103/PhysRevA.20.36.
[96] R.N. Fell, Order $\alpha^4 \ln \alpha^{-1} f_{\mathrm{RYD}}$ corrections to the $n = 1$ and $n = 2$ energy levels of positronium, Phys. Rev. Lett. 68 (1) (1992) 25–28, http://dx.doi.org/10.1103/PhysRevLett.68.25.
[97] I.B. Khriplovich, A.I. Milstein, A.S. Yelkhovsky, Corrections of $O(\alpha^6 \log \alpha)$ in the two-body qed problem, Phys. Lett. B 282 (1–2) (1992) 237–242.
[98] A.S. Elkhovsky, A.I. Milstein, I.B. Khriplovich, Logarithmic corrections in the two-body problem in QED, Sov. Phys. JETP 75 (6) (1992) 954–959, Originally published as Zh. Eksp. Teor. Fiz. 102, 1768-1780 (1992), URL http://www.jetp.ac.ru/cgi-bin/dn/e_075_06_0954.pdf.
[99] R.N. Fell, Single-transverse-photon contributions of order $\alpha^6 \ln(\alpha)$ to the energy levels of positronium, Phys. Rev. A 48 (4) (1993) 2634–2667, http://dx.doi.org/10.1103/PhysRevA.48.2634.
[100] T. Fulton, Is there a need to calculate positronium and muonium hfs to higher order? Phys. Rev. A 7 (1) (1973) 377–379, http://dx.doi.org/10.1103/PhysRevA.7.377.
[101] M.A. Samuel, An order-α^2 correction to the hyperfine structure of positronium due to the Källen-Sabry potential, Phys. Rev. A 10 (4) (1974) 1450–1451, http://dx.doi.org/10.1103/PhysRevA.10.1450.

[102] V.K. Cung, A. Devoto, T. Fulton, W.W. Repko, Three photon virtual annihilation contributions to positronium hyperfine structure, Phys. Lett. B 68 (5) (1977) 474–476, http://dx.doi.org/10.1016/0370-2693(77)90474-9.

[103] V.K. Cung, A. Devoto, T. Fulton, W.W. Repko, Order α^2 corrections to the positronium hyperfine interval arising from three-photon virtual annihilation, Il Nuovo Cimento 43 A (1978) 643–657, http://dx.doi.org/10.1007/BF02730349.

[104] V.K. Cung, A. Devoto, T. Fulton, W.W. Repko, $m\alpha^6$ Contributions to the positronium hyperfine structure from two-photon virtual annihilation, Phys. Lett. B 78 (1) (1978) 116–118, http://dx.doi.org/10.1016/0370-2693(78)90361-1.

[105] W.E. Caswell, G.P. Lepage, Reduction of the Bethe-Salpeter equation to an equivalent Schrödinger equation, with applications, Phys. Rev. A 18 (1978) 810–819, http://dx.doi.org/10.1103/PhysRevA.18.810.

[106] V.K. Cung, A. Devoto, T. Fulton, W.W. Repko, Order-$\alpha^4 R_\infty$ contributions to positronium hyperfine structure from radiative corrections to two-photon virtual annihilation, Phys. Rev. A 19 (5) (1979) 1886–1892, http://dx.doi.org/10.1103/PhysRevA.19.1886.

[107] W. Buchmüller, E. Remiddi, Radiative corrections to positronium energy levels, Nuclear Phys. B 162 (2) (1980) 250–270, http://dx.doi.org/10.1016/0550-3213(80)90263-1.

[108] W. Buchmüller, E. Remiddi, Contributions to positronium hyperfine splitting from second-order perturbation theory, Il Nuovo Cimento 60 A (2) (1980) 109–119, http://dx.doi.org/10.1007/BF02902439.

[109] L.C. Hostler, W.W. Repko, Corrections to positronium levels using a coordinate representation of the reduced green's function, Phys. Rev. A 23 (5) (1981) 2425–2429, http://dx.doi.org/10.1103/PhysRevA.23.2425.

[110] T. Fulton, Corrections to the balmer-energy differences in positronium, Phys. Rev. A 26 (3) (1982) 1794–1795, http://dx.doi.org/10.1103/PhysRevA.26.1794.

[111] J.R. Sapirstein, E.A. Terray, D.R. Yennie, Additional radiative-recoil corrections to muonium and positronium hyperfine splitting, Phys. Rev. Lett. 51 (11) (1983) 982–984, http://dx.doi.org/10.1103/PhysRevLett.51.982.

[112] J.R. Sapirstein, E.A. Terray, D.R. Yennie, Radiative-recoil corrections to muonium and positronium hyperfine splitting, Phys. Rev. D 29 (10) (1984) 2290–2314, http://dx.doi.org/10.1103/PhysRevD.29.2290.

[113] G.S. Adkins, M.H.T. Bui, D. Zhu, New calculation of the three-photon-annihilation contribution to the positronium hyperfine interval, Phys. Rev. A 37 (1988) 4071–4078, http://dx.doi.org/10.1103/PhysRevA.37.4071.

[114] G.S. Adkins, Y.M. Aksu, M.H.T. Bui, Calculation of the two-photon-annihilation contribution to the positronium hyperfine interval at order $m\alpha^6$, Phys. Rev. A 47 (4) (1993) 2640–2652, http://dx.doi.org/10.1103/PhysRevA.47.2640.

[115] S.G. Karshenboim, Corrections of order α^2 to the hyperfine splitting in positronium, Phys. At. Nucl. 56 (12) (1993) 1710–1719.

[116] T. Zhang, L. Xiao, Hyperfine corrections to order α^6 in a relativistic formalism for positronium, Phys. Rev. A 49 (4) (1994) 2411–2414, http://dx.doi.org/10.1103/PhysRevA.49.2411.

[117] T. Zhang, G.W.F. Drake, QED correction of $O(\alpha^6 mc^2)$ to the fine structure splittings of helium and positronium, Phys. Rev. Lett. 72 (26) (1994) 4078–4081, http://dx.doi.org/10.1103/PhysRevLett.72.4078, Erratum published as PRL 73, 2637 (1994): DOI: 10.1103/PhysRevLett.73.2637.

[118] M.I. Eides, H. Grotch, Corrections of order α^6 to s levels of two-body systems, Phys. Rev. A 52 (2) (1995) 1757–1760, http://dx.doi.org/10.1103/PhysRevA.52.1757.

[119] G.S. Adkins, R.N. Fell, P.M. Mitrikov, Calculation of the positronium hyperfine interval, Phys. Rev. Lett. 79 (18) (1997) 3383–3386, http://dx.doi.org/10.1103/PhysRevLett.79.3383.

[120] A.H. Hoang, P. Labelle, S.M. Zebarjad, Single photon annihilation contributions to the positronium hyperfine splitting to order $m_e\alpha^6$, Phys. Rev. Lett. 79 (18) (1997) 3387–3390, http://dx.doi.org/10.1103/PhysRevLett.79.3387.

[121] K. Pachucki, Effective Hamiltonian approach to the bound state: Positronium hyperfine structure, Phys. Rev. A 56 (1) (1997) 297–304, http://dx.doi.org/10.1103/PhysRevA.56.297.

[122] K. Pachucki, Recoil effects in positronium energy levels to order α^6, Phys. Rev. Lett. 79 (21) (1997) 4120–4123, http://dx.doi.org/10.1103/PhysRevLett.79.4120.

[123] G.S. Adkins, J.R. Sapirstein, Order $m\alpha^6$ contributions to ground-state hyperfine splitting in positronium, Phys. Rev. A 58 (5) (1998) 3552–3560, http://dx.doi.org/10.1103/PhysRevA.58.3552.

[124] G.S. Adkins, J.R. Sapirstein, Erratum: Order $m\alpha^6$ contributions to ground-state hyperfine splitting in positronium [phys. Rev. a 58, 3552 (1998)],, Phys. Rev. A 61 (6) (2000) 069902(E), http://dx.doi.org/10.1103/PhysRevA.61.069902.

[125] K. Pachucki, S.G. Karshenboim, Complete results for positronium energy levels at order $m\alpha^6$, Phys. Rev. Lett. 80 (10) (1998) 2101–2104, http://dx.doi.org/10.1103/PhysRevLett.80.2101.

[126] A. Czarnecki, K. Melnikov, A. Yelkhovsky, Positronium $\boldsymbol{s}$-state spectrum: Analytic results at $O(m\alpha^6)$, Phys. Rev. A 59 (1999) 4316–4330, http://dx.doi.org/10.1103/PhysRevA.59.4316.

[127] A.H. Hoang, P. Labelle, S.M. Zebarjad, $O(m_e\alpha^6)$ Positronium hyperfine splitting due to single-photon annihilation, Phys. Rev. A 62 (1) (2000) 012109, http://dx.doi.org/10.1103/PhysRevA.62.012109.

[128] A.P. Burichenko, "Recoil"-effect-induced contribution of order $m\alpha^6$ to the hyperfine splitting of the positronium ground state, Phys. At. Nucl. 64 (2001) 1628–1636, http://dx.doi.org/10.1134/1.1409504.

[129] G.S. Adkins, R.N. Fell, P.M. Mitrikov, Calculation of the positronium hyperfine interval using the bethe-salpeter formalism, Phys. Rev. A 65 (4) (2002) 042103, http://dx.doi.org/10.1103/PhysRevA.65.042103.

[130] I.B. Khriplovich, A.I. Milstein, A.S. Yelkhovsky, Order $\alpha^4 R_\infty$ corrections to the fine-structure splitting of positronium p levels, Phys. Rev. Lett. 71 (26) (1993) 4323–4325, http://dx.doi.org/10.1103/PhysRevLett.71.4323.

[131] A.S. Elkhovsky, I.B. Khriplovich, A.I. Mil'stein, Corrections of order $\alpha^4 R_\infty$ to the positronium p levels, Sov. Phys. JETP 78 (2) (1994) 159–164, URL http://www.jetp.ac.ru/cgi-bin/dn/e_078_02_0159.pdf.

[132] E.A. Golosov, A.S. Elkhovskii, A.I. Milshtein, I.B. Khriplovich, Order $\alpha^4(m/M)R_\infty$ corrections to hydrogen p levels, Sov. Phys. JETP 80 (2) (1995) 208–211, URL http://jetp.ac.ru/cgi-bin/dn/e_080_02_0208.pdf.

[133] G.S. Adkins, B. Akers, M.F. Alam, L.M. Tran, X. Zhang, Calculation of higher order corrections to positronium energy levels, Proc. Sci. 353 (2019) 004, http://dx.doi.org/10.22323/1.353.0004, (FFK2019).

[134] S.G. Karshenboim, New logarithmic contributions in muonium and positronium, JETP 78 (4) (1993) 541–546, URL http://jetp.ac.ru/cgi-bin/e/index/e/76/4/p541?a=list.

[135] K. Melnikov, A. Yelkhovsky, $O(m\alpha^7 \ln^2 \alpha)$ Corrections to positronium energy levels, Phys. Lett. B 458 (1) (1999) 143–151, http://dx.doi.org/10.1016/S0370-2693(99)00566-3.

[136] K. Pachucki, S.G. Karshenboim, Higher-order recoil corrections to energy levels of two-body systems, Phys. Rev. A 60 (4) (1999) 2792–2798, http://dx.doi.org/10.1103/PhysRevA.60.2792.

[137] B.A. Kniehl, A.A. Penin, Order $\alpha^7 \ln(1/\alpha)$ contribution to positronium hyperfine splitting, Phys. Rev. Lett. 85 (24) (2000) 5094–5097, http://dx.doi.org/10.1103/PhysRevLett.85.5094.

[138] K. Melnikov, A. Yelkhovsky, $O(\alpha^3 \ln \alpha)$ Corrections to muonium and positronium hyperfine splitting, Phys. Rev. Lett. 86 (8) (2001) 1498–1501, http://dx.doi.org/10.1103/PhysRevLett.86.1498.

[139] R.J. Hill, New value of m_μ/m_e from muonium hyperfine splitting, Phys. Rev. Lett. 86 (15) (2001) 3280–3283, http://dx.doi.org/10.1103/PhysRevLett.86.3280.

[140] A. Czarnecki, U.D. Jentschura, K. Pachucki, Calculation of the one- and two-loop lamb shift for arbitrary excited hydrogenic states, Phys. Rev. Lett. 95 (18) (2005) 180404, http://dx.doi.org/10.1103/PhysRevLett.95.180404, See also the erratum: DOI: 10.1103/PhysRevLett.95.199903.

[141] U.D. Jentschura, A. Czarnecki, K. Pachucki, Nonrelativistic QED approach to the lamb shift, Phys. Rev. A 72 (6) (2005) 062102, http://dx.doi.org/10.1103/PhysRevA.72.062102.

[142] S.R. Marcu, Ultrasoft Contribution to the Positronium Hyperfine Splitting (Master's thesis), University of Alberta, 2011.

[143] M. Baker, P. Marquard, A.A. Penin, J. Piclum, M. Steinhauser, Hyperfine splitting in positronium to $O(\alpha^7 m_e)$: One photon annihilation contribution, Phys. Rev. Lett. 112 (2014) 120407, http://dx.doi.org/10.1103/PhysRevLett.112.120407.

[144] G.S. Adkins, R.N. Fell, Positronium hyperfine splitting at order $m\alpha^7$: Light-by-light scattering in the two-photon-exchange channel, Phys. Rev. A 89 (2014) 052518, http://dx.doi.org/10.1103/PhysRevA.89.052518.

[145] M.I. Eides, V.A. Shelyuto, Hard nonlogarithmic corrections of order $m\alpha^7$ to hyperfine splitting in positronium, Phys. Rev. D 89 (11) (2014) http://dx.doi.org/10.1103/PhysRevD.89.111301, 111301(R).

[146] G.S. Adkins, C. Parsons, M.D. Salinger, R. Wang, R.N. Fell, Positronium energy levels at order $m\alpha^7$: Light-by-light scattering in the two-photon-annihilation channel, Phys. Rev. A 90 (2014) 042502, http://dx.doi.org/10.1103/PhysRevA.90.042502.

[147] M.I. Eides, V.A. Shelyuto, Hard three-loop corrections to hyperfine splitting in positronium and muonium, Phys. Rev. D 92 (1) (2015) 013010, http://dx.doi.org/10.1103/PhysRevD.92.013010.

[148] G.S. Adkins, M. Kim, C. Parsons, R.N. Fell, Three-photon-annihilation contributions to positronium energies at order $m\alpha^7$, Phys. Rev. Lett. 115 (23) (2015) 233401, http://dx.doi.org/10.1103/PhysRevLett.115.233401.

[149] G.S. Adkins, C. Parsons, M.D. Salinger, R. Wang, Positronium energy levels at order $m\alpha^7$: Vacuum polarization corrections in the two-photon-annihilation channel, Phys. Lett. B 747 (2015) 551–555, http://dx.doi.org/10.1016/j.physletb.2015.06.050.

[150] M.I. Eides, V.A. Shelyuto, Hard three-loop corrections to hyperfine splitting, Internat. J. Modern Phys. A 31 (2–3) (2016) 1641030, http://dx.doi.org/10.1142/S0217751X1641030X.

[151] M.I. Eides, V.A. Shelyuto, Hyperfine splitting in muonium and positronium, Internat. J. Modern Phys. A 31 (2016) 1645034, http://dx.doi.org/10.1142/S0217751X16450342.

[152] G.S. Adkins, L.M. Tran, R. Wang, Positronium energy levels at order $m\alpha^7$: Product contributions in the two-photon-annihilation channel, Phys. Rev. A 93 (5) (2016) 052511, http://dx.doi.org/10.1103/PhysRevA.93.052511.

[153] M.I. Eides, V.A. Shelyuto, One more hard three-loop correction to parapositronium energy levels, Phys. Rev. D 96 (2017) 011301, http://dx.doi.org/10.1103/PhysRevD.96.011301.

[154] G.S. Adkins, Higher order corrections to positronium energy levels, J. Phys.: Conf. Ser. 1138 (2018) 012005, http://dx.doi.org/10.1088/1742-6596/1138/1/012005.

[155] A.V. Manohar, I.W. Stewart, Logarithms of α in QED bound states from the renormalization group, Phys. Rev. Lett. 85 (11) (2000) 2248–2251, http://dx.doi.org/10.1103/PhysRevLett.85.2248.

[156] H. Lamm, P-state positronium for precision physics: An ultrafine splitting at α^6, Phys. Rev. A 96 (2) (2017) 022515, http://dx.doi.org/10.1103/PhysRevA.96.022515.

[157] R.F. Lebed, E.S. Swanson, Quarkonium h states as arbiters of exoticity, Phys. Rev. D 96 (5) (2017) 056015, http://dx.doi.org/10.1103/PhysRevD.96.056015.

[158] A. Czarnecki, S.G. Karshenboim, Decays of positronium, in: B.B. Levchenko, V.I. Savrin (Eds.), Proceedings of the 14th International Workshop on High Energy Physics and Quantum Field Theory (QFTHEP99, Moscow, 1999), MSU Press, 2000, pp. 538–544, Available as hep-ph/9911410, URL https://arxiv.org/abs/hep-ph/9911410.

[159] S.N. Gninenko, N.V. Krasnikov, A. Rubbia, Positronium physics beyond the standard model, Modern Phys. Lett. A 17 (26) (2002) 1713–1724, http://dx.doi.org/10.1142/S0217732302008162.

[160] A.H. Al-Ramadhan, D.W. Gidley, New precision measurement of the decay rate of singlet positronium, Phys. Rev. Lett. 72 (1994) 1632–1635, http://dx.doi.org/10.1103/PhysRevLett.72.1632.

[161] Y. Kataoka, S. Asai, T. Kobayashi, First test of $O(\alpha^2)$ correction of the orthopositronium decay rate, Phys. Lett. B 671 (2) (2009) 219–223, http://dx.doi.org/10.1016/j.physletb.2008.12.008, URL http://www.sciencedirect.com/science/article/pii/S0370269308014688.

[162] I. Harris, L.M. Brown, Radiative corrections to pair annihilation, Phys. Rev. 105 (5) (1957) 1656–1661, http://dx.doi.org/10.1103/PhysRev.105.1656.

[163] L.M. Brown, R.P. Feynman, Radiative corrections to compton scattering, Phys. Rev. 85 (2) (1952) 231–244, http://dx.doi.org/10.1103/PhysRev.85.231.

[164] I.B. Khriplovich, A.S. Yelkhovsky, On the radiative corrections $\alpha^2 ln\alpha$ to the positronium decay rate, Phys. Lett. B 246 (3–4) (1990) 520–522, http://dx.doi.org/10.1016/0370-2693(90)90641-I.

[165] A. Czarnecki, K. Melnikov, A. Yelkhovsky, α^2 Corrections to parapositronium decay, Phys. Rev. Lett. 83 (6) (1999) 1135–1138, http://dx.doi.org/10.1103/PhysRevLett.83.1135.

[166] A. Czarnecki, K. Melnikov, A. Yelkhovsky, Erratum: α^2 corrections to parapositronium decay [Phys. Rev. Lett. 83, 1135 (1999)], Phys. Rev. Lett. 85 (10) (2000) 2221, http://dx.doi.org/10.1103/PhysRevLett.85.2221.

[167] A. Czarnecki, K. Melnikov, A. Yelkhovsky, Calculation of α^2 corrections to parapositronium decay, Phys. Rev. A 61 (5) (2000) 052502, http://dx.doi.org/10.1103/PhysRevA.61.052502.

[168] A. Czarnecki, K. Melnikov, A. Yelkhovsky, Erratum: Calculation of α^2 corrections to parapositronium decay [Phys. Rev. A 61, 052502 (2000)], Phys. Rev. A 62 (5) (2000) 059902, http://dx.doi.org/10.1103/PhysRevA.62.059902.

[169] G.S. Adkins, N.M. McGovern, R.N. Fell, J. Sapirstein, Two-loop corrections to the decay rate of parapositronium, Phys. Rev. A 68 (2003) 032512, http://dx.doi.org/10.1103/PhysRevA.68.032512, URL http://link.aps.org/doi/10.1103/PhysRevA.68.032512.

[170] B.A. Kniehl, A.A. Penin, Order $\alpha^3 \ln(1/\alpha)$ corrections to positronium decays, Phys. Rev. Lett. 85 (6) (2000) 1210–1213, http://dx.doi.org/10.1103/PhysRevLett.85.1210, [Erratum: Phys. Rev. Lett. 85, 3065 (2000)].

[171] A. Billoire, R. Lacaze, A. Morel, H. Navelet, The OZI rule violating radiative decays of the heavy pseudoscalars, Phys. Lett. B 78 (1978) 140–143, http://dx.doi.org/10.1016/0370-2693(78)90367-2.

[172] T. Muta, T. Niuya, Nonplanar 4-jets in quarkonium decays as a probe for 3-gluon coupling, Progr. Theoret. Phys. 68 (5) (1982) 1735–1748, http://dx.doi.org/10.1143/PTP.68.1735.

[173] G.P. Lepage, P.B. Mackenzie, K.H. Streng, P.W. Zerwas, Multiphoton decays of positronium, Phys. Rev. A 28 (5) (1983) 3090–3091, http://dx.doi.org/10.1103/PhysRevA.28.3090.

[174] G.S. Adkins, F.R. Brown, Rate for positronium decay to five photons, Phys. Rev. A 28 (1983) 1164–1165, http://dx.doi.org/10.1103/PhysRevA.28.1164.

[175] S. Adachi, Bachelor's thesis, Tokyo Metropolitan University, 1990, as reported in [425].

[176] G.S. Adkins, E.D. Pfahl, Order-α radiative correction to the rate for parapositronium decay to four photons, Phys. Rev. A (1999) R915–R918, http://dx.doi.org/10.1103/PhysRevA.59.R915.

[177] A. Pokraka, A. Czarnecki, Parapositronium can decay into three photons, Phys. Rev. D 96 (2017) 093002, http://dx.doi.org/10.1103/PhysRevD.96.093002, URL https://link.aps.org/doi/10.1103/PhysRevD.96.093002.

[178] J. Pérez-Ríos, S.T. Love, Effective single photon decay mode of positronium via electroweak interactions, J. Phys. B: At. Mol. Opt. Phys. 48 (24) (2015) 244009, http://dx.doi.org/10.1088/0953-4075/48/24/244009.

[179] A. Pokraka, A. Czarnecki, Positronium decay into a photon and neutrinos, Phys. Rev. D 94 (2016) 113012, http://dx.doi.org/10.1103/PhysRevD.94.113012, URL https://link.aps.org/doi/10.1103/PhysRevD.94.113012.

[180] P. Pascual, E. de Rafael, Photon-photon scattering contribution to the decay rate of orthopositronium, Lett. Nuovo Cimento IV (24) (1970) 1144–1146, http://dx.doi.org/10.1007/BF02753661.

[181] M.A. Stroscio, J.M. Holt, Radiative corrections to the decay rate of orthopositronium, Phys. Rev. A 10 (3) (1974) 749–755, http://dx.doi.org/10.1103/PhysRevA.10.749.

[182] W.E. Caswell, G.P. Lepage, J. Sapirstein, $O(\alpha)$ Corrections to the decay rate of orthopositronium, Phys. Rev. Lett. 38 (1977) 488–491, http://dx.doi.org/10.1103/PhysRevLett.38.488.

[183] G.S. Adkins, Radiative corrections to positronium decay, Ann. Physics 146 (1983) 78–128, http://dx.doi.org/10.1016/0003-4916(83)90053-2.

[184] M.A. Stroscio, Exact first-order electron self-energy contribution to the decay rate of orthopositronium, Phys. Rev. Lett. 48 (9) (1982) 571–573, http://dx.doi.org/10.1103/PhysRevLett.48.571.

[185] G.S. Adkins, Analytic evaluation of an $O(\alpha)$ vertex correction to the decay rate of orthopositronium, Phys. Rev. A 27 (1) (1983) 530–532, http://dx.doi.org/10.1103/PhysRevA.27.530.

[186] G.S. Adkins, Inner vertex contribution to the decay rate of orthopositronium, Phys. Rev. A 31 (3) (1985) 1250–1252, http://dx.doi.org/10.1103/PhysRevA.31.1250.

[187] V.V. Dvoeglazov, R.N. Faustov, Y.N. Tyukhtyaev, Decay rate of a positronium. Review of theory and experiment, Modern Phys. Lett. A 8 (34) (1993) 3263–3272, http://dx.doi.org/10.1142/S0217732393002191.

[188] M.I. Dobroliubov, S.N. Gninenko, A.Y. Ignatiev, V.A. Matveev, Orthopositronium lifetime problem, Internat. J. Modern Phys. A 8 (17) (1993) 2859–2874, http://dx.doi.org/10.1142/S0217751X93001156.

[189] D. Sillou, Status of orthopositronium decay rate measurements, Internat. J. Modern Phys. A 19 (23) (2004) 3919–3925, http://dx.doi.org/10.1142/S0217751X04020178.

[190] A.P. Burichenko, Large contribution to the correction $\sim \alpha^2$ to the width of orthopositronium, Phys. At. Nucl. 56 (1993) 640–642, [Yad. Fiz. 56, 123-127 (1993)].

[191] G.S. Adkins, Analytic evaluation of the orthopositronium-to-three-photon decay amplitudes to one-loop order, Phys. Rev. Lett. 76 (1996) 4903–4906, http://dx.doi.org/10.1103/PhysRevLett.76.4903.

[192] A.P. Burichenko, D.Y. Ivanov, Contribution of vacuum polarization to a correction of order α^2 to the positronium width, Phys. At. Nucl. 58 (1995) 832–834.

[193] G.S. Adkins, Y. Shiferaw, Two-loop corrections to the orthopositronium and parapositronium decay rates due to vacuum polarization, Phys. Rev. A 52 (3) (1995) 2442–2445, http://dx.doi.org/10.1103/PhysRevA.52.2442, URL http://link.aps.org/doi/10.1103/PhysRevA.52.2442.

[194] G.S. Adkins, M. Lymberopoulos, Light-by-light scattering contribution to the decay rate of orthopositronium at order α^2 ?$Gamma_{LO}$, Phys. Rev. A 51 (1995) R875–R878, http://dx.doi.org/10.1103/PhysRevA.51.R875, URL http://link.aps.org/doi/10.1103/PhysRevA.51.R875.

[195] G.S. Adkins, M. Lymberopoulos, Contribution of light-by-light scattering to the orders $O(m\alpha^8)$ and $O(m\alpha^8 \ln \alpha)$ orthopositronium decay rate, Phys. Rev. A 51 (4) (1995) 2908–2918, http://dx.doi.org/10.1103/PhysRevA.51.2908.

[196] G.S. Adkins, K. Melnikov, A. Yelkhovsky, Virtual annihilation contribution to orthopositronium decay rate, Phys. Rev. A 60 (1999) 3306–3307, http://dx.doi.org/10.1103/PhysRevA.60.3306, URL http://link.aps.org/doi/10.1103/PhysRevA.60.3306.

[197] G.S. Adkins, R.N. Fell, J. Sapirstein, Light-by-light scattering contributions to positronium decay rates, Phys. Rev. A 63 (2001) 032511, http://dx.doi.org/10.1103/PhysRevA.63.032511, URL http://link.aps.org/doi/10.1103/PhysRevA.63.032511.

[198] G.S. Adkins, R.N. Fell, J. Sapirstein, Order α^2 corrections to the decay rate of orthopositronium, Phys. Rev. Lett. 84 (2000) 5086–5089, http://dx.doi.org/10.1103/PhysRevLett.84.5086, URL https://journals.aps.org/prl/abstract/10.1103/PhysRevLett.84.5086.

[199] G.S. Adkins, R.N. Fell, J. Sapirstein, Two-loop correction to the orthopositronium decay rate, Ann. Physics 295 (2) (2002) 136–193, http://dx.doi.org/10.1006/aphy.2001.6219.

[200] R.J. Hill, G.P. Lepage, $O(\alpha^2$?$Gamma$, α^3 ?$Gamma$) Binding effects in orthopositronium decay, Phys. Rev. D 62 (11) (2000) http://dx.doi.org/10.1103/PhysRevD.62.111301, 111301(R).

[201] K. Melnikov, A. Yelkhovsky, $O(\alpha^3 \ln \alpha)$ Corrections to positronium decay rates, Phys. Rev. D 62 (11) (2000) 116003, http://dx.doi.org/10.1103/PhysRevD.62.116003.

[202] O. Jinnouchi, S. Asai, T. Kobayashi, Precision measurement of orthopositronium decay rate using sio_2 powder, Phys. Lett. B 572 (2003) 117–126, http://dx.doi.org/10.1016/j.physletb.2003.08.018, URL http://www.sciencedirect.com/science/article/pii/S0370269303012607.

[203] R.S. Vallery, P.W. Zitzewitz, D.W. Gidley, Resolution of the orthopositronium-lifetime puzzle, Phys. Rev. Lett. 90 (2003) 203402, http://dx.doi.org/10.1103/PhysRevLett.90.203402, URL http://link.aps.org/doi/10.1103/PhysRevLett.90.203402.

[204] S. Asai, O. Jinnouchi, T. Kobayashi, Solution of the orthopositronium lifetime puzzle, Internat. J. Modern Phys. A 19 (23) (2004) 3927–3938, http://dx.doi.org/10.1142/S0217751X0402018X.

[205] G.S. Adkins, Analytic evaluation of the amplitudes for orthopositronium decay to three photons to one-loop order, Phys. Rev. A 72 (2005) 032501, http://dx.doi.org/10.1103/PhysRevA.72.032501, URL http://link.aps.org/doi/10.1103/PhysRevA.72.032501.

[206] B.A. Kniehl, A.V. Kotikov, O.L. Veretin, Orthopositronium lifetime: Analytic results in $O(\alpha)$ and $O(\alpha^3 \ln \alpha)$, Phys. Rev. Lett. 101 (19) (2008) 193401, http://dx.doi.org/10.1103/PhysRevLett.101.193401.

[207] P.A.M. Dirac, The quantum theory of the electron, Proc. R. Soc. London A: Math. Phys. Eng. Sci. 117 (778) (1928) 610–624, http://dx.doi.org/10.1098/rspa.1928.0023.

[208] W. Gordon, Die energieniveaus des wasserstoffatoms nach der Dirac schen quantentheorie des elektrons, Z. Phys. 48 (1–2) (1928) 11–14.

[209] L.L. Foldy, S.A. Wouthuysen, On the Dirac theory of spin 1/2 particles and its non-relativistic limit, Phys. Rev. 78 (1950) 29–36, http://dx.doi.org/10.1103/PhysRev.78.29w.

[210] G. Breit, The effect of retardation on the interaction of two electrons, Phys. Rev. 34 (4) (1929) 553–573, http://dx.doi.org/10.1103/PhysRev.34.553.

[211] C.G. Darwin, The dynamical motions of charged particles, Phil. Mag. 39 (233) (1920) 537–551.

[212] Z.V. Chraplyvy, Reduction of relativistic two-particle wave equations to approximate forms. i., Phys. Rev. 91 (2) (1953) 388–391, http://dx.doi.org/10.1103/PhysRev.91.388.

[213] W.A. Barker, F.N. Glover, Reduction of relativistic two-particle wave equations to approximate forms. III., Phys. Rev. 99 (1) (1955) 317–324, http://dx.doi.org/10.1103/PhysRev.99.317.

[214] G. Breit, The fine structure of he as a test of the spin interaction of two electrons, Phys. Rev. 36 (3) (1930) 383–397, http://dx.doi.org/10.1103/PhysRev.36.383.

[215] G.E. Brown, D.G. Ravenhall, On the interaction of two electrons, Proc. R. Soc. London, Ser. A 208 (1951) 552–559, http://dx.doi.org/10.1098/rspa.1951.0181.

[216] E.E. Salpeter, Mass corrections to the fine structure of hydrogen-like atoms, Phys. Rev. 87 (2) (1952) 328–343, http://dx.doi.org/10.1103/PhysRev.87.328.
[217] H.A. Bethe, E.E. Salpeter, Quantum Mechanics of One- and Two-Electron Atoms, Plenum, New York, 1977.
[218] K. Bechert, J. Meixner, Uber die struktur die wasserstofflinien, Ann. Phys. 414 (6) (1935) 525–536, http://dx.doi.org/10.1002/andp.19354140603.
[219] W.E. Lamb Jr., Fine structure of the hydrogen atom. III, Phys. Rev. 85 (2) (1952) 259–276, http://dx.doi.org/10.1103/PhysRev.85.259.
[220] C. Itzykson, J.-B. Zuber, Quantum Field Theory, McGraw-Hill, 1980.
[221] V.B. Berestetskii, E.M. Lifshitz, L.P. Pitaevskii, Quantum Electrodynamics, 2, in: Landau and Lifshitz Course of Theoretical Physics, vol. 4, Butterworth-Heinemann, Oxford, 1982.
[222] H.A. Bethe, E.E. Salpeter, A relativistic equation for bound state problems, Phys. Rev. 82 (2) (1951) 309, http://dx.doi.org/10.1103/PhysRev.82.291.
[223] J. Schwinger, On the green's functions of quantized fields. II, Proc. Natl. Acad. Sci. (USA) 37 (5) (1951) 455–459, http://dx.doi.org/10.1073/pnas.37.7.455, URL http://www.jstor.org/stable/88018.
[224] H. Kita, Relativistic two-body problem, Progr. Theoret. Phys. 7 (2) (1952) 217–224, http://dx.doi.org/10.1143/ptp/7.2.217.
[225] C. Hayashi, Y. Munakata, On a relativistic integral equation for bound states, Progr. Theoret. Phys. 7 (5–6) (1952) 481–516, http://dx.doi.org/10.1143/PTP.7.5.481.
[226] M. Gell-Mann, F. Low, Bound states in quantum field theory, Phys. Rev. 84 (2) (1951) 350–354, http://dx.doi.org/10.1103/PhysRev.84.350.
[227] R. Barbieri, E. Remiddi, Solving the Bethe-Salpeter equation for positronium, Nuclear Phys. B 141 (1978) 413–422, http://dx.doi.org/10.1016/0550-3213(78)90036-6.
[228] N. Nakanishi, A general survey of the theory of the Bethe-Salpeter equation, Suppl. Prog. Theor. Phys. 43 (1969) 1–81, http://dx.doi.org/10.1143/PTPS.43.1.
[229] G.R. Allcock, Normalization of bethe-salpeter wave functions, Phys. Rev. 104 (6) (1956) 1799–1802, http://dx.doi.org/10.1103/PhysRev.104.1799.
[230] D. Lurié, A.J. Macfarlane, Y. Takahashi, Normalization of Bethe-Salpeter wave functions, Phys. Rev. 140 (1965) B1091–B1099, http://dx.doi.org/10.1103/PhysRev.140.B1091.
[231] S. Love, A study of gauge properties of the Bethe-Salpeter equation for two-fermion electromagnetic bound state systems, Ann. Physics 113 (1978) 153–176, http://dx.doi.org/10.1016/0003-4916(78)90253-1.
[232] V.K. Cung, T. Fulton, W.W. Repko, A. Schaum, A. Devoto, Complete reduction of fermion-antifermion bethe-salpeter equation with static kernel. II, Ann. Phys. (N.Y.) 98 (2) (1976) 516–552, http://dx.doi.org/10.1016/0003-4916(76)90164-0.
[233] R.M. Woloshyn, A.D. Jackson, Comparison of three-dimensional relativistic scattering equations, Nuclear Phys. B 64 (1973) 269–288, http://dx.doi.org/10.1016/0550-3213(73)90626-3.
[234] F. Gross, Relativistic few-body problem. I. Two-body equations, Phys. Rev. C 26 (5) (1982) http://dx.doi.org/10.1103/PhysRevC.26.2203, 2303–2225.
[235] J.R. Sapirstein, D.R. Yennie, Theory of hydrogenic bound states, in: T. Kinoshita (Ed.), Quantum Electrodynamics, in: Advanced Series on Directions in High Energy Physics, vol. 7, World Scientific, Singapore, 1990, pp. 560–672.
[236] H. Grotch, D.A. Owen, Bound states in quantum electrodynamics: theory and applications, Found. Phys. 32 (2002) 1419–1457.
[237] G.T. Bodwin, D.R. Yennie, M.A. Gregorio, Recoil effects in the hyperfine structure of QED bound states, Rev. Modern Phys. 57 (3) (1985) 723–782, http://dx.doi.org/10.1103/RevModPhys.57.723.
[238] S.N. Gupta, Particle-particle and particle-antiparticle interactions, Nucl. Phys. 57 (1964) 19–28, http://dx.doi.org/10.1016/0029-5582(64)90312-8.
[239] M.I. Eides, I.B. Khroplovich, A.I. Milstein, Radiative corrections to P-levels in the two-body QED problem, Phys. Lett. B 339 (3) (1994) 275–277, http://dx.doi.org/10.1016/0370-2693(94)90644-0.
[240] T. Kinoshita, G.P. Lepage, Quantum electrodynamics for nonrelativistic systems and high precision determination of α, in: T. Kinoshita (Ed.), Quantum Electrodynamics, in: Advanced Series on Directions in High Energy Physics, vol. 7, World Scientific, Singapore, 1990, pp. 81–91.
[241] T. Kinoshita, M. Nio, Radiative corrections to the muonium hyperfine structure: The $\alpha^2(Z\alpha)$ correction, Phys. Rev. D 53 (9) (1996) 4909–4929, http://dx.doi.org/10.1103/PhysRevD.53.4909.
[242] P. Labelle, Effective field theories for QED bound states: Extending nonrelativistic QED to study retardation effects, Phys. Rev. D 58 (9) (1998) 093013, http://dx.doi.org/10.1103/PhysRevD.58.093013.
[243] R.J. Hill, G. Lee, G. Paz, M.P. Solon, NRQED Lagrangian at order $1/M^4$, Phys. Rev. D 87 (5) (2013) 053017, http://dx.doi.org/10.1103/PhysRevD.87.053017.
[244] G. Paz, An introduction to NRQED, Modern Phys. Lett. A 30 (26) (2015) 1550128, http://dx.doi.org/10.1142/S021773231550128X.
[245] A. Pineda, J. Soto, The lamb shift in dimensional regularization, Phys. Lett. B 420 (3–4) (1998) 391–398, http://dx.doi.org/10.1016/S0370-2693(97)01537-2.
[246] A.H. Hoang, Heavy quarkonium dynamics, in: M. Shifman (Ed.), At the Frontier of Particle Physics/Handbook of QCD, Vol. 4, World Scientific, Singapore, 2002, pp. 2215–2331, arXiv:hep-ph/0204299v1, URL http://arxiv.org/abs/hep-ph/0204299.
[247] N. Brambilla, A. Pineda, J. Soto, A. Vairo, Effective-field theories for heavy quarkonium, Rev. Modern Phys. 77 (4) (2005) 1423–1496, http://dx.doi.org/10.1103/RevModPhys.77.1423, URL http://link.aps.org/doi/10.1103/RevModPhys.77.1423.
[248] A. Pineda, Next-to-leading-log renormalization-group running in heavy-quarkonium creation and annihilation, Phys. Rev. D 66 (2002) 054022.
[249] M.E. Luke, A.V. Manohar, I.Z. Rothstein, Renormalization group scaling in nonrelativistic QCD, Phys. Rev. D 61 (2000) 074025.
[250] I.Z. Rothstein, TASI lectures on effective field theories, 2000, URL arXiv:hep-ph/0308266v2.
[251] A.A. Petrov, A.E. Blechman, Effective Field Theories, World Scientific, Singapore, 2016.
[252] M.S. Fee, A.P. Mills, Jr., S. Chu, E.D. Shaw, K. Danzmann, R.J. Chichester, D.M. Zuckerman, Measurement of the positronium $1\,^3S_1 \rightarrow 2\,^3S_1$ interval by continuous-wave two-photon excitation, Phys. Rev. Lett. 70 (1993) 1397–1400, http://dx.doi.org/10.1103/PhysRevLett.70.1397, URL http://link.aps.org/doi/10.1103/PhysRevLett.70.1397.
[253] D.A. Cooke, P. Crivelli, J. Alnis, A. Antognini, B. Brown, S. Friedreich, A. Gabard, T. Haensch, K. Kirch, A. Rubbia, V. Vrankovic, Observation of positronium annihilation in the 2*S* state: Towards a new measurement of the 1*S*-2*S* transition frequency, Hyperfine Interact. (2015) 1–7, http://dx.doi.org/10.1007/s10751-015-1158-4.
[254] A. Antognini, F. Nez, K. Schuhmann, F.D. Amaro, F. Biraben, J.M.R. Cardoso, D.S. Covita, A. Dax, S. Dhawan, M. Diepold, L.M.P. Fernandes, A. Giesen, A.L. Gouvea, T. Graf, T.W. Hänsch, P. Indelicato, L. Julien, C.-Y. Kao, P. Knowles, F. Kottmann, E.-O. Le Bigot, Y.-W. Liu, J.A.M. Lopes, L. Ludhova, C.M.B. Monteiro, F. Mulhauser, T. Nebel, P. Rabinowitz, J.M.F. dos Santos, L.A. Schaller, C. Schwob, D. Taqqu, J.F.C.A. Veloso, J. Vogelsang, R. Pohl, Proton structure from the measurement of 2S-2p transition frequencies of muonic hydrogen, Science 339 (6118) (2013) 417–420, http://dx.doi.org/10.1126/science.1230016.
[255] E. Tiesinga, P.J. Mohr, D.B. Newell, B.N. Taylor, CODATA recommended values of the fundamental physical constants: 2018, Rev. Modern Phys. 93 (2) (2021) 025010, http://dx.doi.org/10.1103/RevModPhys.93.025010.
[256] J.-P. Karr, D. Marchand, E. Voutier, The proton size, Nature Rev. Phys. 2 (2020) 601–614, http://dx.doi.org/10.1038/s42254-020-0229-x.
[257] R.J. Hughes, B.I. Deutch, Electric charges of positronium and antiprotons, Phys. Rev. Lett. 69 (4) (1992) 578–581, http://dx.doi.org/10.1103/PhysRevLett.69.578.

[258] M. Deutsch, Three-quantum decay of positronium, Phys. Rev. 83 (1951) 866–867, http://dx.doi.org/10.1103/PhysRev.83.866, URL http://link.aps.org/doi/10.1103/PhysRev.83.866.

[259] M. Deutsch, E. Dulit, Short range interaction of electrons and fine structure of positronium, Phys. Rev. 84 (1951) 601–602, http://dx.doi.org/10.1103/PhysRev.84.601, URL http://link.aps.org/doi/10.1103/PhysRev.84.601.

[260] M. Deutsch, S.C. Brown, Zeeman effect and hyperfine splitting of positronium, Phys. Rev. 85 (1952) 1047–1048, http://dx.doi.org/10.1103/PhysRev.85.1047, URL http://link.aps.org/doi/10.1103/PhysRev.85.1047.

[261] G. Bearman, A. Mills, Calculation of the pressure shift of the positronium hyperfine interval, Phys. Lett. A 56 (5) (1976) 350–352, http://dx.doi.org/10.1016/0375-9601(76)90368-6, URL http://www.sciencedirect.com/science/article/pii/0375960176903686.

[262] A. Ishida, T. Namba, S. Asai, Measurement of positronium thermalization in isobutane gas for precision measurement of ground-state hyperfine splitting, J. Phys. B: At. Mol. Opt. Phys. 49 (6) (2016) 064008, URL http://stacks.iop.org/0953-4075/49/i=6/a=064008.

[263] D.B. Cassidy, S.H.M. Deng, H.K.M. Tanaka, A.P. Mills, Jr., Single shot positron annihilation lifetime spectroscopy, Appl. Phys. Lett. 88 (19) (2006) 194105, http://dx.doi.org/10.1063/1.2203336.

[264] P.J. Schultz, K.G. Lynn, Interaction of positron beams with surfaces, thin films, and interfaces, Rev. Modern Phys. 60 (1988) 701–779, http://dx.doi.org/10.1103/RevModPhys.60.701.

[265] D.B. Cassidy, S.H.M. Deng, R.G. Greaves, A.P. Mills, Jr., Accumulator for the production of intense positron pulses, Rev. Sci. Instrum. 77 (7) (2006) 073106, http://dx.doi.org/10.1063/1.2221509.

[266] D.B. Cassidy, S.H.M. Deng, R.G. Greaves, T. Maruo, N. Nishiyama, J.B. Snyder, H.K.M. Tanaka, A.P. Mills, Jr., Experiments with a high-density positronium gas, Phys. Rev. Lett. 95 (2005) 195006, http://dx.doi.org/10.1103/PhysRevLett.95.195006, URL http://link.aps.org/doi/10.1103/PhysRevLett.95.195006.

[267] K.F. Canter, P.G. Coleman, T.C. Griffith, G.R. Heyland, Measurement of total cross sections for low energy positron-helium collisions. (positron backscattering from metal surface), J. Phys. B 5 (8) (1972) L167, URL http://stacks.iop.org/0022-3700/5/i=8/a=007.

[268] D.G. Costello, D.E. Groce, D.F. Herring, J.W. McGowan, Evidence for the negative work function associated with positrons in gold, Phys. Rev. B 5 (1972) 1433–1436, http://dx.doi.org/10.1103/PhysRevB.5.1433, URL http://link.aps.org/doi/10.1103/PhysRevB.5.1433.

[269] S. Pendyala, P. Zitzewitz, J. McGowan, P. Orth, Low-energy positrons from metallic moderators in a back scattering mode, Phys. Lett. A 43 (3) (1973) 298–300, http://dx.doi.org/10.1016/0375-9601(73)90314-9, URL http://www.sciencedirect.com/science/article/pii/0375960173903149.

[270] A.P. Mills, Jr., Positron solid state physics, in: W. Brandt, A. Dupasquier (Eds.), Course LXXXIII "Positron Solid-State Physics", IOS Press, Proceedings of the International School of Physics 'Enrico Fermi', Amsterdam, 1983, pp. 77–187.

[271] A.P. Mills, Jr., E.M. Gullikson, Solid neon moderator for producing slow positrons, Appl. Phys. Lett. 49 (1986) 1121, http://dx.doi.org/10.1063/1.97441.

[272] C. Hugenschmidt, C. Piochacz, M. Reiner, K. Schreckenbach, The NEPOMUC upgrade and advanced positron beam experiments, New J. Phys. 14 (5) (2012) 055027, URL http://stacks.iop.org/1367-2630/14/i=5/a=055027.

[273] R.H. Howell, R.A. Alvarez, M. Stanek, Production of slow positrons with a 100 MeV electron linac, Appl. Phys. Lett. 40 (8) (1982) 751–752, http://dx.doi.org/10.1063/1.93215, URL http://scitation.aip.org/content/aip/journal/apl/40/8/10.1063/1.93215.

[274] D.B. Cassidy, A.W. Hunt, P. Asoka-Kumar, B.V. Bhat, T.E. Cowan, R.H. Howell, K.G. Lynn, A.P. Mills, Jr., J.C. Palathingal, J.A. Golovchenko, Resonant versus nonresonant nuclear excitation of ^{115}In by positron annihilation, Phys. Rev. C 64 (2001) 054603, http://dx.doi.org/10.1103/PhysRevC.64.054603, URL https://link.aps.org/doi/10.1103/PhysRevC.64.054603.

[275] C.M. Surko, M. Leventhal, A. Passner, Positron plasma in the laboratory, Phys. Rev. Lett. 62 (1989) 901–904, http://dx.doi.org/10.1103/PhysRevLett.62.901, URL http://link.aps.org/doi/10.1103/PhysRevLett.62.901.

[276] C.M. Surko, T.J. Murphy, Positron trapping in an electrostatic well by inelastic collisions with nitrogen molecules, Phys. Rev. A 46 (1992) 5696, http://dx.doi.org/10.1103/PhysRevA.46.5696.

[277] M.J. Puska, R.M. Nieminen, Theory of positrons in solids and on solid surfaces, Rev. Modern Phys. 66 (1994) 841–897, http://dx.doi.org/10.1103/RevModPhys.66.841, URL https://link.aps.org/doi/10.1103/RevModPhys.66.841.

[278] A.P. Mills, Jr., Thermal activation measurement of positron binding energies at surfaces, Solid State Commun. 31 (9) (1979) 623–626, http://dx.doi.org/10.1016/0038-1098(79)90310-7, URL http://www.sciencedirect.com/science/article/pii/0038109879903107.

[279] S. Mariazzi, P. Bettotti, R.S. Brusa, Positronium cooling and emission in vacuum from nanochannels at cryogenic temperature, Phys. Rev. Lett. 104 (2010) 243401, http://dx.doi.org/10.1103/PhysRevLett.104.243401, URL http://link.aps.org/doi/10.1103/PhysRevLett.104.243401.

[280] A.P. Mills, Jr., E.D. Shaw, M. Leventhal, R.J. Chichester, D.M. Zuckerman, Thermal desorption of cold positronium from oxygen-treated al(111) surfaces, Phys. Rev. B 44 (1991) 5791–5799, http://dx.doi.org/10.1103/PhysRevB.44.5791, URL http://link.aps.org/doi/10.1103/PhysRevB.44.5791.

[281] G. Laricchia, S. Armitage, A. Kövér, D. Murtagh, Ionizing collisions by positrons and positronium impact on the inert atoms, in: Advances in Atomic, Molecular, and Optical Physics, in: Advances In Atomic, Molecular, and Optical Physics, vol. 56, Academic Press, 2008, pp. 1–47.

[282] S.J. Brawley, S.E. Fayer, M. Shipman, G. Laricchia, Positronium production and scattering below its breakup threshold, Phys. Rev. Lett. 115 (2015) 223201, http://dx.doi.org/10.1103/PhysRevLett.115.223201, URL http://link.aps.org/doi/10.1103/PhysRevLett.115.223201.

[283] G. Laricchia, M. Charlton, G. Clark, T. Griffith, Excited state positronium formation in low density gases, Phys. Lett. A 109 (3) (1985) 97–100, http://dx.doi.org/10.1016/0375-9601(85)90264-6, URL http://www.sciencedirect.com/science/article/pii/0375960185902646.

[284] D.J. Murtagh, D.A. Cooke, G. Laricchia, Excited-state positronium formation from helium, argon, and xenon, Phys. Rev. Lett. 102 (2009) 133202, http://dx.doi.org/10.1103/PhysRevLett.102.133202, URL http://link.aps.org/doi/10.1103/PhysRevLett.102.133202.

[285] N.F. Ramsey, Experiments with separated oscillatory fields and hydrogen masers, Rev. Modern Phys. 62 (1990) 541–552, http://dx.doi.org/10.1103/RevModPhys.62.541, URL https://link.aps.org/doi/10.1103/RevModPhys.62.541.

[286] A. Held, S. Kahana, Quasi-positronium in metals, Can. J. Phys. 42 (10) (1964) 1908–1913, http://dx.doi.org/10.1139/p64-180.

[287] H. Kanazawa, Y.H. Ohtsuki, S. Yanagawa, Positronium formation in metals, Phys. Rev. 138 (1965) A1155–A1157, http://dx.doi.org/10.1103/PhysRev.138.A1155, URL http://link.aps.org/doi/10.1103/PhysRev.138.A1155.

[288] A.P. Mills, Jr., Positronium formation at surfaces, Phys. Rev. Lett. 41 (1978) 1828–1831, http://dx.doi.org/10.1103/PhysRevLett.41.1828, URL http://link.aps.org/doi/10.1103/PhysRevLett.41.1828.

[289] A.P. Mills, Jr., L. Pfeiffer, Desorption of surface positrons: A source of free positronium at thermal velocities, Phys. Rev. Lett. 43 (1979) 1961–1964, http://dx.doi.org/10.1103/PhysRevLett.43.1961, URL http://link.aps.org/doi/10.1103/PhysRevLett.43.1961.

[290] K.F. Canter, A.P. Mills, Jr., S. Berko, Observations of positronium lyman-α radiation, Phys. Rev. Lett. 34 (1975) 177–180, http://dx.doi.org/10.1103/PhysRevLett.34.177, URL http://link.aps.org/doi/10.1103/PhysRevLett.34.177.

[291] D.B. Cassidy, T.H. Hisakado, H.W.K. Tom, A.P. Mills, Jr., New mechanism for positronium formation on a silicon surface, Phys. Rev. Lett. 106 (2011) 133401, http://dx.doi.org/10.1103/PhysRevLett.106.133401.

[292] D. Cassidy, T. Hisakado, H. Tom, A.P. Mills, Jr., Positronium formation via excitonlike states on si and ge surfaces, Phys. Rev. B 84 (2011) 195312, http://dx.doi.org/10.1103/PhysRevB.84.195312, URL http://link.aps.org/doi/10.1103/PhysRevB.84.195312.

[293] D.B. Cassidy, T.H. Hisakado, H.W.K. Tom, A.P. Mills, Jr., Photoemission of positronium from si, Phys. Rev. Lett. 107 (2011) 033401, http://dx.doi.org/10.1103/PhysRevLett.107.033401, URL http://link.aps.org/doi/10.1103/PhysRevLett.107.033401.

[294] D.B. Cassidy, T.H. Hisakado, H.W.K. Tom, A.P. Mills, Excitonic positronium emission from n-Si(111), Phys. Rev. B 86 (2012) 155303, http://dx.doi.org/10.1103/PhysRevB.86.155303, URL https://link.aps.org/doi/10.1103/PhysRevB.86.155303.

[295] A. Kawasuso, M. Maekawa, A. Miyashita, K. Wada, T. Kaiwa, Y. Nagashima, Positronium formation at Si surfaces, Phys. Rev. B 97 (2018) 245303, http://dx.doi.org/10.1103/PhysRevB.97.245303, URL https://link.aps.org/doi/10.1103/PhysRevB.97.245303.

[296] B.S. Cooper, A.M. Alonso, A. Deller, L. Liszkay, D.B. Cassidy, Positronium production in cryogenic environments, Phys. Rev. B 93 (2016) 125305, http://dx.doi.org/10.1103/PhysRevB.93.125305, URL http://link.aps.org/doi/10.1103/PhysRevB.93.125305.

[297] S.J. Tao, The formation of positronium in molecular substances, Appl. Phys. 10 (1) (1976) 67–79, http://dx.doi.org/10.1007/BF00929530.

[298] Y. Nagashima, Y. Morinaka, T. Kurihara, Y. Nagai, T. Hyodo, T. Shidara, K. Nakahara, Origins of positronium emitted from SiO_2, Phys. Rev. B 58 (1998) 12676–12679, http://dx.doi.org/10.1103/PhysRevB.58.12676, URL http://link.aps.org/doi/10.1103/PhysRevB.58.12676.

[299] R. Paulin, G. Ambrosino, Annihilation libre de l'ortho-positonium formé dans certaines poudres de grande surface spécifique, J. Phys. France 29 (4) (1968) 263–270, http://dx.doi.org/10.1051/jphys:01968002904026300.

[300] P. Sen, A.P. Patro, Positron annihilation studies in oxides, Il Nuovo Cimento B (1965-1970) 64 (2) (1969) 324–336, http://dx.doi.org/10.1007/BF02711014.

[301] Y. Nagashima, M. Kakimoto, T. Hyodo, K. Fujiwara, A. Ichimura, T. Chang, J. Deng, T. Akahane, T. Chiba, K. Suzuki, B.T.A. McKee, A.T. Stewart, Thermalization of free positronium atoms by collisions with silica-powder grains, aerogel grains, and gas molecules, Phys. Rev. A 52 (1995) 258–265, http://dx.doi.org/10.1103/PhysRevA.52.258, URL https://link.aps.org/doi/10.1103/PhysRevA.52.258.

[302] L. Liszkay, C. Corbel, P. Perez, P. Desgardin, M.F. Barthe, T. Ohdaira, R. Suzuki, P. Crivelli, U. Gendotti, A. Rubbia, M. Etienne, A. Walcarius, Positronium reemission yield from mesostructured silica films, Appl. Phys. Lett. 92 (6) (2008) 063114, http://dx.doi.org/10.1063/1.2844888.

[303] L. Liszkay, M.F. Barthe, C. Corbel, P. Crivelli, P. Desgardin, M. Etienne, T. Ohdaira, P. Perez, R. Suzuki, V. Valtchev, A. Walcarius, Orthopositronium annihilation and emission in mesostructured thin silica and silicalite-1 films, Appl. Surf. Sci. 255 (1) (2008) 187–190, http://dx.doi.org/10.1016/j.apsusc.2008.05.210.

[304] L. Liszkay, C. Corbel, L. Raboin, J.-P. Boilot, P. Perez, A. Brunet-Bruneau, P. Crivelli, U. Gendotti, A. Rubbia, T. Ohdaira, R. Suzuki, Mesoporous silica films with varying porous volume fraction: Direct correlation between ortho-positronium annihilation decay and escape yield into vacuum, Appl. Phys. Lett. 95 (12) (2009) 124103, http://dx.doi.org/10.1063/1.3234381.

[305] L. Liszkay, F. Guillemot, C. Corbel, J.-P. Boilot, T. Gacoin, E. Barthel, P. Perez, M.-F. Barthe, P. Desgardin, P. Crivelli, U. Gendotti, A. Rubbia, Positron annihilation in latex-templated macroporous silica films: pore size and ortho-positronium escape, New J. Phys. 14 (6) (2012) 065009, URL http://stacks.iop.org/1367-2630/14/i=6/a=065009.

[306] W. Brandt, R. Paulin, Positronium diffusion in solids, Phys. Rev. Lett. 21 (1968) 193–195, http://dx.doi.org/10.1103/PhysRevLett.21.193, URL http://link.aps.org/doi/10.1103/PhysRevLett.21.193.

[307] S. Curry, A. Schawlow, Measurements of the kinetic energy of free positronium formed in mgo , Phys. Lett. A 37 (1) (1971) 5–6, http://dx.doi.org/10.1016/0375-9601(71)90304-5, URL http://www.sciencedirect.com/science/article/pii/0375960171903045.

[308] D.B. Cassidy, P. Crivelli, T.H. Hisakado, L. Liszkay, V.E. Meligne, P. Perez, H.W.K. Tom, A.P. Mills, Jr., Positronium cooling in porous silica measured via Doppler spectroscopy, Phys. Rev. A 81 (2010) 012715, http://dx.doi.org/10.1103/PhysRevA.81.012715.

[309] P. Crivelli, U. Gendotti, A. Rubbia, L. Liszkay, P. Perez, C. Corbel, Measurement of the orthopositronium confinement energy in mesoporous thin films, Phys. Rev. A 81 (2010) 052703, http://dx.doi.org/10.1103/PhysRevA.81.052703.

[310] L. Gurung, A.M. Alonso, T.J. Babij, B.S. Cooper, A.L. Shluger, D.B. Cassidy, Positronium emission from mgo smoke nanocrystals, J. Phys. B: At. Mol. Opt. Phys. 52 (10) (2019) 105004, http://dx.doi.org/10.1088/1361-6455/ab0f06.

[311] J.L. Rowsell, O.M. Yaghi, Metal organic frameworks: a new class of porous materials, Microporous and Mesoporous Mater. 73 (1) (2004) 3–14, http://dx.doi.org/10.1016/j.micromeso.2004.03.034, Metal-Organic Open Frameworks, URL http://www.sciencedirect.com/science/article/pii/S1387181104001295.

[312] D. Dutta, J.I. Feldblyum, D.W. Gidley, J. Imirzian, M. Liu, A.J. Matzger, R.S. Vallery, A.G. Wong-Foy, Evidence of positronium Bloch states in porous crystals of Zn_4O-coordination polymers, Phys. Rev. Lett. 110 (2013) 197403, http://dx.doi.org/10.1103/PhysRevLett.110.197403, URL http://link.aps.org/doi/10.1103/PhysRevLett.110.197403.

[313] P. Crivelli, D. Cooke, B. Barbiellini, B.L. Brown, J.I. Feldblyum, P. Guo, D.W. Gidley, L. Gerchow, A.J. Matzger, Positronium emission spectra from self-assembled metal-organic frameworks, Phys. Rev. B 89 (2014) 241103, http://dx.doi.org/10.1103/PhysRevB.89.241103, URL http://link.aps.org/doi/10.1103/PhysRevB.89.241103.

[314] A.C.L. Jones, H.J. Goldman, Q. Zhai, P. Feng, H.W.K. Tom, A.P. Mills, Jr., Monoenergetic positronium emission from metal-organic framework crystals, Phys. Rev. Lett. 114 (2015) 153201, http://dx.doi.org/10.1103/PhysRevLett.114.153201, URL http://link.aps.org/doi/10.1103/PhysRevLett.114.153201.

[315] A. Deller, A.M. Alonso, B.S. Cooper, S.D. Hogan, D.B. Cassidy, Electrostatically guided Rydberg positronium, Phys. Rev. Lett. 117 (2016) 073202, http://dx.doi.org/10.1103/PhysRevLett.117.073202, URL http://link.aps.org/doi/10.1103/PhysRevLett.117.073202.

[316] D.B. Cassidy, S.H.M. Deng, A.P. Mills, Evidence for positronium molecule formation at a metal surface, Phys. Rev. A 76 (2007) 062511, http://dx.doi.org/10.1103/PhysRevA.76.062511, URL https://link.aps.org/doi/10.1103/PhysRevA.76.062511.

[317] D.B. Cassidy, A.P. Mills, Jr., Enhanced Ps-Ps interactions due to quantum confinement, Phys. Rev. Lett. 107 (2011) 213401, http://dx.doi.org/10.1103/PhysRevLett.107.213401, URL http://link.aps.org/doi/10.1103/PhysRevLett.107.213401.

[318] H. Saito, Y. Nagashima, T. Hyodo, T. Chang, Detection of paramagnetic centers on amorphous-SiO_2 grain surfaces using positronium, Phys. Rev. B 52 (1995) R689–R692, http://dx.doi.org/10.1103/PhysRevB.52.R689, URL https://link.aps.org/doi/10.1103/PhysRevB.52.R689.

[319] H. Saito, T. Hyodo, Quenching of positronium by surface paramagnetic centers in ultraviolet- and positron-irradiated fine oxide grains, Phys. Rev. B 60 (1999) 11070–11077, http://dx.doi.org/10.1103/PhysRevB.60.11070, URL https://link.aps.org/doi/10.1103/PhysRevB.60.11070.

[320] C.M. Surko, F.A. Gianturco (Eds.), Cooling and Quenching of Positronium in Porous Material, Springer Netherlands, Dordrecht, 2001, http://dx.doi.org/10.1007/0-306-47613-4_7.

[321] D.B. Cassidy, K.T. Yokoyama, S.H.M. Deng, D.L. Griscom, H. Miyadera, H.W.K. Tom, C.M. Varma, A.P. Mills, Jr., Positronium as a probe of transient paramagnetic centers in $a-SiO_2$, Phys. Rev. B 75 (2007) 085415, http://dx.doi.org/10.1103/PhysRevB.75.085415, URL http://link.aps.org/doi/10.1103/PhysRevB.75.085415.

[322] D.B. Cassidy, Physics with many positrons, in: R.S. Brusa, A. Dupasquier, A.P. Mills, Jr. (Eds.), Course CLXXIV "Physics with Many Positrons", IOS Press, Proceedings of the International School of Physics 'Enrico Fermi', Amserdam, 2010, pp. 1–75.

[323] K.P. Ziock, C.D. Dermer, R.H. Howell, F. Magnotta, K.M. Jones, Optical saturation of the $1^3S - 2^3P$ transition in positronium, J. Phys. B 23 (2) (1990) 329, http://dx.doi.org/10.1088/0953-4075/23/2/015.

[324] M.S. Fee, S. Chu, A.P. Mills, Jr., R.J. Chichester, D.M. Zuckerman, E.D. Shaw, K. Danzmann, Measurement of the positronium $1\,^3S_1 \rightarrow 2\,^3S_1$ interval by continuous-wave two-photon excitation, Phys. Rev. A 48 (1993) 192–219, http://dx.doi.org/10.1103/PhysRevA.48.192, URL http://link.aps.org/doi/10.1103/PhysRevA.48.192.

[325] A.C.L. Jones, A.M. Piñeiro, E.E. Roeder, H.J. Rutbeck-Goldman, H.W.K. Tom, A.P. Mills, Jr., Large-area field-ionization detector for the study of Rydberg atoms, Rev. Sci. Instrum. 87 (11) (2016) http://dx.doi.org/10.1063/1.4967305, URL https://www.scopus.com/inward/record.uri?eid=2-s2.0-84999264461&doi=10.1063%2f1.4967305&partnerID=40&md5=eebd8d67b780660e15af7ee583a4d100.

[326] W. Demtröder, Laser Spectroscopy, third, Springer, New York, 2003.

[327] C. Vigo, L. Gerchow, B. Radics, M. Raaijmakers, A. Rubbia, P. Crivelli, New bounds from positronium decays on massless mirror dark photons, Phys. Rev. Lett. 124 (2020) 101803, http://dx.doi.org/10.1103/PhysRevLett.124.101803, URL https://link.aps.org/doi/10.1103/PhysRevLett.124.101803.

[328] L. Gurung, T.J. Babij, S.D. Hogan, D.B. Cassidy, Precision microwave spectroscopy of the positronium $n = 2$ fine structure, Phys. Rev. Lett. 125 (2020) 073002, http://dx.doi.org/10.1103/PhysRevLett.125.073002, URL https://link.aps.org/doi/10.1103/PhysRevLett.125.073002.

[329] D.B. Cassidy, T.H. Hisakado, H.W.K. Tom, A.P. Mills, Jr., Positronium hyperfine interval measured via saturated absorption spectroscopy, Phys. Rev. Lett. 109 (2012) 073401, http://dx.doi.org/10.1103/PhysRevLett.109.073401, URL http://link.aps.org/doi/10.1103/PhysRevLett.109.073401.

[330] A.P. Mills, Jr., Line-shape effects in the measurement of the positronium hyperfine interval, Phys. Rev. A 27 (1983) 262–267, http://dx.doi.org/10.1103/PhysRevA.27.262, URL http://link.aps.org/doi/10.1103/PhysRevA.27.262.

[331] M.W. Ritter, P.O. Egan, V.W. Hughes, K.A. Woodle, Precision determination of the hyperfine-structure interval in the ground state of positronium. V, Phys. Rev. A 30 (1984) 1331–1338, http://dx.doi.org/10.1103/PhysRevA.30.1331, URL http://link.aps.org/doi/10.1103/PhysRevA.30.1331.

[332] R. Ley, D. Hagena, D. Weil, G. Werth, W. Arnold, H. Schneider, Spectroscopy of excited state positronium, Hyperfine Interact. 89 (1) (1994) 327–341, http://dx.doi.org/10.1007/BF02064517.

[333] D. Hagena, R. Ley, D. Weil, G. Werth, W. Arnold, H. Schneider, Precise measurement of n=2 positronium fine-structure intervals, Phys. Rev. Lett. 71 (1993) 2887–2890, http://dx.doi.org/10.1103/PhysRevLett.71.2887, URL http://link.aps.org/doi/10.1103/PhysRevLett.71.2887.

[334] C.I. Westbrook, D.W. Gidley, R.S. Conti, A. Rich, New precision measurement of the orthopositronium decay rate: A discrepancy with theory, Phys. Rev. Lett. 58 (1987) 1328–1331, http://dx.doi.org/10.1103/PhysRevLett.58.1328, URL https://link.aps.org/doi/10.1103/PhysRevLett.58.1328.

[335] A.M. Alonso, B.S. Cooper, A. Deller, S.D. Hogan, D.B. Cassidy, Positronium decay from $n = 2$ states in electric and magnetic fields, Phys. Rev. A 93 (2016) 012506, http://dx.doi.org/10.1103/PhysRevA.93.012506, URL http://link.aps.org/doi/10.1103/PhysRevA.93.012506.

[336] B.S. Cooper, A.M. Alonso, A. Deller, T.E. Wall, D.B. Cassidy, A trap-based pulsed positron beam optimised for positronium laser spectroscopy, Rev. Sci. Instrum. 86 (10) (2015) http://dx.doi.org/10.1063/1.4931690, URL http://scitation.aip.org/content/aip/journal/rsi/86/10/10.1063/1.4931690.

[337] A.P. Mills, Jr., S. Berko, K.F. Canter, Fine-structure measurement in the first excited state of positronium, Phys. Rev. Lett. 34 (1975) 1541–1544, http://dx.doi.org/10.1103/PhysRevLett.34.1541, URL http://link.aps.org/doi/10.1103/PhysRevLett.34.1541.

[338] L. Gurung, T.J. Babij, J. Pérez-Ríos, S.D. Hogan, D.B. Cassidy, Observation of asymmetric lineshapes in precision microwave spectroscopy of the positronium $2\,^3s_1 \rightarrow 2\,^3p_J$ ($J = 1, 2$) fine structure intervals, Phys. Rev. A (2021) in press.

[339] H.W. Kendall, The First Excited State of Positronium, (Ph.D. thesis), Massachusetts Institute of Technology, 1954.

[340] S. Varghese, E. Ensberg, V. Hughes, I. Lindgren, Evidence for formation of the first excited state of positronium, Phys. Lett. A 49 (6) (1974) 415–417, http://dx.doi.org/10.1016/0375-9601(74)90295-3, URL http://www.sciencedirect.com/science/article/pii/0375960174902953.

[341] L.S. Vasilenko, V.P. Chebotaev, A.V. Shishaev, Line shape of two-photon absorption in a standing-wave field in a gas, Sov. Phys. JETP Lett. 12 (1970) 113.

[342] F. Biraben, B. Cagnac, G. Grynberg, Experimental evidence of two-photon transition without Doppler broadening, Phys. Rev. Lett. 32 (1974) 643–645, http://dx.doi.org/10.1103/PhysRevLett.32.643, URL http://link.aps.org/doi/10.1103/PhysRevLett.32.643.

[343] T.W. Hänsch, S.A. Lee, R. Wallenstein, C. Wieman, Doppler-free two-photon spectroscopy of hydrogen $1S - 2S$, Phys. Rev. Lett. 34 (1975) 307–309, http://dx.doi.org/10.1103/PhysRevLett.34.307, URL http://link.aps.org/doi/10.1103/PhysRevLett.34.307.

[344] F. Biraben, Spectroscopy of atomic hydrogen, Eur. Phys. J. Spec. Top. 172 (1) (2009) 109–119, http://dx.doi.org/10.1140/epjst/e2009-01045-3.

[345] T.W. Hänsch, Nobel lecture: Passion for precision, Rev. Modern Phys. 78 (2006) 1297–1309, http://dx.doi.org/10.1103/RevModPhys.78.1297, URL https://link.aps.org/doi/10.1103/RevModPhys.78.1297.

[346] C.G. Parthey, A. Matveev, J. Alnis, B. Bernhardt, A. Beyer, R. Holzwarth, A. Maistrou, R. Pohl, K. Predehl, T. Udem, T. Wilken, N. Kolachevsky, M. Abgrall, D. Rovera, C. Salomon, P. Laurent, T.W. Hänsch, Improved measurement of the hydrogen $1S - 2S$ transition frequency, Phys. Rev. Lett. 107 (2011) 203001, http://dx.doi.org/10.1103/PhysRevLett.107.203001, URL http://link.aps.org/doi/10.1103/PhysRevLett.107.203001.

[347] S. Chu, A.P. Mills, Jr., J.L. Hall, Measurement of the positronium $1\,^3S_1 \rightarrow 2\,^3S_1$ interval by Doppler-free two-photon spectroscopy, Phys. Rev. Lett. 52 (1984) 1689–1692, http://dx.doi.org/10.1103/PhysRevLett.52.1689, URL http://link.aps.org/doi/10.1103/PhysRevLett.52.1689.

[348] M.S. Fee, K. Danzmann, S. Chu, Optical heterodyne measurement of pulsed lasers: Toward high-precision pulsed spectroscopy, Phys. Rev. A 45 (1992) 4911–4924, http://dx.doi.org/10.1103/PhysRevA.45.4911, URL http://link.aps.org/doi/10.1103/PhysRevA.45.4911.

[349] K. Danzmann, M.S. Fee, S. Chu, Doppler-free laser spectroscopy of positronium and muonium: Reanalysis of the 1 s-2 s measurements, Phys. Rev. A 39 (1989) 6072–6073, http://dx.doi.org/10.1103/PhysRevA.39.6072, URL http://link.aps.org/doi/10.1103/PhysRevA.39.6072.

[350] A.P. Mills, Jr., E.D. Shaw, R.J. Chichester, D.M. Zuckerman, Production of slow positron bunches using a microtron accelerator, Rev. Sci. Instrum. 60 (5) (1989) 825–830, http://dx.doi.org/10.1063/1.1141030, URL http://scitation.aip.org/content/aip/journal/rsi/60/5/10.1063/1.1141030.

[351] M.S. Fee, A.P. Mills, Jr., E.D. Shaw, R.J. Chichester, D.M. Zuckerman, S. Chu, K. Danzmann, Sensitive detection of Doppler-free two-photon-excited 2 s positronium by spatially separated photoionization, Phys. Rev. A 44 (1991) R5–R8, http://dx.doi.org/10.1103/PhysRevA.44.R5, URL http://link.aps.org/doi/10.1103/PhysRevA.44.R5.

[352] A. Deller, D. Edwards, T. Mortensen, C.A. Isaac, D.P. van der Werf, H.H. Telle, M. Charlton, Exciting positronium with a solid-state UV laser: the Doppler-broadened lyman-alpha transition, J. Phys. B: At. Mol. Opt. Phys. 48 (17) (2015) 175001, URL http://stacks.iop.org/0953-4075/48/i=17/a=175001.

[353] S. Aghion, C. Amsler, A. Ariga, T. Ariga, G. Bonomi, P. Bräunig, J. Bremer, R.S. Brusa, L. Cabaret, M. Caccia, R. Caravita, F. Castelli, G. Cerchiari, K. Chlouba, S. Cialdi, D. Comparat, G. Consolati, A. Demetrio, L. Di Noto, M. Doser, A. Dudarev, A. Ereditato, C. Evans, R. Ferragut, J. Fesel, A. Fontana, O.K. Forslund, S. Gerber, M. Giammarchi, A. Gligorova, S. Gninenko, F. Guatieri, S. Haider, H. Holmestad, T. Huse, I.L. Jernelv, E. Jordan, A. Kellerbauer, M. Kimura, T. Koettig, D. Krasnicky, V. Lagomarsino, P. Lansonneur, P. Lebrun, S. Lehner, J. Liberadzka, C. Malbrunot, S. Mariazzi, L. Marx, V. Matveev, Z. Mazzotta, G. Nebbia, P. Nedelec, M. Oberthaler, N. Pacifico, D. Pagano, L. Penasa, V. Petracek, C. Pistillo, F. Prelz, M. Prevedelli, L. Ravelli, L. Resch, B. Rienäcker, O.M. Røhne, A. Rotondi, M. Sacerdoti, H. Sandaker, R. Santoro, P. Scampoli, L. Smestad, F. Sorrentino, M. Spacek, J. Storey, I.M. Strojek, G. Testera, I. Tietje, S. Vamosi, E. Widmann, P. Yzombard, J. Zmeskal, N. Zurlo, AEgIS Collaboration Collaboration Collaboration, Laser excitation of the $n = 3$ level of positronium for antihydrogen production, Phys. Rev. A 94 (2016) 012507, http://dx.doi.org/10.1103/PhysRevA.94.012507, URL http://link.aps.org/doi/10.1103/PhysRevA.94.012507.

[354] T.F. Gallagher, Rydberg atoms, Rep. Progr. Phys. 51 (2) (1988) 143, URL http://stacks.iop.org/0034-4885/51/i=2/a=001.

[355] K.P. Ziock, R.H. Howell, F. Magnotta, R.A. Failor, K.M. Jones, First observation of resonant excitation of high- n states in positronium, Phys. Rev. Lett. 64 (1990) 2366–2369, http://dx.doi.org/10.1103/PhysRevLett.64.2366, URL http://link.aps.org/doi/10.1103/PhysRevLett.64.2366.

[356] D.B. Cassidy, T.H. Hisakado, H.W.K. Tom, A.P. Mills, Jr., Efficient production of rydberg positronium, Phys. Rev. Lett. 108 (2012) 043401, http://dx.doi.org/10.1103/PhysRevLett.108.043401, URL http://link.aps.org/doi/10.1103/PhysRevLett.108.043401.

[357] C.J. Baker, D. Edwards, C.A. Isaac, H.H. Telle, D.P. van der Werf, M. Charlton, Excitation of positronium: from the ground state to rydberg levels, J. Phys. B: At. Mol. Opt. Phys. 51 (3) (2018) 035006, URL http://stacks.iop.org/0953-4075/51/i=3/a=035006.

[358] A. Deller, A.M. Alonso, B.S. Cooper, S.D. Hogan, D.B. Cassidy, Measurement of Rydberg positronium fluorescence lifetimes, Phys. Rev. A 93 (2016) 062513, http://dx.doi.org/10.1103/PhysRevA.93.062513, URL https://link.aps.org/doi/10.1103/PhysRevA.93.062513.

[359] A.C.L. Jones, T.H. Hisakado, H.J. Goldman, H.W.K. Tom, A.P. Mills, Jr., D.B. Cassidy, Doppler-corrected balmer spectroscopy of Rydberg positronium, Phys. Rev. A 90 (2014) 012503, http://dx.doi.org/10.1103/PhysRevA.90.012503, URL http://link.aps.org/doi/10.1103/PhysRevA.90.012503.
[360] S.D. Hogan, Rydberg-stark deceleration of atoms and molecules, EPJ Tech. Instrum. 3 (2016) 1, http://dx.doi.org/10.1140/epjti/s40485-015-0028-4.
[361] A. Osterwalder, F. Merkt, Using high rydberg states as electric field sensors, Phys. Rev. Lett. 82 (1999) 1831–1834, http://dx.doi.org/10.1103/PhysRevLett.82.1831, URL http://link.aps.org/doi/10.1103/PhysRevLett.82.1831.
[362] A. Beyer, J. Alnis, K. Khabarova, A. Matveev, C.G. Parthey, D.C. Yost, R. Pohl, T. Udem, T.W. Hänsch, N. Kolachevsky, Precision spectroscopy of the 2S-4P transition in atomic hydrogen on a cryogenic beam of optically excited 2S atoms, Ann. Phys. 525 (8–9) (2013) 671–679, http://dx.doi.org/10.1002/andp.201300075.
[363] W.E. Lamb, R.C. Retherford, Fine structure of the hydrogen atom by a microwave method, Phys. Rev. 72 (1947) 241–243, http://dx.doi.org/10.1103/PhysRev.72.241, URL http://link.aps.org/doi/10.1103/PhysRev.72.241.
[364] W.E. Lamb, R.C. Retherford, Fine structure of the hydrogen atom. Part I, Phys. Rev. 79 (1950) 549–572, http://dx.doi.org/10.1103/PhysRev.79.549, URL https://link.aps.org/doi/10.1103/PhysRev.79.549.
[365] S.R. Furlanetto, Physical cosmology from the 21-cm line, 2019, arXiv:1909.12430.
[366] J.P. Gordon, H.J. Zeiger, C.H. Townes, The maser—New type of microwave amplifier, frequency standard, and spectrometer, Phys. Rev. 99 (1955) 1264–1274, http://dx.doi.org/10.1103/PhysRev.99.1264, URL https://link.aps.org/doi/10.1103/PhysRev.99.1264.
[367] A. Miyazaki, T. Yamazaki, T. Suehara, T. Namba, S. Asai, T. Kobayashi, H. Saito, T. Idehara, I. Ogawa, Y. Tatematsu, The direct spectroscopy of positronium hyperfine structure using a sub-THz gyrotron, J. Infrared, Millim. Terahertz Waves 35 (1) (2014) 91–100, http://dx.doi.org/10.1007/s10762-013-0001-8.
[368] T. Yamazaki, A. Miyazaki, T. Suehara, T. Namba, S. Asai, T. Kobayashi, H. Saito, I. Ogawa, T. Idehara, S. Sabchevski, Direct observation of the hyperfine transition of ground-state positronium, Phys. Rev. Lett. 108 (2012) 253401, http://dx.doi.org/10.1103/PhysRevLett.108.253401, URL http://link.aps.org/doi/10.1103/PhysRevLett.108.253401.
[369] S.M. Curry, Combined zeeman and motional stark effects in the first excited state of positronium, Phys. Rev. A 7 (1973) 447–450, http://dx.doi.org/10.1103/PhysRevA.7.447.
[370] C.D. Dermer, J.C. Weisheit, Perturbative analysis of simultaneous stark and zeeman effects on $n = 1 \rightarrow n = 2$ radiative transitions in positronium, Phys. Rev. A 40 (1989) 5526–5532, http://dx.doi.org/10.1103/PhysRevA.40.5526.
[371] G. Breit, I.I. Rabi, Measurement of nuclear spin, Phys. Rev. 38 (1931) 2082–2083, http://dx.doi.org/10.1103/PhysRev.38.2082.2, URL http://link.aps.org/doi/10.1103/PhysRev.38.2082.2.
[372] V.W. Hughes, S. Marder, C.S. Wu, Hyperfine structure of positronium in its ground state, Phys. Rev. 106 (1957) 934–947, http://dx.doi.org/10.1103/PhysRev.106.934, URL http://link.aps.org/doi/10.1103/PhysRev.106.934.
[373] E.D. Theriot, R.H. Beers, V.W. Hughes, Precision redetermination of the hyperfine structure interval of positronium, Phys. Rev. Lett. 18 (1967) 767–769, http://dx.doi.org/10.1103/PhysRevLett.18.767, URL http://link.aps.org/doi/10.1103/PhysRevLett.18.767.
[374] E.D. Theriot, R.H. Beers, V.W. Hughes, K.O.H. Ziock, Precision redetermination of the fine-structure interval of the ground state of positronium and a direct measurement of the decay rate of parapositronium, Phys. Rev. A 2 (1970) 707–721, http://dx.doi.org/10.1103/PhysRevA.2.707, URL https://link.aps.org/doi/10.1103/PhysRevA.2.707.
[375] E.R. Carlson, V.W. Hughes, M.L. Lewis, I. Lindgren, Higher-precision determination of the fine-structure interval in the ground state of positronium, and the fine-structure density shift in nitrogen, Phys. Rev. Lett. 29 (1972) 1059–1061, http://dx.doi.org/10.1103/PhysRevLett.29.1059, URL https://link.aps.org/doi/10.1103/PhysRevLett.29.1059.
[376] E.R. Carlson, V.W. Hughes, I. Lindgren, Precision determination of the fine-structure interval in the ground state of positronium. III, Phys. Rev. A 15 (1977) 241–250, http://dx.doi.org/10.1103/PhysRevA.15.241, URL https://link.aps.org/doi/10.1103/PhysRevA.15.241.
[377] P.O. Egan, V.W. Hughes, M.H. Yam, Precision determination of the fine-structure interval in the ground state of positronium. IV. Measurement of positronium fine-structure density shifts in noble gases, Phys. Rev. A 15 (1977) 251–260, http://dx.doi.org/10.1103/PhysRevA.15.251, URL https://link.aps.org/doi/10.1103/PhysRevA.15.251.
[378] M.H. Yam, P.O. Egan, W.E. Frieze, V.W. Hughes, Positronium fine-structure interval $\Delta\nu$ in oxide powders, Phys. Rev. A 18 (1978) 350–353, http://dx.doi.org/10.1103/PhysRevA.18.350, URL https://link.aps.org/doi/10.1103/PhysRevA.18.350.
[379] A.P. Mills, Jr., G.H. Bearman, New measurement of the positronium hyperfine interval, Phys. Rev. Lett. 34 (1975) 246–250, http://dx.doi.org/10.1103/PhysRevLett.34.246, URL http://link.aps.org/doi/10.1103/PhysRevLett.34.246.
[380] A. Rich, Corrections to the measured $n = 1$ hyperfine interval of positronium due to annihilation effects, Phys. Rev. A 23 (1981) 2747–2750, http://dx.doi.org/10.1103/PhysRevA.23.2747, URL http://link.aps.org/doi/10.1103/PhysRevA.23.2747.
[381] A.P. Mills, Jr., Effects of collisions on the magnetic quenching of positronium, J. Chem. Phys. 62 (7) (1975) 2646–2659, http://dx.doi.org/10.1063/1.430850, URL http://scitation.aip.org/content/aip/journal/jcp/62/7/10.1063/1.430850.
[382] V. Baryshevsky, O. Metelitsa, V. Tikhomirov, S. Andrukhovich, A. Berestov, B. Martsinkevich, E. Rudak, Observation of time oscillation in 3γ-annihilation of positronium in a magnetic field, Phys. Lett. A 136 (7) (1989) 428–432, http://dx.doi.org/10.1016/0375-9601(89)90428-3, URL http://www.sciencedirect.com/science/article/pii/0375960189904283.
[383] V.G. Baryshevsky, O.N. Metelitsa, V.V. Tikhomirov, Oscillations of the positronium decay γ-quantum angular distribution in a magnetic field, J. Phys. B: At. Mol. Opt. Phys. 22 (17) (1989) 2835, URL http://stacks.iop.org/0953-4075/22/i=17/a=020.
[384] S. Fan, C. Beling, S. Fung, Hyperfine splitting in positronium measured through quantum beats in the 3γ decay, Phys. Lett. A 216 (1) (1996) 129–136, http://dx.doi.org/10.1016/0375-9601(96)00273-3, URL http://www.sciencedirect.com/science/article/pii/0375960196002733.
[385] Y. Nagata, K. Michishio, T. Iizuka, H. Kikutani, L. Chiari, F. Tanaka, Y. Nagashima, Motion-induced transition of positronium through a static periodic magnetic field in the sub-THz region, Phys. Rev. Lett. 124 (2020) 173202, http://dx.doi.org/10.1103/PhysRevLett.124.173202, URL https://link.aps.org/doi/10.1103/PhysRevLett.124.173202.
[386] S. Hatamian, R.S. Conti, A. Rich, Measurements of the 2^3S_1-2^3P_J ($J = 0, 1, 2$) fine-structure splittings in positronium, Phys. Rev. Lett. 58 (1987) 1833–1836, http://dx.doi.org/10.1103/PhysRevLett.58.1833, URL http://link.aps.org/doi/10.1103/PhysRevLett.58.1833.
[387] R.S. Conti, S. Hatamian, L. Lapidus, A. Rich, M. Skalsey, Search for C-violating, P-conserving interactions and observation of 2^3s_1 to 2^1p_1 transitions in positronium, Phys. Lett. A 177 (1) (1993) 43–48, http://dx.doi.org/10.1016/0375-9601(93)90371-6.
[388] R. Ley, K.D. Niebling, R. Schwarz, G. Werth, Evidence from n=2 fine structure transitions for the production of fast excited state positronium, J. Phys. B: At. Mol. Opt. Phys. 23 (11) (1990) 1915, URL http://stacks.iop.org/0953-4075/23/i=11/a=024.
[389] R. Ley, K.D. Niebling, G. Werth, C. Hahn, H. Schneider, I. Tobehn, Energy dependence of excited positronium formation at a molybdenum surface, J. Phys. B: At. Mol. Opt. Phys. 23 (19) (1990) 3437, URL http://stacks.iop.org/0953-4075/23/i=19/a=024.
[390] D.C. Schoepf, S. Berko, K.F. Canter, P. Sferlazzo, Observation of ps($n = 2$) from well-characterized metal surfaces in ultrahigh vacuum, Phys. Rev. A 45 (1992) 1407–1411, http://dx.doi.org/10.1103/PhysRevA.45.1407, URL http://link.aps.org/doi/10.1103/PhysRevA.45.1407.
[391] T.D. Steiger, R.S. Conti, Formation of $n = 2$ positronium from untreated metal surfaces, Phys. Rev. A 45 (1992) 2744–2752, http://dx.doi.org/10.1103/PhysRevA.45.2744, URL http://link.aps.org/doi/10.1103/PhysRevA.45.2744.

[392] D.J. Day, M. Charlton, G. Laricchia, On the formation of excited state positronium in vacuum by positron impact on untreated surfaces, J. Phys. B: At. Mol. Opt. Phys. 34 (18) (2001) 3617, URL http://stacks.iop.org/0953-4075/34/i=18/a=301.

[393] A. Marsman, M. Horbatsch, E.A. Hessels, Interference between two resonant transitions with distinct initial and final states connected by radiative decay, Phys. Rev. A 96 (2017) 062111, http://dx.doi.org/10.1103/PhysRevA.96.062111, URL https://link.aps.org/doi/10.1103/PhysRevA.96.062111.

[394] U. Fano, Effects of configuration interaction on intensities and phase shifts, Phys. Rev. 124 (1961) 1866–1878, http://dx.doi.org/10.1103/PhysRev.124.1866, URL https://link.aps.org/doi/10.1103/PhysRev.124.1866.

[395] A.L. Stancik, E.B. Brauns, A simple asymmetric lineshape for fitting infrared absorption spectra, Vib. Spectrosc. 47 (1) (2008) 66–69, http://dx.doi.org/10.1016/j.vibspec.2008.02.009, URL http://www.sciencedirect.com/science/article/pii/S0924203108000453.

[396] L.A. Akopyan, T.J. Babij, K. Lakhmanskiy, D.B. Cassidy, A. Matveev, Line-shape modeling in microwave spectroscopy of the positronium $n = 2$ fine-structure intervals, Phys. Rev. A 104 (2021) 062810, http://dx.doi.org/10.1103/PhysRevA.104.062810, URL https://link.aps.org/doi/10.1103/PhysRevA.104.062810.

[397] M. Haghighat, S.M. Zebarjad, F. Loran, Positronium hyperfine splitting in noncommutative space at order α^6, Phys. Rev. D 66 (2002) 016005, http://dx.doi.org/10.1103/PhysRevD.66.016005, URL http://link.aps.org/doi/10.1103/PhysRevD.66.016005.

[398] A.C. Vutha, E.A. Hessels, Frequency-offset separated oscillatory fields, Phys. Rev. A 92 (2015) 052504, http://dx.doi.org/10.1103/PhysRevA.92.052504, URL https://link.aps.org/doi/10.1103/PhysRevA.92.052504.

[399] N. Bezginov, T. Valdez, M. Horbatsch, A. Marsman, A.C. Vutha, E.A. Hessels, A measurement of the atomic hydrogen lamb shift and the proton charge radius, Science 365 (6457) (2019) 1007–1012, http://dx.doi.org/10.1126/science.aau7807, URL https://science.sciencemag.org/content/365/6457/1007.

[400] M. Heiss, G. Wichmann, A. Rubbia, P. Crivelli, The positronium hyperfine structure: Progress towards a direct measurement of the $2^3S_1 \rightarrow 2^1S_0$ transition in vacuum, 2018, arXiv:1805.05886.

[401] T.C. Griffith, G.R. Heyland, The mean lifetime of orthopositronium in vacuum, Nature 269 (5624) (1977) 109–112, http://dx.doi.org/10.1038/269109a0.

[402] A.I. Alekseev, Two-photon annihilation of positronium in the P-state, Sov. Phys. JETP 7 (1958) 826.

[403] A.I. Alekseev, Three-photon annihilation of positronium in the P-state, Sov. Phys. JETP 9 (1959) 1312.

[404] A.M. Alonso, B.S. Cooper, A. Deller, S.D. Hogan, D.B. Cassidy, Controlling positronium annihilation with electric fields, Phys. Rev. Lett. 115 (2015) 183401, http://dx.doi.org/10.1103/PhysRevLett.115.183401, URL http://link.aps.org/doi/10.1103/PhysRevLett.115.183401.

[405] R.E. Sheldon, T.J. Babij, B.A. Devlin-Hill, L. Gurung, D.B. Cassidy, Measurement of the annihilation decay rate of $2\,^3S_1$ positronium, EPL (Europhys. Lett.) 132 (1) (2020) 13001, http://dx.doi.org/10.1209/0295-5075/132/13001.

[406] D.W. Gidley, A. Rich, E. Sweetman, D. West, New precision measurements of the decay rates of singlet and triplet positronium, Phys. Rev. Lett. 49 (1982) 525–528, http://dx.doi.org/10.1103/PhysRevLett.49.525, URL https://link.aps.org/doi/10.1103/PhysRevLett.49.525.

[407] K.G. Lynn, W.E. Frieze, P.J. Schultz, Measurement of the positron surface-state lifetime for Al, Phys. Rev. Lett. 52 (1984) 1137–1140, http://dx.doi.org/10.1103/PhysRevLett.52.1137, URL https://link.aps.org/doi/10.1103/PhysRevLett.52.1137.

[408] D.W. Gidley, K.A. Marko, A. Rich, Precision measurement of the decay rate of orthopositronium in SiO_2 powders, Phys. Rev. Lett. 36 (1976) 395–398, http://dx.doi.org/10.1103/PhysRevLett.36.395, URL https://link.aps.org/doi/10.1103/PhysRevLett.36.395.

[409] D.W. Gidley, P.W. Zitzewitz, K.A. Marko, A. Rich, Measurement of the vacuum decay rate of orthopositronium, Phys. Rev. Lett. 37 (1976) 729–732, http://dx.doi.org/10.1103/PhysRevLett.37.729, URL http://link.aps.org/doi/10.1103/PhysRevLett.37.729.

[410] D.W. Gidley, A. Rich, P.W. Zitzewitz, D.A.L. Paul, New experimental value for the orthopositronium decay rate, Phys. Rev. Lett. 40 (1978) 737–740, http://dx.doi.org/10.1103/PhysRevLett.40.737, URL http://link.aps.org/doi/10.1103/PhysRevLett.40.737.

[411] T.C. Griffith, G.R. Heyland, K.S. Lines, T.R. Twomey, The decay rate of ortho-positronium in vacuum, J. Phys. B: At. Mol. Phys. 11 (23) (1978) L743, URL http://stacks.iop.org/0022-3700/11/i=23/a=007.

[412] J.S. Nico, D.W. Gidley, A. Rich, P.W. Zitzewitz, Precision measurement of the orthopositronium decay rate using the vacuum technique, Phys. Rev. Lett. 65 (1990) 1344–1347, http://dx.doi.org/10.1103/PhysRevLett.65.1344, URL https://link.aps.org/doi/10.1103/PhysRevLett.65.1344.

[413] S. Asai, S. Orito, N. Shinohara, New measurement of the orthopositronium decay rate, Phys. Lett. B 357 (3) (1995) 475–480, http://dx.doi.org/10.1016/0370-2693(95)00916-9, URL http://www.sciencedirect.com/science/article/pii/0370269395009169.

[414] Y. Kataoka, S. Asai, T. Kobayashi, First test of order α^2 correction of the orthopositronium decay rate, Phys. Lett. B 671 (2) (2009) 219–223, http://dx.doi.org/10.1016/j.physletb.2008.12.008, URL http://www.sciencedirect.com/science/article/pii/S0370269308014688.

[415] P. Moskal, D. Alfs, T. Bednarski, P. Białas, E. Czerwiński, C. Curceanu, A. Gajos, B. Głowacz, M. Gorgol, B. Hiesmayr, et al., Potential of the J-PET detector for studies of discrete symmetries in decays of positronium atom — A purely leptonic system, Acta Phys. Polon. B 47 (2) (2016) 509, http://dx.doi.org/10.5506/aphyspolb.47.509.

[416] P. Moskal, N. Krawczyk, B.C. Hiesmayr, M. Bała, C. Curceanu, E. Czerwiński, K. Dulski, A. Gajos, M. Gorgol, R. Del Grande, et al., Feasibility studies of the polarization of photons beyond the optical wavelength regime with the J-PET detector, Eur. Phys. J. C 78 (11) (2018) http://dx.doi.org/10.1140/epjc/s10052-018-6461-1.

[417] S. Asai, S. Orito, K. Yoshimura, T. Haga, Search for long-lived neutral bosons in orthopositronium decay, Phys. Rev. Lett. 66 (1991) 2440–2443, http://dx.doi.org/10.1103/PhysRevLett.66.2440, URL http://link.aps.org/doi/10.1103/PhysRevLett.66.2440.

[418] S. Asai, K. Shigekuni, T. Sanuki, S. Orito, Search for short-lived neutral bosons in orthopositronium decay, Phys. Lett. B 323 (1) (1994) 90–94, http://dx.doi.org/10.1016/0370-2693(94)90459-6, URL http://www.sciencedirect.com/science/article/pii/0370269394904596.

[419] T. Maeno, M. Fujikawa, J. Kataoka, Y. Nishihara, S. Orito, K. Shigekuni, Y. Watanabe, A search for massive neutral bosons in orthopositronium decay, Phys. Lett. B 351 (4) (1995) 574–578, http://dx.doi.org/10.1016/0370-2693(95)00425-K, URL https://www.sciencedirect.com/science/article/pii/037026939500425K.

[420] T. Mitsui, K. Maki, S. Asai, Y. Ishisaki, R. Fujimoto, N. Muramoto, T. Sato, Y. Ueda, Y. Yamazaki, S. Orito, Limit on an exotic three-body decay of orthopositronium, Europhys. Lett. 33 (2) (1996) 111, URL http://stacks.iop.org/0295-5075/33/i=2/a=111.

[421] M. Skalsey, R.S. Conti, Search for very weakly interacting, short-lived, C-odd bosons and the orthopositronium decay rate problem, Phys. Rev. A 55 (1997) 984–987, http://dx.doi.org/10.1103/PhysRevA.55.984, URL http://link.aps.org/doi/10.1103/PhysRevA.55.984.

[422] J. Pérez-Ríos, S.T. Love, Searching for light dark matter through positronium decay, Eur. Phys. J. D 72 (3) (2018) 44, http://dx.doi.org/10.1140/epjd/e2017-80614-7.

[423] A.P. Mills, Jr., S. Berko, Search for C nonconservation in electron-positron annihilation, Phys. Rev. Lett. 18 (1967) 420–425, http://dx.doi.org/10.1103/PhysRevLett.18.420, URL http://link.aps.org/doi/10.1103/PhysRevLett.18.420.

[424] K. Marko, A. Rich, Search for orthopositronium decay into four photons as a test of charge-conjugation invariance, Phys. Rev. Lett. 33 (1974) 980–983, http://dx.doi.org/10.1103/PhysRevLett.33.980, URL https://link.aps.org/doi/10.1103/PhysRevLett.33.980.

[425] S. Adachi, M. Chiba, T. Hirose, S. Nagayama, Y. Nakamitsu, T. Sato, T. Yamada, Measurement of $e^+\ e^-$ annihilation at rest into four γ-rays, Phys. Rev. Lett. 65 (1990) 2634–2637, http://dx.doi.org/10.1103/PhysRevLett.65.2634, URL http://link.aps.org/doi/10.1103/PhysRevLett.65.2634.

[426] J. Yang, M. Chiba, R. Hamatsu, T. Hirose, T. Matsumoto, J. Yu, Four-photon decay of orthopositronium: A test of charge-conjugation invariance, Phys. Rev. A 54 (1996) 1952–1956, http://dx.doi.org/10.1103/PhysRevA.54.1952, URL https://link.aps.org/doi/10.1103/PhysRevA.54.1952.

[427] T. Matsumoto, M. Chiba, R. Hamatsu, T. Hirose, J. Yang, J. Yu, Measurement of five-photon decay in orthopositronium, Phys. Rev. A 54 (1996) 1947–1951, http://dx.doi.org/10.1103/PhysRevA.54.1947, URL http://link.aps.org/doi/10.1103/PhysRevA.54.1947.

[428] P.A. Vetter, S.J. Freedman, Branching-ratio measurements of multiphoton decays of positronium, Phys. Rev. A 66 (2002) 052505, http://dx.doi.org/10.1103/PhysRevA.66.052505, URL http://link.aps.org/doi/10.1103/PhysRevA.66.052505.

[429] M. Chiba, J. Nakagawa, H. Tsugawa, R. Ogata, T. Nishimura, A detector with high detection efficiency in 4- and 5-photon-positronium annihilations, Can. J. Phys. 80 (11) (2002) 1287–1295, http://dx.doi.org/10.1139/p02-107, http://arxiv.org/abs/DOI: 10.1139/p02-107[arXiv:DOI: 10.1139/p02-107].

[430] I.-Y. Lee, The GAMMASPHERE, Nuclear Phys. A 520 (1990) c641–c655, http://dx.doi.org/10.1016/0375-9474(90)91181-P, Nuclear Structure in the Nineties, URL https://www.sciencedirect.com/science/article/pii/037594749091181P.

[431] C. Bartram, R. Henning, D. Primosch, Demonstration of o-Ps detection with a cylindrical array of NaI detectors, Nucl. Instrum. Methods Phys. Res. A 966 (2020) 163856, http://dx.doi.org/10.1016/j.nima.2020.163856, URL https://www.sciencedirect.com/science/article/pii/S0168900220303624.

[432] D.W. Jeong, A. Khan, H.W. Park, J. Lee, H. Kim, Optimization and characterization of detector and trigger system for a KAPAE design, Nucl. Instrum. Methods Phys. Res. A 989 (2021) 164941, http://dx.doi.org/10.1016/j.nima.2020.164941.

[433] T. Mitsui, R. Fujimoto, Y. Ishisaki, Y. Ueda, Y. Yamazaki, S. Asai, S. Orito, Search for invisible decay of orthopositronium, Phys. Rev. Lett. 70 (1993) 2265–2268, http://dx.doi.org/10.1103/PhysRevLett.70.2265, URL http://link.aps.org/doi/10.1103/PhysRevLett.70.2265.

[434] A. Badertscher, P. Crivelli, M. Felcini, S. Gninenko, N. Goloubev, P. Năcdăclec, J. Peigneux, V. Postoev, A. Rubbia, D. Sillou, Search for an exotic three-body decay of orthopositronium, Phys. Lett. B 542 (2002) 29–34, http://dx.doi.org/10.1016/S0370-2693(02)02237-2, URL http://www.sciencedirect.com/science/article/pii/S0370269302022372.

[435] A. Badertscher, P. Crivelli, W. Fetscher, U. Gendotti, S.N. Gninenko, V. Postoev, A. Rubbia, V. Samoylenko, D. Sillou, Improved limit on invisible decays of positronium, Phys. Rev. D 75 (2007) 032004, http://dx.doi.org/10.1103/PhysRevD.75.032004, URL http://link.aps.org/doi/10.1103/PhysRevD.75.032004.

[436] I.Y. Kobzarev, L.B. Okun, I.Y. Pomeranchuk, On the possibility of experimental observation of mirror particles, Sov. J. Nucl. Phys. 3 (6) (1966) 837–841.

[437] L.B. Okun, Mirror particles and mirror matter: 50 years of speculation and searching, Phys.-Usp. 50 (4) (2007) 380–389, http://dx.doi.org/10.1070/pu2007v050n04abeh006227.

[438] P. Crivelli, A. Belov, U. Gendotti, S. Gninenko, A. Rubbia, Positronium portal into hidden sector: a new experiment to search for mirror dark matter, J. Instrum. 5 (08) (2010) P08001, URL http://stacks.iop.org/1748-0221/5/i=08/a=P08001.

[439] S. Glashow, Positronium versus the mirror universe, Phys. Lett. B 167 (1) (1986) 35–36, http://dx.doi.org/10.1016/0370-2693(86)90540-X, URL http://www.sciencedirect.com/science/article/pii/037026938690540X.

[440] R. Foot, S. Gninenko, Can the mirror world explain the ortho-positronium lifetime puzzle? Phys. Lett. B 480 (2000) 171–175, http://dx.doi.org/10.1016/S0370-2693(00)00357-9, URL http://www.sciencedirect.com/science/article/pii/S0370269300003579.

[441] T.D. Lee, C.N. Yang, Question of parity conservation in weak interactions, Phys. Rev. 104 (1956) 254–258, http://dx.doi.org/10.1103/PhysRev.104.254, URL http://link.aps.org/doi/10.1103/PhysRev.104.254.

[442] R.L. Garwin, L.M. Lederman, M. Weinrich, Observations of the failure of conservation of parity and charge conjugation in meson decays: the magnetic moment of the free muon, Phys. Rev. 105 (1957) 1415–1417, http://dx.doi.org/10.1103/PhysRev.105.1415, URL https://link.aps.org/doi/10.1103/PhysRev.105.1415.

[443] C.S. Wu, E. Ambler, R.W. Hayward, D.D. Hoppes, R.P. Hudson, Experimental test of parity conservation in beta decay, Phys. Rev. 105 (1957) 1413–1415, http://dx.doi.org/10.1103/PhysRev.105.1413, URL http://link.aps.org/doi/10.1103/PhysRev.105.1413.

[444] J.H. Christenson, J.W. Cronin, V.L. Fitch, R. Turlay, Evidence for the 2π decay of the K_2^0 meson, Phys. Rev. Lett. 13 (1964) 138–140, http://dx.doi.org/10.1103/PhysRevLett.13.138, URL https://link.aps.org/doi/10.1103/PhysRevLett.13.138.

[445] J.S. Bell, R.E. Peierls, Time reversal in field theory, Proc. R. Soc. London Ser. A Math. Phys. Sci. 231 (1187) (1955) 479–495, http://dx.doi.org/10.1098/rspa.1955.0189, arXiv:https://royalsocietypublishing.org/doi/pdf/10.1098/rspa.1955.0189, URL https://royalsocietypublishing.org/doi/abs/10.1098/rspa.1955.0189.

[446] R.D. Peccei, H.R. Quinn, CP Conservation in the presence of pseudoparticles, Phys. Rev. Lett. 38 (1977) 1440–1443, http://dx.doi.org/10.1103/PhysRevLett.38.1440, URL https://link.aps.org/doi/10.1103/PhysRevLett.38.1440.

[447] M. Dine, A. Kusenko, Origin of the matter-antimatter asymmetry, Rev. Modern Phys. 76 (2003) 1–30, http://dx.doi.org/10.1103/RevModPhys.76.1, URL https://link.aps.org/doi/10.1103/RevModPhys.76.1.

[448] T. Ibrahim, P. Nath, *CP* Violation from the standard model to strings, Rev. Modern Phys. 80 (2008) 577–631, http://dx.doi.org/10.1103/RevModPhys.80.577, URL https://link.aps.org/doi/10.1103/RevModPhys.80.577.

[449] A. Pilaftsis, CP Violation and baryogenesis due to heavy majorana neutrinos, Phys. Rev. D 56 (1997) 5431–5451, http://dx.doi.org/10.1103/PhysRevD.56.5431, URL https://link.aps.org/doi/10.1103/PhysRevD.56.5431.

[450] G.S. Adkins, D.R. Droz, D. Rastawicki, R.N. Fell, Orthopositronium decay form factors and two-photon correlations, Phys. Rev. A 81 (2010) 042507, http://dx.doi.org/10.1103/PhysRevA.81.042507, URL https://link.aps.org/doi/10.1103/PhysRevA.81.042507.

[451] S.K. Andrukhovich, N. Antovich, A.V. Berestov, P. Vukotich, A.A. Gurinovich, O.N. Metelitsa, A.A. Khrushchinskii, A method for selecting three-photon positronium-annihilation events with a multidetector coincidence spectrometer, Instrum. Exp. Tech. 43 (3) (2000) 295–299, http://dx.doi.org/10.1007/BF02759022.

[452] P.A. Vetter, S.J. Freedman, Search for *CPT*-odd decays of positronium, Phys. Rev. Lett. 91 (2003) 263401, http://dx.doi.org/10.1103/PhysRevLett.91.263401, URL http://link.aps.org/doi/10.1103/PhysRevLett.91.263401.

[453] M. Skalsey, J. Van House, First test of *CP* invariance in the decay of positronium, Phys. Rev. Lett. 67 (1991) 1993–1996, http://dx.doi.org/10.1103/PhysRevLett.67.1993, URL http://link.aps.org/doi/10.1103/PhysRevLett.67.1993.

[454] T. Yamazaki, T. Namba, S. Asai, T. Kobayashi, Search for *CP* violation in positronium decay, Phys. Rev. Lett. 104 (2010) 083401, http://dx.doi.org/10.1103/PhysRevLett.104.083401, URL http://link.aps.org/doi/10.1103/PhysRevLett.104.083401.

[455] B.K. Arbic, S. Hatamian, M. Skalsey, J. Van House, W. Zheng, Angular-correlation test of *CPT* in polarized positronium, Phys. Rev. A 37 (1988) 3189–3194, http://dx.doi.org/10.1103/PhysRevA.37.3189, URL http://link.aps.org/doi/10.1103/PhysRevA.37.3189.

[456] G. Adkins, Search for CP and CPT violation in positronium decay, CPT Lorentz Symmetry (2010) http://dx.doi.org/10.1142/9789814327688_0050.

[457] T. Yamazaki, T. Namba, S. Asai, T. Kobayashi, Erratum: Search for *CP* violation in positronium decay [Phys. Rev. Lett. 104, 083401 (2010)]„ Phys. Rev. Lett. 120 (2018) 239902, http://dx.doi.org/10.1103/PhysRevLett.120.239902, URL https://link.aps.org/doi/10.1103/PhysRevLett.120.239902.

[458] J. Donoghue, E. Golowich, B.R. Holstein, Dynamics of the Standard Model, Vol. 2, CUP, 2014, http://dx.doi.org/10.1017/CBO9780511524370.

[459] W. Cottingham, D. Greenwood, An Introduction to the Standard Model of Particle Physics, Cambridge University Press, 2007.

[460] M.D. Schwartz, Quantum Field Theory and the Standard Model, Cambridge University Press, 2014.

[461] F. Englert, R. Brout, Broken symmetry and the mass of gauge vector mesons, Phys. Rev. Lett. 13 (1964) 321–323, http://dx.doi.org/10.1103/PhysRevLett.13.321, URL https://link.aps.org/doi/10.1103/PhysRevLett.13.321.

[462] P.W. Higgs, Broken symmetries and the masses of gauge bosons, Phys. Rev. Lett. 13 (1964) 508–509, http://dx.doi.org/10.1103/PhysRevLett.13.508, URL https://link.aps.org/doi/10.1103/PhysRevLett.13.508.

[463] N. Haba, H. Ishida, R. Takahashi, Y. Yamaguchi, Hierarchy problem, gauge coupling unification at the Planck scale, and vacuum stability, Nuclear Phys. B 900 (2015) 244–258, http://dx.doi.org/10.1016/j.nuclphysb.2015.09.004, URL http://www.sciencedirect.com/science/article/pii/S0550321315003120.

[464] C. Froggatt, H. Nielsen, Standard model criticality prediction top mass 173 ± 5 GeV and Higgs mass 135 ± 9 GeV, Phys. Lett. B 368 (1) (1996) 96–102, http://dx.doi.org/10.1016/0370-2693(95)01480-2, URL http://www.sciencedirect.com/science/article/pii/0370269395014802.

[465] I. Masina, The Higgs boson and top quark masses as tests of electroweak vacuum stability, Nuclear Phys. B Proc. Suppl. 237–238 (2013) 323–325, http://dx.doi.org/10.1016/j.nuclphysbps.2013.04.117, Proceedings of the Neutrino Oscillation Workshop, URL http://www.sciencedirect.com/science/article/pii/S0920563213002387.

[466] Y. Fukuda, T. Hayakawa, E. Ichihara, K. Inoue, K. Ishihara, H. Ishino, Y. Itow, T. Kajita, J. Kameda, S. Kasuga, K. Kobayashi, Y. Kobayashi, Y. Koshio, M. Miura, M. Nakahata, S. Nakayama, A. Okada, K. Okumura, N. Sakurai, M. Shiozawa, Y. Suzuki, Y. Takeuchi, Y. Totsuka, S. Yamada, M. Earl, A. Habig, E. Kearns, M.D. Messier, K. Scholberg, J.L. Stone, L.R. Sulak, C.W. Walter, M. Goldhaber, T. Barszczak, D. Casper, W. Gajewski, P.G. Halverson, J. Hsu, W.R. Kropp, L.R. Price, F. Reines, M. Smy, H.W. Sobel, M.R. Vagins, K.S. Ganezer, W.E. Keig, R.W. Ellsworth, S. Tasaka, J.W. Flanagan, A. Kibayashi, J.G. Learned, S. Matsuno, V.J. Stenger, D. Takemori, T. Ishii, J. Kanzaki, T. Kobayashi, S. Mine, K. Nakamura, K. Nishikawa, Y. Oyama, A. Sakai, M. Sakuda, O. Sasaki, S. Echigo, M. Kohama, A.T. Suzuki, T.J. Haines, E. Blaufuss, B.K. Kim, R. Sanford, R. Svoboda, M.L. Chen, Z. Conner, J.A. Goodman, G.W. Sullivan, J. Hill, C.K. Jung, K. Martens, C. Mauger, C. McGrew, E. Sharkey, B. Viren, C. Yanagisawa, W. Doki, K. Miyano, H. Okazawa, C. Saji, M. Takahata, Y. Nagashima, M. Takita, T. Yamaguchi, M. Yoshida, S.B. Kim, M. Etoh, K. Fujita, A. Hasegawa, T. Hasegawa, S. Hatakeyama, T. Iwamoto, M. Koga, T. Maruyama, H. Ogawa, J. Shirai, A. Suzuki, F. Tsushima, M. Koshiba, M. Nemoto, K. Nishijima, T. Futagami, Y. Hayato, Y. Kanaya, K. Kaneyuki, Y. Watanabe, D. Kielczewska, R.A. Doyle, J.S. George, A.L. Stachyra, L.L. Wai, R.J. Wilkes, K.K. Young, Super-Kamiokande Collaboration Collaboration Collaboration, Evidence for oscillation of atmospheric neutrinos, Phys. Rev. Lett. 81 (1998) 1562–1567, http://dx.doi.org/10.1103/PhysRevLett.81.1562, URL https://link.aps.org/doi/10.1103/PhysRevLett.81.1562.

[467] R.D. Peccei, H.R. Quinn, Constraints imposed by CP conservation in the presence of pseudoparticles, Phys. Rev. D 16 (1977) 1791–1797, http://dx.doi.org/10.1103/PhysRevD.16.1791, URL https://link.aps.org/doi/10.1103/PhysRevD.16.1791.

[468] N.A. Bahcall, J.P. Ostriker, S. Perlmutter, P.J. Steinhardt, The cosmic triangle: Revealing the state of the universe, Science 284 (5419) (1999) 1481–1488, http://dx.doi.org/10.1126/science.284.5419.1481, arXiv:https://science.sciencemag.org/content/284/5419/1481.full.pdf, URL https://science.sciencemag.org/content/284/5419/1481.

[469] Planck Collaboration, N. Aghanim, Y. Akrami, F. Arroja, M. Ashdown, J. Aumont, C. Baccigalupi, M. Ballardini, A.J. Banday, R.B. Barreiro, N. Bartolo, S. Basak, R. Battye, K. Benabed, J.-P. Bernard, M. Bersanelli, P. Bielewicz, J.J. Bock, J.R. Bond, et al., Planck 2018 results. I. Overview and the cosmological legacy of Planck, Astron. Astrophys. (2019) http://dx.doi.org/10.1051/0004-6361/201833880.

[470] P. Collaboration, Planck 2018 results. VI. Cosmological parameters, Astron. Astrophys. (2020) http://dx.doi.org/10.1051/0004-6361/201833910.

[471] R. Essig, J. Mardon, T. Volansky, Direct detection of sub-GeV dark matter, Phys. Rev. D 85 (2012) 076007, http://dx.doi.org/10.1103/PhysRevD.85.076007, URL https://link.aps.org/doi/10.1103/PhysRevD.85.076007.

[472] J. Va'vra, Molecular excitations: A new way to detect dark matter, Phys. Lett. B 736 (2014) 169–173, http://dx.doi.org/10.1016/j.physletb.2014.07.023, URL http://www.sciencedirect.com/science/article/pii/S0370269314005255.

[473] A. Arvanitaki, S. Dimopoulos, K. Van Tilburg, Resonant absorption of bosonic dark matter in molecules, Phys. Rev. X 8 (2018) 041001, http://dx.doi.org/10.1103/PhysRevX.8.041001, URL https://link.aps.org/doi/10.1103/PhysRevX.8.041001.

[474] R. Essig, J. Pérez-Ríos, H. Ramani, O. Slone, Direct detection of nuclear scattering of sub-GeV dark matter using molecular excitations, Phys. Rev. Res. 1 (2019) 033105, http://dx.doi.org/10.1103/PhysRevResearch.1.033105, URL https://link.aps.org/doi/10.1103/PhysRevResearch.1.033105.

[475] A.D. Sakharov, Violation of CP invariance, C asymmetry, and baryon asymmetry of the universe, Sov. Phys. Uspekhi 34 (5) (1991) 392–393, http://dx.doi.org/10.1070/pu1991v034n05abeh002497.

[476] J.J. Hudson, D.M. Kara, I.J. Smallman, B.E. Sauer, M.R. Tarbutt, E.A. Hinds, Improved measurement of the shape of the electron, Nature 473 (7348) (2011) 493–496, http://dx.doi.org/10.1038/nature10104.

[477] J. Baron, W.C. Campbell, D. DeMille, J.M. Doyle, G. Gabrielse, Y.V. Gurevich, P.W. Hess, N.R. Hutzler, E. Kirilov, I. Kozyryev, B.R. O'Leary, C.D. Panda, M.F. Parsons, E.S. Petrik, B. Spaun, A.C. Vutha, A.D. West, Order of magnitude smaller limit on the electric dipole moment of the electron, Science 343 (6168) (2014) 269–272, http://dx.doi.org/10.1126/science.1248213, URL http://science.sciencemag.org/content/343/6168/269.

[478] N. Arkani-Hamed, S. Dimopoulos, G. Dvali, The hierarchy problem and new dimensions at a millimeter, Phys. Lett. B 429 (3) (1998) 263–272, http://dx.doi.org/10.1016/S0370-2693(98)00466-3, URL http://www.sciencedirect.com/science/article/pii/S0370269398004663.

[479] M. Borkowski, A.A. Buchachenko, R. Ciuryło, P.S. Julienne, H. Yamada, K. Yuu, K. Takahashi, Y. Takasu, Y. Takahashi, Probing non-Newtonian gravity by photoassociation spectroscopy, J. Phys. Conf. Ser. 810 (2017) 012014, http://dx.doi.org/10.1088/1742-6596/810/1/012014.

[480] B. Gato-Rivera, Constraining extra space dimensions using precision molecular spectroscopy, J. Phys. Conf. Ser. 626 (2015) 012052, http://dx.doi.org/10.1088/1742-6596/626/1/012052.

[481] J. Biesheuvel, J.P. Karr, L. Hilico, K.S.E. Eikema, W. Ubachs, J.C.J. Koelemeij, Probing QED and fundamental constants through laser spectroscopy of vibrational transitions in HD+, Nature Commun. 7 (1) (2016) 10385, http://dx.doi.org/10.1038/ncomms10385.

[482] W. Ubachs, J. Koelemeij, K. Eikema, E. Salumbides, Physics beyond the standard model from hydrogen spectroscopy, J. Mol. Spectrosc. 320 (2016) 1–12, http://dx.doi.org/10.1016/j.jms.2015.12.003, URL http://www.sciencedirect.com/science/article/pii/S0022285215300217.

[483] J. Pérez-Ríos, An Introduction to Cold and Ultracold Chemistry, Springer International Publishing, 2020, URL https://www.ebook.de/de/product/39345358/jesus_perez_rios_an_introduction_to_cold_and_ultracold_chemistry.html.

[484] E. Reinhold, R. Buning, U. Hollenstein, A. Ivanchik, P. Petitjean, W. Ubachs, Indication of a cosmological variation of the proton-electron mass ratio based on laboratory measurement and reanalysis of H_2 spectra, Phys. Rev. Lett. 96 (2006) 151101, http://dx.doi.org/10.1103/PhysRevLett.96.151101, URL https://link.aps.org/doi/10.1103/PhysRevLett.96.151101.

[485] V.V. Flambaum, M.G. Kozlov, Limit on the cosmological variation of m_p/m_e from the inversion spectrum of ammonia, Phys. Rev. Lett. 98 (2007) 240801, http://dx.doi.org/10.1103/PhysRevLett.98.240801, URL https://link.aps.org/doi/10.1103/PhysRevLett.98.240801.

[486] D. DeMille, S. Sainis, J. Sage, T. Bergeman, S. Kotochigova, E. Tiesinga, Enhanced sensitivity to variation of m_e/m_p in molecular spectra, Phys. Rev. Lett. 100 (2008) 043202, http://dx.doi.org/10.1103/PhysRevLett.100.043202, URL https://link.aps.org/doi/10.1103/PhysRevLett.100.043202.

[487] E.R. Hudson, H.J. Lewandowski, B.C. Sawyer, J. Ye, Cold molecule spectroscopy for constraining the evolution of the fine structure constant, Phys. Rev. Lett. 96 (2006) 143004, http://dx.doi.org/10.1103/PhysRevLett.96.143004, URL https://link.aps.org/doi/10.1103/PhysRevLett.96.143004.

[488] E. Salumbides, W. Ubachs, V. Korobov, Bounds on fifth forces at the sub-å length scale, J. Mol. Spectrosc. 300 (2014) 65–69, http://dx.doi.org/10.1016/j.jms.2014.04.003, Spectroscopic Tests of Fundamental Physics, URL http://www.sciencedirect.com/science/article/pii/S0022285214000885.

[489] W. Ubachs, W. Vassen, E.J. Salumbides, K.S.E. Eikema, Precision metrology on the hydrogen atom in search for new physics, Ann. Phys. 525 (7) (2013) A113–A115, http://dx.doi.org/10.1002/andp.201300730, arXiv:https://onlinelibrary.wiley.com/doi/pdf/10.1002/andp.201300730, URL https://onlinelibrary.wiley.com/doi/abs/10.1002/andp.201300730.

[490] R. Essig, J. Mardon, O. Slone, T. Volansky, Detection of sub-GeV dark matter and solar neutrinos via chemical-bond breaking, Phys. Rev. D 95 (2017) 056011, http://dx.doi.org/10.1103/PhysRevD.95.056011, URL https://link.aps.org/doi/10.1103/PhysRevD.95.056011.

[491] R. Essig, P. Schuster, N. Toro, Probing dark forces and light hidden sectors at low-energy e^+e^- colliders, Phys. Rev. D 80 (2009) 015003, http://dx.doi.org/10.1103/PhysRevD.80.015003, URL https://link.aps.org/doi/10.1103/PhysRevD.80.015003.

[492] J.L. Feng, Dark matter candidates from particle physics and methods of detection, Ann. Rev. Astron. Astrophys. 48 (2010) 495–545, http://dx.doi.org/10.1146/annurev-astro-082708-101659, arXiv:1003.0904.
[493] J. Alexander, et al., Dark sectors 2016 workshop: Community report, 2016, arXiv:1608.08632.
[494] J.L. Feng, M. Kaplinghat, H. Tu, H.-B. Yu, Hidden charged dark matter, J. Cosmol. Astropart. Phys. 07 (2009) 004, http://dx.doi.org/10.1088/1475-7516/2009/07/004, arXiv:0905.3039.
[495] T. Hambye, Hidden vector dark matter, J. High Energy Phys. 01 (2009) 028, http://dx.doi.org/10.1088/1126-6708/2009/01/028, arXiv:0811.0172.
[496] C. Englert, T. Plehn, D. Zerwas, P.M. Zerwas, Exploring the Higgs portal, Phys. Lett. B 703 (2011) 298–305, http://dx.doi.org/10.1016/j.physletb.2011.08.002, arXiv:1106.3097.
[497] T. Flacke, C. Frugiuele, E. Fuchs, R.S. Gupta, G. Perez, Phenomenology of relaxion-higgs mixing, J. High Energy Phys. 06 (2017) 050, http://dx.doi.org/10.1007/JHEP06(2017)050, arXiv:1610.02025.
[498] B.A. Dobrescu, C. Frugiuele, Hidden gev-scale interactions of quarks, Phys. Rev. Lett. 113 (2014) 061801, http://dx.doi.org/10.1103/PhysRevLett.113.061801, arXiv:1404.3947.
[499] A. Costantino, S. Fichet, P. Tanedo, Exotic spin-dependent forces from a hidden sector, J. High Energy Phys. 03 (2020) 148, http://dx.doi.org/10.1007/JHEP03(2020)148, arXiv:1910.02972.
[500] K.R. Dienes, C. Kolda, J. March-Russell, Kinetic mixing and the supersymmetric gauge hierarchy, Nuclear Phys. B 492 (1) (1997) 104–118, http://dx.doi.org/10.1016/S0550-3213(97)80028-4, URL http://www.sciencedirect.com/science/article/pii/S0550321397800284.
[501] B. Holdom, Two $U(1)$'s and ϵcharge shifts, Phys. Lett. B 166 (2) (1986) 196–198, http://dx.doi.org/10.1016/0370-2693(86)91377-8, URL http://www.sciencedirect.com/science/article/pii/0370269386913778.
[502] B. Wojtsekhowski, G. Baranov, M. Blinov, E. Levichev, S. Mishnev, D. Nikolenko, I. Rachek, Y. Shestakov, Y. Tikhonov, D. Toporkov, J. Alexander, M. Battaglieri, A. Celentano, R.D. Vita, L. Marsicano, M. Bondì, M.D. Napoli, A. Italiano, E. Leonora, N. Randazzo, Searching for a dark photon: project of the experiment at VEPP-3, J. Instrum. 13 (02) (2018) P02021, http://dx.doi.org/10.1088/1748-0221/13/02/p02021.
[503] P.H. Adrian, N.A. Baltzell, M. Battaglieri, M. Bondí, S. Boyarinov, S. Bueltmann, V.D. Burkert, D. Calvo, M. Carpinelli, A. Celentano, G. Charles, L. Colaneri, W. Cooper, C. Cuevas, A. D'Angelo, N. Dashyan, M. De Napoli, R. De Vita, A. Deur, R. Dupre, H. Egiyan, L. Elouadrhiri, R. Essig, V. Fadeyev, C. Field, A. Filippi, A. Freyberger, M. Garçon, N. Gevorgyan, F.X. Girod, N. Graf, M. Graham, K.A. Griffioen, A. Grillo, M. Guidal, R. Herbst, M. Holtrop, J. Jaros, G. Kalicy, M. Khandaker, V. Kubarovsky, E. Leonora, K. Livingston, T. Maruyama, K. McCarty, J. McCormick, B. McKinnon, K. Moffeit, O. Moreno, C. Munoz Camacho, T. Nelson, S. Niccolai, A. Odian, M. Oriunno, M. Osipenko, R. Paremuzyan, S. Paul, N. Randazzo, B. Raydo, B. Reese, A. Rizzo, P. Schuster, Y.G. Sharabian, G. Simi, A. Simonyan, V. Sipala, D. Sokhan, M. Solt, S. Stepanyan, H. Szumila-Vance, N. Toro, S. Uemura, M. Ungaro, H. Voskanyan, L.B. Weinstein, B. Wojtsekhowski, B. Yale, Heavy Photon Search Collaboration Collaboration Collaboration, Search for a dark photon in electroproduced e^+e^- pairs with the heavy photon search experiment at jlab, Phys. Rev. D 98 (2018) 091101, http://dx.doi.org/10.1103/PhysRevD.98.091101, URL https://link.aps.org/doi/10.1103/PhysRevD.98.091101.
[504] J.P. Lees, V. Poireau, V. Tisserand, E. Grauges, A. Palano, G. Eigen, B. Stugu, D.N. Brown, M. Feng, L.T. Kerth, Y.G. Kolomensky, M.J. Lee, G. Lynch, H. Koch, T. Schroeder, C. Hearty, T.S. Mattison, J.A. McKenna, R.Y. So, A. Khan, V.E. Blinov, A.R. Buzykaev, V.P. Druzhinin, V.B. Golubev, E.A. Kravchenko, A.P. Onuchin, S.I. Serednyakov, Y.I. Skovpen, E.P. Solodov, K.Y. Todyshev, A.J. Lankford, M. Mandelkern, B. Dey, J.W. Gary, O. Long, C. Campagnari, M. Franco Sevilla, T.M. Hong, D. Kovalskyi, J.D. Richman, C.A. West, A.M. Eisner, W.S. Lockman, W. Panduro Vazquez, B.A. Schumm, A. Seiden, D.S. Chao, C.H. Cheng, B. Echenard, K.T. Flood, D.G. Hitlin, T.S. Miyashita, P. Ongmongkolkul, F.C. Porter, R. Andreassen, Z. Huard, B.T. Meadows, B.G. Pushpawela, M.D. Sokoloff, L. Sun, P.C. Bloom, W.T. Ford, A. Gaz, J.G. Smith, S.R. Wagner, R. Ayad, W.H. Toki, B. Spaan, D. Bernard, M. Verderi, S. Playfer, D. Bettoni, C. Bozzi, R. Calabrese, G. Cibinetto, E. Fioravanti, I. Garzia, E. Luppi, L. Piemontese, V. Santoro, A. Calcaterra, R. de Sangro, G. Finocchiaro, S. Martellotti, P. Patteri, I.M. Peruzzi, M. Piccolo, M. Rama, A. Zallo, R. Contri, M. Lo Vetere, M.R. Monge, S. Passaggio, C. Patrignani, E. Robutti, B. Bhuyan, V. Prasad, A. Adametz, U. Uwer, H.M. Lacker, P.D. Dauncey, U. Mallik, C. Chen, J. Cochran, S. Prell, H. Ahmed, A.V. Gritsan, N. Arnaud, M. Davier, D. Derkach, G. Grosdidier, F. Le Diberder, A.M. Lutz, B. Malaescu, P. Roudeau, A. Stocchi, G. Wormser, D.J. Lange, D.M. Wright, J.P. Coleman, J.R. Fry, E. Gabathuler, D.E. Hutchcroft, D.J. Payne, C. Touramanis, A.J. Bevan, F. Di Lodovico, R. Sacco, G. Cowan, J. Bougher, D.N. Brown, C.L. Davis, A.G. Denig, M. Fritsch, W. Gradl, K. Griessinger, A. Hafner, K.R. Schubert, R.J. Barlow, G.D. Lafferty, R. Cenci, B. Hamilton, A. Jawahery, D.A. Roberts, R. Cowan, G. Sciolla, R. Cheaib, P.M. Patel, S.H. Robertson, N. Neri, F. Palombo, L. Cremaldi, R. Godang, P. Sonnek, D.J. Summers, M. Simard, P. Taras, G. De Nardo, G. Onorato, C. Sciacca, M. Martinelli, G. Raven, C.P. Jessop, J.M. LoSecco, K. Honscheid, R. Kass, E. Feltresi, M. Margoni, M. Morandin, M. Posocco, M. Rotondo, G. Simi, F. Simonetto, R. Stroili, S. Akar, E. Ben-Haim, M. Bomben, G.R. Bonneaud, H. Briand, G. Calderini, J. Chauveau, P. Leruste, G. Marchiori, J. Ocariz, M. Biasini, E. Manoni, S. Pacetti, A. Rossi, C. Angelini, G. Batignani, S. Bettarini, M. Carpinelli, G. Casarosa, A. Cervelli, M. Chrzaszcz, F. Forti, M.A. Giorgi, A. Lusiani, B. Oberhof, E. Paoloni, A. Perez, G. Rizzo, J.J. Walsh, D. Lopes Pegna, J. Olsen, A.J.S. Smith, R. Faccini, F. Ferrarotto, F. Ferroni, M. Gaspero, L. Li Gioi, A. Pilloni, G. Piredda, C. Bünger, S. Dittrich, O. Grünberg, T. Hartmann, M. Hess, T. Leddig, C. Voß, R. Waldi, T. Adye, E.O. Olaiya, F.F. Wilson, S. Emery, G. Vasseur, F. Anulli, D. Aston, D.J. Bard, C. Cartaro, M.R. Convery, J. Dorfan, G.P. Dubois-Felsmann, W. Dunwoodie, M. Ebert, R.C. Field, B.G. Fulsom, M.T. Graham, C. Hast, W.R. Innes, P. Kim, D.W.G.S. Leith, P. Lewis, D. Lindemann, S. Luitz, V. Luth, H.L. Lynch, D.B. MacFarlane, D.R. Muller, H. Neal, M. Perl, T. Pulliam, B.N. Ratcliff, A. Roodman, A.A. Salnikov, R.H. Schindler, A. Snyder, D. Su, M.K. Sullivan, J. Va'vra, W.J. Wisniewski, H.W. Wulsin, M.V. Purohit, R.M. White, J.R. Wilson, A. Randle-Conde, S.J. Sekula, M. Bellis, P.R. Burchat, E.M.T. Puccio, M.S. Alam, J.A. Ernst, R. Gorodeisky, N. Guttman, D.R. Peimer, A. Soffer, S.M. Spanier, J.L. Ritchie, A.M. Ruland, R.F. Schwitters, B.C. Wray, J.M. Izen, X.C. Lou, F. Bianchi, F. De Mori, A. Filippi, D. Gamba, L. Lanceri, L. Vitale, F. Martinez-Vidal, A. Oyanguren, P. Villanueva-Perez, J. Albert, S. Banerjee, A. Beaulieu, F.U. Bernlochner, H.H.F. Choi, G.J. King, R. Kowalewski, M.J. Lewczuk, T. Lueck, I.M. Nugent, J.M. Roney, R.J. Sobie, N. Tasneem, T.J. Gershon, P.F. Harrison, T.E. Latham, H.R. Band, S. Dasu, Y. Pan, R. Prepost, S.L. Wu, BaBar Collaboration Collaboration Collaboration, Search for a dark photon in e^+e^- collisions at babar, Phys. Rev. Lett. 113 (2014) 201801, http://dx.doi.org/10.1103/PhysRevLett.113.201801, URL https://link.aps.org/doi/10.1103/PhysRevLett.113.201801.
[505] S. Bilmiş, I. Turan, T.M. Aliev, M. Deniz, L. Singh, H.T. Wong, Constraints on dark photon from neutrino-electron scattering experiments, Phys. Rev. D 92 (2015) 033009, http://dx.doi.org/10.1103/PhysRevD.92.033009, URL https://link.aps.org/doi/10.1103/PhysRevD.92.033009.
[506] P.-F. Yin, S.-H. Zhu, Light dark sector searches at low-energy high-luminosity e^+e^- colliders, Front. Phys. 11 (5) (2016) 111403, http://dx.doi.org/10.1007/s11467-016-0541-1.
[507] T. Lin, TASI lectures on dark matter models and direct detection, 2019, arXiv:1904.07915.
[508] J.D. Bjorken, R. Essig, P. Schuster, N. Toro, New fixed-target experiments to search for dark gauge forces, Phys. Rev. D 80 (2009) 075018, http://dx.doi.org/10.1103/PhysRevD.80.075018, URL https://link.aps.org/doi/10.1103/PhysRevD.80.075018.
[509] M. Pospelov, Secluded U(1) below the weak scale, Phys. Rev. D 80 (2009) 095002, http://dx.doi.org/10.1103/PhysRevD.80.095002, URL https://link.aps.org/doi/10.1103/PhysRevD.80.095002.
[510] D. Banerjee, V. Burtsev, D. Cooke, P. Crivelli, E. Depero, A.V. Dermenev, S.V. Donskov, F. Dubinin, R.R. Dusaev, S. Emmenegger, A. Fabich, V.N. Frolov, A. Gardikiotis, S.N. Gninenko, M. Hösgen, V.A. Kachanov, A.E. Karneyeu, B. Ketzer, D.V. Kirpichnikov, M.M. Kirsanov, S.G. Kovalenko, V.A. Kramarenko, L.V. Kravchuk, N.V. Krasnikov, S.V. Kuleshov, V.E. Lyubovitskij, V. Lysan, V.A. Matveev, Y.V. Mikhailov, V.V. Myalkovskiy, V.D. Peshekhonov, D.V. Peshekhonov, O. Petuhov, V.A. Polyakov, B. Radics, A. Rubbia, V.D. Samoylenko, V.O. Tikhomirov, D.A. Tlisov, A.N. Toropin, A.Y. Trifonov, B. Vasilishin, G. Vasquez Arenas, P. Ulloa, K. Zhukov, K. Zioutas, NA64 Collaboration Collaboration Collaboration, Search for invisible decays of sub-GeV dark photons in missing-energy events at the CERN SPS, Phys. Rev. Lett. 118 (2017) 011802, http://dx.doi.org/10.1103/PhysRevLett.118.011802, URL https://link.aps.org/doi/10.1103/PhysRevLett.118.011802.

[511] D. Banerjee, V.E. Burtsev, A.G. Chumakov, D. Cooke, P. Crivelli, E. Depero, A.V. Dermenev, S.V. Donskov, F. Dubinin, R.R. Dusaev, S. Emmenegger, A. Fabich, V.N. Frolov, A. Gardikiotis, S.G. Gerassimov, S.N. Gninenko, M. Hösgen, A.E. Karneyeu, B. Ketzer, D.V. Kirpichnikov, M.M. Kirsanov, I.V. Konorov, S.G. Kovalenko, V.A. Kramarenko, L.V. Kravchuk, N.V. Krasnikov, S.V. Kuleshov, V.E. Lyubovitskij, V. Lysan, V.A. Matveev, Y.V. Mikhailov, D.V. Peshekhonov, V.A. Polyakov, B. Radics, R. Rojas, A. Rubbia, V.D. Samoylenko, V.O. Tikhomirov, D.A. Tlisov, A.N. Toropin, A.Y. Trifonov, B.I. Vasilishin, G. Vasquez Arenas, P. Ulloa, The NA64 Collaboration Collaboration Collaboration, Search for vector mediator of dark matter production in invisible decay mode, Phys. Rev. D 97 (2018) 072002, http://dx.doi.org/10.1103/PhysRevD.97.072002, URL https://link.aps.org/doi/10.1103/PhysRevD.97.072002.
[512] L. Morel, Z. Yao, P. Cladé, S. Guellati-Khélifa, Determination of the fine-structure constant with an accuracy of 81 parts per trillion, Nature 588 (7836) (2020) 61–65, http://dx.doi.org/10.1038/s41586-020-2964-7.
[513] B.A. Dobrescu, I. Mocioiu, Spin-dependent macroscopic forces from new particle exchange, J. High Energy Phys. 11 (2006) 005, http://dx.doi.org/10.1088/1126-6708/2006/11/005, arXiv:hep-ph/0605342.
[514] P. Fadeev, Y.V. Stadnik, F. Ficek, M.G. Kozlov, V.V. Flambaum, D. Budker, Revisiting spin-dependent forces mediated by new bosons: Potentials in the coordinate-space representation for macroscopic- and atomic-scale experiments, Phys. Rev. A 99 (2019) 022113, http://dx.doi.org/10.1103/PhysRevA.99.022113, URL https://link.aps.org/doi/10.1103/PhysRevA.99.022113.
[515] J.A. Frieman, S. Dimopoulos, M.S. Turner, Axions and stars, Phys. Rev. D 36 (1987) 2201–2210, http://dx.doi.org/10.1103/PhysRevD.36.2201, URL https://link.aps.org/doi/10.1103/PhysRevD.36.2201.
[516] G.G. Raffelt, D.S. Dearborn, Bounds on hadronic axions from stellar evolution, Phys. Rev. D 36 (1987) 2211, http://dx.doi.org/10.1103/PhysRevD.36.2211.
[517] G.G. Raffelt, D.S.P. Dearborn, Bounds on light, weakly interacting particles from observational lifetimes of helium-burning stars, Phys. Rev. D 37 (1988) 549–551, http://dx.doi.org/10.1103/PhysRevD.37.549, URL https://link.aps.org/doi/10.1103/PhysRevD.37.549.
[518] G. Raffelt, Horizontal branch stars and the neutrino signal from SN 1987a, Phys. Rev. D 38 (1988) 3811–3812, http://dx.doi.org/10.1103/PhysRevD.38.3811, URL https://link.aps.org/doi/10.1103/PhysRevD.38.3811.
[519] G.G. Raffelt, Astrophysical methods to constrain axions and other novel particle phenomena, Phys. Rep. 198 (1) (1990) 1–113, http://dx.doi.org/10.1016/0370-1573(90)90054-6, URL http://www.sciencedirect.com/science/article/pii/0370157390900546.
[520] W.C. Haxton, K.Y. Lee, Red-giant evolution, metallicity, and new bounds on hadronic axions, Phys. Rev. Lett. 66 (1991) 2557–2560, http://dx.doi.org/10.1103/PhysRevLett.66.2557, URL https://link.aps.org/doi/10.1103/PhysRevLett.66.2557.
[521] G. Raffelt, Stars As Laboratories for Fundamental Physics: The Astrophysics of Neutrinos, Axions, and Other Weakly Interacting Particles, University of Chicago, 1996.
[522] G.G. Raffelt, Particle physics from stars, Ann. Rev. Nucl. Part. Sci. 49 (1999) 163–216, http://dx.doi.org/10.1146/annurev.nucl.49.1.163, arXiv:hep-ph/9903472.
[523] G. Raffelt, D. Seckel, Bounds on exotic particle interactions from SN 1987a, Phys. Rev. Lett. 60 (1988) 1793, http://dx.doi.org/10.1103/PhysRevLett.60.1793.
[524] G.G. Raffelt, Astrophysics probes of particle physics, Phys. Rep. 333–334 (2000) 593–618, http://dx.doi.org/10.1016/S0370-1573(00)00039-9, URL http://www.sciencedirect.com/science/article/pii/S0370157300000399.
[525] N. Viaux, M. Catelan, P.B. Stetson, G. Raffelt, J. Redondo, A.A.R. Valcarce, A. Weiss, Neutrino and axion bounds from the globular cluster M5 (NGC 5904), Phys. Rev. Lett. 111 (2013) 231301, http://dx.doi.org/10.1103/PhysRevLett.111.231301, arXiv:1311.1669.
[526] A. Ayala Gómez, Beyond Standard Model Particle Constraints from Stellar Evolution, (Ph.D. thesis), Granada U., 2017.
[527] S. Moehler, Hot stars in globular clusters: A spectroscopist's view, Publ. Astron. Soc. Pac. 113 (788) (2001) 1162–1177, URL http://www.jstor.org/stable/10.1086/323297.
[528] H. Baumgardt, M. Hilker, A catalogue of masses, structural parameters, and velocity dispersion profiles of 112 milky way globular clusters, Mon. Not. R. Astron. Soc. 478 (2) (2018) 1520–1557, http://dx.doi.org/10.1093/mnras/sty1057, arXiv:https://academic.oup.com/mnras/article-pdf/478/2/1520/25060036/sty1057.pdf.
[529] D.A. Forbes, N. Bastian, M. Gieles, R.A. Crain, J.M.D. Kruijssen, S.r.S. Larsen, S. Ploeckinger, O. Agertz, M. Trenti, A.M.N. Ferguson, J. Pfeffer, O.Y. Gnedin, Globular cluster formation and evolution in the context of cosmological galaxy assembly: open questions, Proc. R. Soc. A: Math. Phys. Eng. Sci. 474 (2210) (2018) 20170616, http://dx.doi.org/10.1098/rspa.2017.0616, arXiv:https://royalsocietypublishing.org/doi/pdf/10.1098/rspa.2017.0616, URL https://royalsocietypublishing.org/doi/abs/10.1098/rspa.2017.0616.
[530] J. Grifols, E. Massó, Constraints on finite-range baryonic and leptonic forces from stellar evolution, Phys. Lett. B 173 (3) (1986) 237–240, http://dx.doi.org/10.1016/0370-2693(86)90509-5, URL https://www.sciencedirect.com/science/article/pii/0370269386905095.
[531] J.A. Grifols, E. Massó, S. Peris, Energy loss from the sun and red giants: bounds on short-range baryonic and leptonic forces, Modern Phys. Lett. A 04 (04) (1989) 311–323, http://dx.doi.org/10.1142/S0217732389000381, http://arxiv.org/abs/DOI: 10.1142/S0217732389000381[arXiv:DOI: 10.1142/S0217732389000381].
[532] D.A. Dicus, E.W. Kolb, V.L. Teplitz, R.V. Wagoner, Astrophysical bounds on the masses of axions and Higgs particles, Phys. Rev. D 18 (1978) 1829–1834, http://dx.doi.org/10.1103/PhysRevD.18.1829, URL https://link.aps.org/doi/10.1103/PhysRevD.18.1829.
[533] D.A. Dicus, E.W. Kolb, V.L. Teplitz, R.V. Wagoner, Astrophysical bounds on very-low-mass axions, Phys. Rev. D 22 (1980) 839–845, http://dx.doi.org/10.1103/PhysRevD.22.839, URL https://link.aps.org/doi/10.1103/PhysRevD.22.839.
[534] M. Fukugita, S. Watamura, M. Yoshimura, Light pseudoscalar particle and stellar energy loss, Phys. Rev. Lett. 48 (1982) 1522–1525, http://dx.doi.org/10.1103/PhysRevLett.48.1522, URL https://link.aps.org/doi/10.1103/PhysRevLett.48.1522.
[535] M. Fukugita, S. Watamura, M. Yoshimura, Astrophysical constraints on a new light axion and other weakly interacting particles, Phys. Rev. D 26 (1982) 1840–1853, http://dx.doi.org/10.1103/PhysRevD.26.1840, URL https://link.aps.org/doi/10.1103/PhysRevD.26.1840.
[536] A. Barroso, G.C. Branco, Constraints on light axions, Phys. Lett. B 116 (4) (1982) 247–250, http://dx.doi.org/10.1016/0370-2693(82)90335-5, URL https://www.sciencedirect.com/science/article/pii/0370269382903355.
[537] A. Pantziris, K. Kang, Axion emission rates in stars and constraints on its mass, Phys. Rev. D 33 (1986) 3509–3518, http://dx.doi.org/10.1103/PhysRevD.33.3509, URL https://link.aps.org/doi/10.1103/PhysRevD.33.3509.
[538] G.G. Raffelt, Astrophysical axion bounds diminished by screening effects, Phys. Rev. D 33 (1986) 897–909, http://dx.doi.org/10.1103/PhysRevD.33.897, URL https://link.aps.org/doi/10.1103/PhysRevD.33.897.
[539] A.M. Alonso, B.S. Cooper, A. Deller, L. Gurung, S.D. Hogan, D.B. Cassidy, Velocity selection of Rydberg positronium using a curved electrostatic guide, Phys. Rev. A 95 (2017) 053409, http://dx.doi.org/10.1103/PhysRevA.95.053409, URL https://link.aps.org/doi/10.1103/PhysRevA.95.053409.
[540] J. Khoury, A. Weltman, Chameleon fields: Awaiting surprises for tests of gravity in space, Phys. Rev. Lett. 93 (2004) 171104, http://dx.doi.org/10.1103/PhysRevLett.93.171104, URL https://link.aps.org/doi/10.1103/PhysRevLett.93.171104.